

Identification and design of a novel family mitochondrial protonophores for bioenergetics
analysis and the treatment of ischemia-reperfusion injury

Brandon Merrill Kenwood

Brookside, NJ

MS, Biological and Physical Science, University of Virginia, 2011

BA, Molecular, Cellular, and Developmental Biology, University of Colorado at Boulder,
2009

A Dissertation Presented to the Graduate Faculty
of the University of Virginia in Candidacy for the Degree of
Doctor of Philosophy

Department of Pharmacology

University of Virginia

September 2014

Kyle L. Hoehn, Ph.D.

Kevin R. Lynch, Ph.D.

Jeffrey S. Smith, Ph.D.

Chien Li, Ph.D.

Thurl E. Harris, Ph.D.

Jeffrey W. Holmes, M.D., Ph.D.

ABSTRACT

Nutrient oxidation is normally coupled to ATP production via a proton cycle across the mitochondrial inner membrane. Small molecule proton transporters (protonophores) enable protons to enter the mitochondrial matrix independently of ATP production and thereby ‘uncouple’ mitochondrial respiration. Mitochondrial protonophore uncouplers improve the efficiency of electron transfer to reduce the production of reactive oxygen species (ROS) and cause mitochondria to respire at a maximal rate. Therefore, mitochondrial uncouplers are used as chemical tools to assess mitochondrial function/dysfunction, and may have clinical applicability in disorders involving mitochondria-derived ROS such as ischemia-reperfusion injury.

A handful of small molecule mitochondrial protonophore uncouplers are known, but they have unwanted activity at other membranes. The primary objective of my thesis project was to identify a mitochondrial uncoupler that lacks activity at the plasma membrane. Herein I report the discovery and validation of BAM15, a novel mitochondrial uncoupler that does not have protonophore activity at the plasma membrane. Structure-activity relationship studies were performed to define the mechanism by which BAM15 uncouples mitochondria. Finally, we demonstrate that BAM15 treatment protects mice from renal ischemia-reperfusion injury. In sum, we conclude that BAM15 is a novel mitochondrial uncoupler that enables a more accurate analysis of cellular and mitochondrial bioenergetics and may have clinical applicability for renal ischemia-reperfusion injury. This work provides a foundation for future chemical engineering and medicinal chemistry to optimize BAM15 for advanced experimental and therapeutic applications.

ACKNOWLEDGEMENTS

There were many individuals that were instrumental to my success. First, I would like to thank my family and friends, for without them this would not be possible. My parents, Carol and Alan, have provided me with constant support throughout my life. Importantly, I would like to thank my grandparents, Stephanie and Joseph, for always encouraging me to help those in need and be a good person. I would also like to acknowledge my childhood friends, especially Daniel Mahoney and his family. We have come a long way and are surprisingly both still in one piece! Finally, I would like to thank my high school biology teacher Harry Bullock for first introducing me to my passion for science.

During my graduate career the Pharmacology Department was continuously supportive of my training and personal development. I was able to work with scientists from many backgrounds, and it is with great appreciation that I was given the opportunity to be educated in an environment that encourages collaboration and scientific discussion on a regular basis. Specifically, I would like to thank Paula Barrett, Thurl Harris, Michelle Bland, Bimal Desai, Ira Shulman, and Jolene Kidd for their guidance, commitment to graduate student training, and unwavering altruism. Lab meetings with Zhen Yan and his laboratory were also critical to my project and career development. My thesis committee, consisting of Kevin Lynch, Thurl Harris, Jeff Smith, Chien Li, and Jeff Holmes was able to guide both my project and my career goals. I would also like to thank Jeff Smith and Noel Dwyer for allowing me to rotate in their labs at the beginning of my graduate career.

My thesis work was highly collaborative and many researchers made direct contributions to my project. Aman Bajwa and Mark Okusa were critical for our work in renal physiology. Jose Tomsig and Kevin Lynch not only provided expertise in mass spectrometry, pharmacokinetics, and drug metabolism for this project, but also donated their time to provide knowledge that will last a lifetime. The discoveries outlined in this work regarding plasma membrane electrophysiology would not have been possible without the hard work and dedication of Janelle Weaver and Doug Bayliss. I would also like to thank Frances Byrne for her work and knowledge in cytotoxicity, and Beverley Murrow for performing much of the primary screening that led to the discovery of BAM15. Flow cytometry was performed in the middle of the night with Ivan K. Poon.

There are also scientists outside of UVA that made significant contributions. Jose Calderone and Webster Santos at Virginia Tech performed medicinal chemistry that was critical to my thesis work. I would also like to thank George Rogers from Seahorse Biosciences and the University of California, San Diego for his expertise in mitochondrial bioenergetics and continued mentorship.

I would sincerely like to thank my laboratory, as over the years it became a second family to me. It was a wonderful experience to matriculate through graduate school and “grow up” with my graduate student lab mates Evan Taddeo and Marin Healy. Because of you both there was never a dull day at work and I always enjoyed coming to lab. I would also like to thank the postdoctoral fellows in our laboratory, Frances Byrne and Jenny Chow, who helped raise us and somehow managed to keep us (me) in line most of the time. I would like to thank my thesis advisor, Kyle Hoehn, for making me the scientist I am today. Kyle allowed me to pursue my research passions and

taught me the value of hard work, persistence, and thinking positive. Finally, I would like to thank Al Merrill for accepting me into his laboratory for postdoctoral training and allowing me to continue scientific research.

TABLE OF CONTENTS

ABSTRACT	2
ACKNOWLEDGEMENTS	3
TABLE OF CONTENTS	6
SUMMARY OF FIGURES	10
APPENDIX OF ABBREVIATIONS	13
<u>CHAPTER 1: MITOCHONDRIAL BIOENERGETICS AND RENAL</u>	
<u>ISCHEMIA REPERFUSION INJURY</u>	15
1.1 Mitochondrial bioenergetics	16
<i>1.1.1 Electron carrier production by mitochondria</i>	16
<i>1.1.2 Regulation of the mitochondrial proton gradient</i>	20
<i>1.1.3 ATP synthase</i>	21
<i>1.1.4 Mitochondrial uncoupling and proton leak</i>	22
<i>1.1.5 Methods of assessing mitochondrial respiratory dysfunction in whole cells</i> ...	24
1.2 Reactive oxygen species	29
<i>1.2.1 Overview of reactive oxygen species</i>	29
<i>1.2.2 Mitochondrial O₂⁻ production from complex I</i>	31
<i>1.2.3 Mitochondrial O₂⁻ production by complex II</i>	36
<i>1.2.4 Mitochondrial O₂⁻ formation by complex III</i>	39
1.3 Renal Ischemia-reperfusion injury	44
<i>1.3.1 Overview of renal Ischemia-reperfusion injury</i>	44
<i>1.3.2 Readouts of renal health</i>	48

1.3.3 Current treatments for renal IRI	49
1.4 Mitochondrial uncouplers	53
1.4.1 The use of uncoupling agents in humans	53
1.4.2 Small molecule mitochondrial uncouplers	57
1.4.3 Limitations of mitochondrial protonophores	62
1.4.4 Toxicity of mitochondrial protonophores	66
1.5 Concluding remarks.....	66

CHAPTER 2: IDENTIFICATION AND VALIDATION OF A NOVEL

MITOCHONDRIAL UNCOUPLER THAT DOES NOT DEPOLARIZE THE

PLASMA MEMBRANE

2.1 Introduction	70
2.2 Materials and methods	71
2.2.1 Non-quantitative oxygen consumption assay	71
2.2.2 ROS production assay	72
2.2.4 Measurements of OCR and ECAR in whole cells	72
2.2.5 Mitochondria isolation from mouse liver	73
2.2.6 Electron flow assay.....	74
2.2.7 Mitochondrial titration assays.....	74
2.2.8 $\Delta\Psi_m$ in whole cells	74
2.2.9 ANT-independence assay.....	74
2.2.10 Mitochondrial swelling assay.....	75
2.2.11. $\Delta\Psi_m$ in isolated mitochondria.....	75
2.2.12. Plasma membrane electrophysiology.....	76

2.2.13 Cytotoxicity assays	77
2.2.14 ATP Assay.....	77
2.3 Results	79
2.3.1 A biochemical screen to search for new uncouplers	79
2.3.2. BAM15 uncouples mitochondria in whole cells	86
2.3.3 BAM15 stimulates respiration by acting directly on isolated mitochondria....	89
2.3.4 BAM15 is a mitochondrial protonophore.....	93
2.3.5 BAM15's effect on respiration is not complex-specific and independent of ANT	95
2.3.6 BAM15 does not depolarize the plasma membrane	99
2.3.7 BAM15 demonstrates significantly less intracellular acidification than FCCP	102
2.3.8 BAM15 is less cytotoxic than FCCP.....	104
2.4 Discussion.....	108

CHAPTER 3: MECHANISTIC DETERMINATION OF THE PROTONOPHORE

<u>ACTIVITY OF BAM15.....</u>	110
3.1 Introduction	111
3.2 Results	111
3.2.1 The lipophilic furazano 'core' of BAM15 is required for activity.....	111
3.2.2 Determination of the ionizable proton location of BAM15	114
3.2.3 The potency of BAM15 is dependent on the electron withdrawing groups	116
3.2.4 The dynamic range of BAM15 is dependent on symmetric fluorination	124
3.2.5 Alkyl chains can be utilized as a source of electron density	126

3.3 Discussion.....	131
<u>CHAPTER 4: BAM15 PROTECTS FROM RENAL ISCHEMIA-REPERFUSION</u>	
<u>INJURY</u>	135
4.1 Introduction.....	136
4.2 Materials and methods	136
4.2.1 BAM15 mass spec analysis.....	136
4.2.2 Pharmacokinetics	137
4.2.3 Renal ischemic reperfusion injury.....	137
4.2.4. Assessment of kidney function and histology.....	138
4.2.5. Kidney FACS analysis	138
4.3 Results	139
4.3.1 BAM15 can be measured via LC-MS/MS	139
4.3.2 Pharmacokinetic profile of BAM15.....	145
4.3.3. BAM15 decreases immune cell infiltration and protects from renal IRI	148
4.4 Discussion.....	153
<u>CONCLUDING REMARKS AND FUTURE DIRECTIONS.....</u>	
	157
<u>PUBLICATIONS RESULTING FROM THIS WORK.....</u>	
	160
<u>REFERENCES.....</u>	
	161

SUMMARY OF FIGURES

FIGURE 1: THE MITOCHONDRIAL ELECTRON TRANSPORT CHAIN.	18
FIGURE 2: THE TCA CYCLE.....	19
FIGURE 3: MITOCHONDRIAL BIOENERGETICS ANALYSIS IN WHOLE CELLS.	28
FIGURE 4: COMPLEX I CAN GENERATE O_2^- IN THE FORWARD AND REVERSE DIRECTION INTO THE MITOCHONDRIAL MATRIX.	35
FIGURE 5: COMPLEX II CAN GENERATE O_2^- INTO THE MATRIX IN THE FORWARD AND REVERSE DIRECTION.	38
FIGURE 6: COMPLEX III GENERATES O_2^- INTO THE MITOCHONDRIAL MATRIX AND INTERMEMBRANE SPACE.	42
FIGURE 7: MITOCHONDRIAL UNCOUPLERS CAUSE MITOCHONDRIAL FAILURE.	65
FIGURE 8: A BIOCHEMICAL SCREEN IDENTIFIES BAM15 AS AN OXYGEN CONSUMPTION AGONIST THAT DOES NOT INCREASE INTRACELLULAR ROS IN WHOLE CELLS.	82
FIGURE 9: BAM15 INCREASES OCR IN WHOLE CELLS ACROSS A BROAD DOSING RANGE. .	83
FIGURE 10: BAM15 INCREASES ECAR.	84
FIGURE 11: BAM15 CAUSES MITOCHONDRIAL UNCOUPLING IN WHOLE CELLS.	87
FIGURE 12: BAM15 DEPOLARIZES MITOCHONDRIA IN INTACT CELLS.	88
FIGURE 13: BAM15 STIMULATES RESPIRATION IN ISOLATED MITOCHONDRIA.	91
FIGURE 14: BAM15 DEPOLARIZES ISOLATED MITOCHONDRIA.	92
FIGURE 15: BAM15 INDUCES PROTON-DEPENDENT MITOCHONDRIAL SWELLING.	94
FIGURE 16: BAM15-MEDIATED RESPIRATION IS NOT COMPLEX-SPECIFIC AND IS NOT DUE TO ELECTRON DONATION.	97

FIGURE 17: BAM15 INCREASES OXYGEN CONSUMPTION INDEPENDENT OF THE ADENINE NUCLEOTIDE TRANSLOCASE.....	98
FIGURE 18: BAM15 DOES NOT ALTER PLASMA MEMBRANE ELECTROPHYSIOLOGY.	100
FIGURE 19: BAM15 CAUSES LESS INTRACELLULAR ACIDIFICATION COMPARED TO FCCP.	103
FIGURE 20: BAM15 DOES NOT DECREASE ATP CONCENTRATIONS.	105
FIGURE 21: BAM15 IS LESS CYTOTOXIC THAN FCCP.....	106
FIGURE 22: THE FURAZANO CORE OF BAM15 IS REQUIRED FOR UNCOUPLING ACTIVITY.	113
FIGURE 23: IDENTIFICATION OF IONIZABLE PROTONS OF BAM15.....	115
FIGURE 24: ALTERATIONS OF HALOGEN POSITIONING HAVE LITTLE EFFECT ON POTENCY OR DYNAMIC RANGE.	118
FIGURE 25: PARA, BUT NOT META HALOGEN POSITIONING DECREASES ECAR COMPARED TO BAM15.	120
FIGURE 26: MODIFICATION OF ELECTRON DENSITY ALTERS POTENCY OF THE BAM15 FAMILY OF UNCOUPLERS.....	121
FIGURE 27: MODIFICATION OF ELECTRON DENSITY ALTERS POTENCY OF THE BAM15 FAMILY OF UNCOUPLERS WITH RESPECT TO ECAR.....	123
FIGURE 28: ELECTRON-WITHDRAWING FLUORINES ARE CRITICAL FOR DYNAMIC RANGE.	125
FIGURE 29: ALKYL CHAINS CAN BE UTILIZED AS ELECTRON WITHDRAWING GROUPS.....	127
FIGURE 30: EFFECTS OF UTILIZING ALKYL CHAINS AS ELECTRON WITHDRAWING GROUPS ON ECAR ARE SIMILAR TO OCR.....	129
FIGURE 31: BAM15 DERIVATIVES THAT DO NOT CONTAIN BENZYL ELECTRON WITHDRAWING GROUPS UTILIZE THE SAME IONIZABLE PROTON AS BAM15.	130

FIGURE 32: PRECURSOR ION SCAN FOLLOWING DIRECT INJECTION OF BAM15.....	141
FIGURE 33: FRAGMENTATION OF BAM15 FOLLOWING COLLISION.	142
FIGURE 34: NEUTRAL LOSS SCAN OF BAM15 USING THE MOST ABUNDANT PRODUCT ION.	143
FIGURE 35: STANDARD CURVE OF BAM15 AS MEASURED VIA LC-MS/MS.....	144
FIGURE 36: PHARMACOKINETICS OF BAM15.	146
FIGURE 37: BAM15 IS ORALLY AVAILABLE.....	147
FIGURE 38: BAM15 DECREASES IMMUNE CELL INVASION FOLLOWING RENAL IRI.	149
FIGURE 39: BAM15 PROTECTS AGAINST KIDNEY ISCHEMIC-REPERFUSION INJURY.	151
FIGURE 40: BAM15 PRETREATMENT DECREASED ACUTE PROXIMAL TUBULAR NECROSIS OF THE KIDNEY MEDULLA 48 H FOLLOWING REPERFUSION.	152

APPENDIX OF ABBREVIATIONS

ANT	Adenine nucleotide translocase
ATN	Acute tubular necrosis
ATP	Adenosine triphosphate
BAM15	(2-fluorophenyl){6-[(2-fluorophenyl)amino](1,2,5-oxadiazolo[3,4-e]pyrazin-5-yl)}amine
CCCP	Carbonyl cyanide <i>m</i> -chlorophenyl hydrazine
DNC	Dinitroresol
DNP	2,4-Dinitrophenol
ECAR	Extracellular acidification rate
ESI	Electrospray ionization
ETC	Electron transport chain
F ₁	ATP synthase coupling factor 1
FA	Fatty acid
FADH	Flavin adenine dinucleotide
FCCP	Carbonyl cyanide-4-(trifluoromethoxy)phenylhydrazone
FDA	Food and Drug Administration
F ₀	ATP synthase coupling factor 0
GDP	Guanosine disphosphate
GFR	Glomerular filtration rate
H ₂ DCFDA	2',7'-dichlorodihydrofluorescein diacetate

HPCD	β -hydroxypropylcyclodextrine
IRI	Ischemia-reperfusion injury
MnSOD	Mitochondrial superoxide dismutase
NADH	Nicotinamide adenine dinucleotide
OCR	Oxygen consumption rate
PIS	Precursor ion scan
Q	Ubiquinone
QH	Semiubiquinone
QH ₂	Ubiquinol
RET	Reverse electron transfer
ROS	Reactive oxygen species
STC1	Stanniocalcin 1
THP	Tamm-Horsefall Protein
UCP	Uncoupling protein
XO	Xanthine Oxidase
ΔpH_m	Mitochondrial pH gradient
$\Delta\Psi_m$	Mitochondrial membrane potential

**CHAPTER 1: MITOCHONDRIAL BIOENERGETICS AND RENAL ISCHEMIA
REPERFUSION INJURY**

1.1 Mitochondrial bioenergetics

1.1.1 *Electron carrier production by mitochondria*

Mitochondria are organelles that convert nutrients to ATP through a series of redox reactions, and consist of two compartments that are separated by inner and outer membranes. The outer membrane is permeable to metabolites required for energy production, and the inner membrane is used to maintain a pH and electrical gradient to be used for ATP synthesis¹ (**Figure 1**). The primary pathway for energy production in aerobic cells involves the oxidation of nutrients in mitochondria via the tricarboxylic acid (TCA) cycle (**Figure 2**) to produce the electron carriers nicotinamide adenine dinucleotide (NADH) and flavin adenine dinucleotide (FADH₂). Glucose is imported into the cell by glucose transporters² and oxidized to pyruvate³, which is transported into the mitochondria by the mitochondrial pyruvate carrier⁴. Pyruvate is then converted into acetyl-CoA by a coordinated sequence of reactions catalyzed by pyruvate dehydrogenase⁵, which produces CO₂ and NADH^{5,6}. Citrate synthase then forms citrate from acetyl-CoA and oxaloacetate at the expense of one ATP molecule⁷. Aconitase then converts citrate to isocitrate (with aconitate as an intermediate)⁸, which is then dehydrogenated by isocitrate dehydrogenase to produce α -ketoglutarate along with NADH and CO₂⁹. α -ketoglutarate is then converted to succinyl-CoA by α -ketoglutarate dehydrogenase, which produces another NADH electron carrier and CO₂¹⁰. Succinyl-CoA synthetase then converts succinyl-CoA to succinate¹¹, which can feed electrons to the succinate dehydrogenase/FAD⁺ complex (complex II)^{12,13}. This process introduces electrons to complex II by oxidizing succinate to fumarate, which reduces FAD⁺ to FADH₂¹⁴. Fumarate is then converted to malate by fumarase¹⁵. Malate is dehydrogenated

by malate dehydrogenase¹⁶ to produce another NADH molecule¹⁷ and oxaloacetate as a final product to complete the TCA cycle¹⁶.

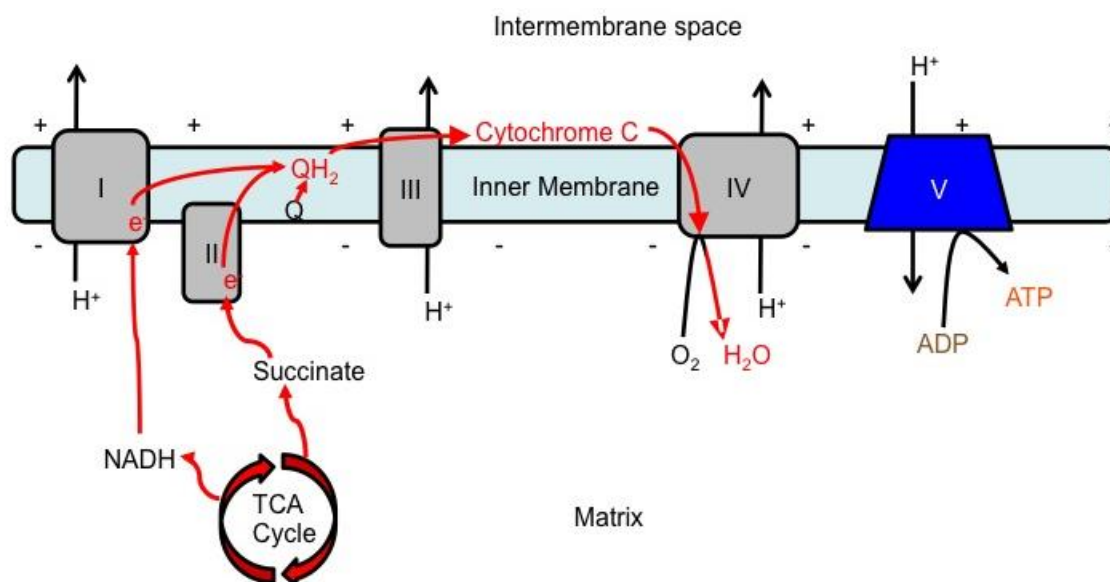


Figure 1: The mitochondrial electron transport chain.

NADH and FADH₂ donate electrons to complexes I and II, respectively. Ubiquinone (Q) is then reduced to ubiquinol by two electrons at either complex I or II. These electrons are then transferred to complex III, which donates electrons to cytochrome C. The final redox reaction occurs at complex IV where cytochrome C is oxidized and O₂ is reduced to H₂O. In our assays, we monitor the depletion of O₂, which allows oxygen consumption to be utilized as a measure of electron flow. Complexes I, III, and IV pump protons from the matrix space into the intermembrane space to create a pH and electrical gradient known as proton motive force (PMF). Protons then reenter the matrix through ATP synthase to generate ATP.

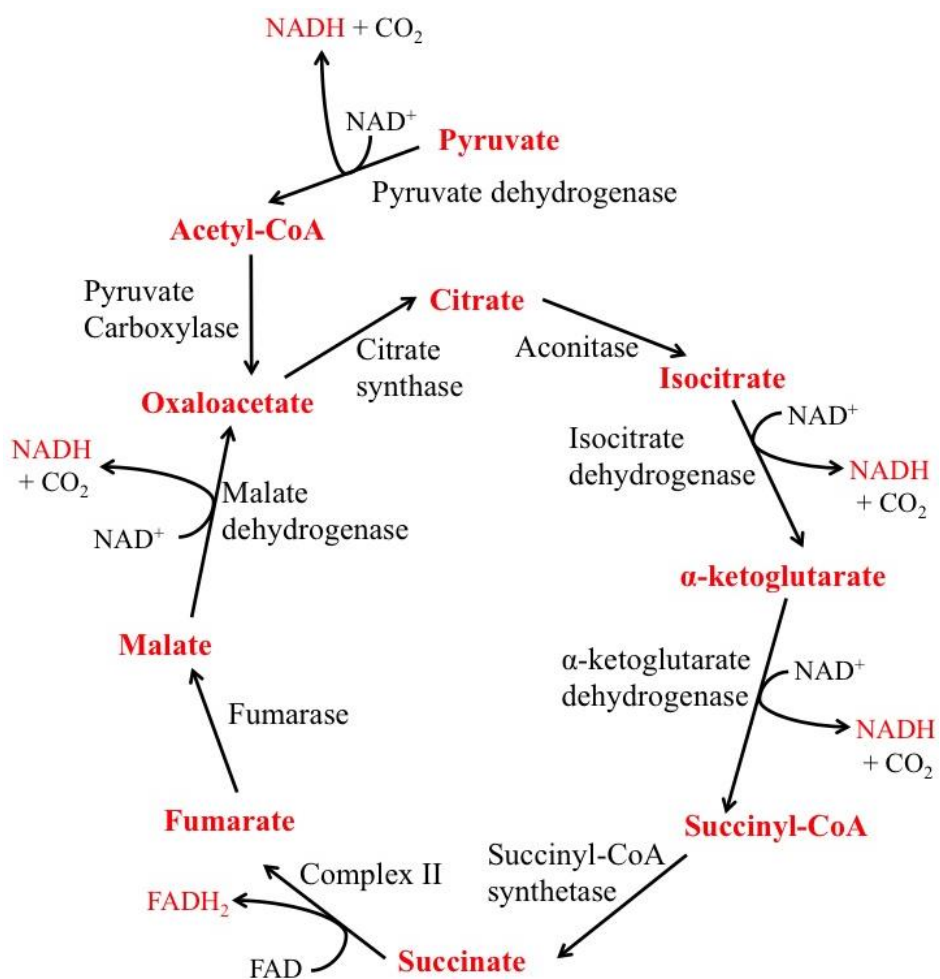


Figure 2: The TCA Cycle

Pyruvate is converted into acetyl-CoA by pyruvate dehydrogenase, which produces CO₂ and NADH^{5,6}. Citrate synthase forms citrate from Acetyl-CoA and oxaloacetate.

Aconitase converts citrate to isocitrate, which is dehydrogenated by isocitrate dehydrogenase to produce α-ketoglutarate with NADH and CO₂⁹. α-ketoglutarate is converted to succinyl-CoA by α-ketoglutarate dehydrogenase, which produces NADH and CO₂. Succinyl-CoA synthetase converts succinyl-CoA to succinate, which is oxidized by complex II to fumarate to reduce FAD⁺ to FADH₂. Fumarate is converted to malate by fumarase. Malate is dehydrogenated by malate dehydrogenase to produce NADH and oxaloacetate as a final product to complete the TCA cycle.

1.1.2 Regulation of the mitochondrial proton gradient

The electron transport chain (ETC) consists of a series of protein complexes which utilize electrons from NADH and FADH₂ generated in the TCA cycle to pump protons from the mitochondrial matrix, across the inner mitochondrial membrane, and into the intermembrane space¹⁸. Electrons can be donated to the ETC by two routes: NADH donates electrons to complex I (NADH:ubiquinone oxidoreductase, NADH dehydrogenase)^{19,20} and oxidation of succinate by complex II/FAD⁺ (succinate dehydrogenase)^{12,13}. Complexes I and II utilize these electrons to reduce ubiquinone to ubisemiquinone with one electron and then ubiquinol with two electrons^{21,22}, which serves as an electron donor for complex III²³. Following complex III oxidation of ubiquinol to ubiquinone, complex III then transfers electrons to Cytochrome C²³, which acts as an electron conduit to complex IV, in which the electrons are transferred to O₂ to form water²⁴.

The first suggestion of how mitochondria can utilize nutrient oxidation to generate ATP was in 1961 by Peter Mitchell. Mitchell proposed the Chemiosmotic Theory, which states that mitochondria create a pH and electrical gradient across the mitochondrial inner membrane that is utilized by ATP synthase to generate ATP²⁵. The energy provided by electrons at complexes I, III, and IV allows them to pump protons across the mitochondrial inner membrane, which results in a high concentration of protons in the intermembrane space²⁶. This creates a pH (ΔpH_m) and an electrical mitochondrial membrane potential ($\Delta\Psi_m$) known as the proton motive force (PMF), which defines how much potential energy exists to “push” a proton back into the mitochondrial matrix²⁶. Protons reenter the mitochondrial matrix through ATP synthase

to generate ATP from ADP. Importantly, the primary limitation of electron flow is PMF²⁷. As PMF increases, electron flow decreases due to the inability of the ETC complexes to pump protons across a higher electrochemical gradient into the intermembrane space²⁸.

1.1.3 ATP synthase

ATP synthase can be separated into two parts, coupling factor 1 (F_1), which contains the catalytic site for ATP synthesis, and coupling factor o (F_o)²⁹. The mechanical part of ATP synthase centers on Subunit-C, which is an 8-subunit membrane protein ring known as the c-ring that spans the mitochondrial inner membrane²⁹. Protons are shuttled through the c-ring by protonation and deprotonation of the carboxylate portion of Glu59 in the c-ring. Resting above the c-ring is Subunit-A, which consists of two aqueous channels that allow protons to the carboxylate group of Glu59, which allows for a protonation and deprotonation reaction³⁰.

Inhibition of ATP synthase is commonly performed to study mitochondrial metabolism. Oligomycin was recognized as an inhibitor of ATP synthase in 1958^{29,31}. Oligomycin binds the F_o subunit²⁹, and it was originally believed that oligomycin binding induced a conformation change in F_o that was transmitted to F_1 , which reversibly altered the catalytic site of ATP synthesis by inhibiting substrate binding³². X-ray crystallography studies now demonstrate that oligomycin likely binds to Subunit-C chains that are in contact with the Subunit-A proton channels, which blocks proton access to Glu59 and thus ATP synthesis and hydrolysis with little change in Subunit-C conformation²⁹. Direct inhibition of ion transport by oligomycin is further supported in its

other target, Na⁺/K⁺ ATPases, in which oligomycin blocks Na⁺ binding without inducing conformational changes³³.

1.1.4 Mitochondrial uncoupling and proton leak

Oxidative phosphorylation in cells is not completely efficient as some electron transfer is not used for ATP synthesis³⁴. This was first documented by David Nicholls, who observed that proton conductance relative to ATP production in mitochondria increases nonlinearly at $\Delta\Psi_m$ above 200 mV. Thus, ATP production was not completely coupled to electron flow and the chemiosmotic theory in its current form was not valid³⁵. This was initially thought to be due to a phenomena described as “proton slip”, in which the electron transport chain complexes were not completely efficient and would accept an electron but not translocate a proton at high PMF^{36–38}. However, an alternative theory suggested that protons could passively leak back into the mitochondrial matrix independent of ATP synthase^{39–41}, and this theory, termed “proton leak”, was quickly favored due to the irreproducibility of primary experiments supporting proton slip^{42,43}.

Protons that reenter the matrix through ATP synthase are said to be “coupled” to ATP production, while electron flow and proton translocation that occurs independent of ATP synthase are described as “uncoupled” because the potential energy used to move the proton into the matrix is not contributing to ATP production^{1,26,44}. Proton leak accounts for 20-30% of respiration in hepatocytes⁴², approximately half of skeletal muscle respiration and is estimated to account for 20-25% of the whole body basal metabolic rate^{34,45}.

Mitochondria have endogenous uncoupling mechanisms known as uncoupling proteins (UCPs), which allow for the passive diffusion of protons into the matrix. UCPs

contribute to proton leak by acting as dimerized proton channels in the mitochondrial inner membrane⁴⁶. There are five known UCP proteins designated UCP1-5. The first UCP to be discovered was UCP1, which is almost exclusively found in brown adipose tissue where it makes up 8% of total mitochondrial protein¹. UCP1's primary function in the production of heat by thermogenesis, as illustrated by the fact that UCP1 is activated by the sympathetic nervous system⁴⁷ and mediates nonshivering thermogenesis and in response to cold exposure in mice^{48,49} and penguins⁵⁰. UCP2 and UCP3 were designated as uncoupling proteins due to protein homology and close amino acid sequence identity. UCP2 and UCP3 are 56-57% identical to UCP1^{51,52}. UCP2⁵³ and UCP4^{54,55} have also been shown to be upregulated in response to cold exposure.

Fatty acids (FAs) are required for UCP1 activation⁵⁶⁻⁵⁹, and the mechanism by which FAs activate UCP1 has been debated since its discovery. FAs were first thought to activate UCP1 through allosteric modulation, which would increase proton channel conductance. A second theory suggests that FAs act as proton donors and acceptors within the channel with or without the aid of aspartate and glutamate residues⁵⁹. A third and most recent theory involves UCP1 not directly transporting protons at all, but transporting protonophoric FAs⁶⁰. At the outer surface anionic fatty acids are protonated and the neutral molecules are flipped inside. The net result is proton flux into the mitochondrial matrix independent of ATP synthesis⁶¹⁻⁶⁴. This may occur via "flip-flop" mechanism by which protonated FAs translocate their protonated head group back and forth from the inner membrane space into the matrix within the UCP1 dimer⁶³. Further studies have suggested that UCP1 transports membrane-impermeable anionic FAs out of the mitochondrial matrix where they can protonate and diffuse back across the

mitochondrial inner membrane⁶⁰. UCP2⁶⁵ and UCP3⁶⁶⁻⁶⁹ also transport FAs, and UCP2 demonstrates FA-mediated proton conductance in a manner thought to be analogous to UCP1⁶⁵. In sum, it is suggested that the function of UCPs is to act as a catalyst to decrease the potential energy required for either FA translocation or ‘flip-flopping’ across or in the mitochondrial inner membrane⁶⁹.

Another method of proton leak is the adenine nucleotide translocase (ANT), a protein that resembles a pore that, when open, allows for the passive diffusion of protons, other ions, and larger macromolecules into the mitochondrial matrix³⁴. It is estimated that two thirds of basal proton conductance in mitochondria is dependent on ANT, and this conductance is independent of ATP/ADP or fatty acid exchange³⁴. Although ANT can increase basal proton conductance of mitochondria independent of FAs³⁴, ANT-mediated respiration can be activated by FAs such as palmitate⁷⁰, which can complicate the studies of UCP-mediated proton conductance in isolated mitochondria⁷¹.

Outside of these proteins, proton leak can also be induced pharmacologically by small molecule mitochondrial uncouplers. Uncouplers act as protonophores which allow for a reduction in PMF and increased energy expenditure in a dose dependent manner. They are commonly used to better understand the role of PMF and to identify defects in mitochondrial respiration²⁶.

1.1.5 Methods of assessing mitochondrial respiratory dysfunction in whole cells

Mitochondrial function in whole cells is determined by measuring mitochondrial respiration and cellular glycolysis simultaneously. Electrons are added to molecular oxygen at complex IV, which allows the O₂ consumption rate (OCR) to be a measure of electron flow⁷². The caveat to this approach is that is not clear as to how these electrons

are contributing to ATP synthesis or if the basal level of electron flow represents the maximal rate²⁶. These questions can be answered by manipulating mitochondria in whole cells to obtain various attributes of mitochondrial bioenergetics that allow for the assessment of mitochondrial function within the context of the cellular environment. There are several important readouts of mitochondrial function that are used to determine mitochondrial health such as basal respiration, ATP-linked respiration, maximal respiration, reserve capacity⁷³, proton leak, coupling efficiency (CE), and respiratory control ratio (RCR). These can be determined by a mitochondrial ‘stress test’ in whole cells, which involves measuring OCR following the sequential addition of oligomycin and a small molecule uncoupler. Following respiratory measurements in whole cells, the electron transport chain inhibitors rotenone and antimycin A²⁶ are added to deplete mitochondrial respiration. Non-mitochondrial respiration is subtracted from all respiratory measurements (**Figure 3**).

Basal respiration, commonly known as *State 3* respiration, is not an accurate indication of mitochondrial function because it does not take into account how protons are being utilized. Once protons are pumped out of the matrix they can reenter via ATP synthase or uncoupled respiration to complete the circuit, the latter of the two referred to as proton leak. Because of this, the relative fluxes of protons through ATP synthase and uncoupled routes can be determined by inhibiting ATP synthase with oligomycin, which removes ATP-dependent respiration and induces a respiration state known as *State 4_o*. The mitochondrial respiration that still occurs is due to endogenous uncoupling, and is not being used for the generation of ATP.

These two respiration rates can be used to calculate Coupling Efficiency (CE) which is the ratio of ATP-linked respiration to basal respiration. This value ranges between 0-1 with 1 being 100% of electron flow being utilized for ATP production. This allows for determination of how efficient mitochondria are at synthesizing ATP without the confounding variables that can affect the basal respiration rate. Following the addition of oligomycin, a mitochondrial uncoupler is added, which decreases PMF and induces the maximal rate of mitochondrial respiration, known as State 3_u. This can be determined in the absence of ATP synthase activity because nearly all respiration will be uncoupled. The maximal respiration rate alone is not informative and is affected by many of the confounding variables that affect the basal respiration rate, so this value is analyzed relative to the State 3 and State 4_o respiration rate. The difference between State 3 and State 3_u respiration is known as 'reserve capacity' which is the measure of mitochondria to respond to increased ATP demand or metabolic stress^{73,74}. Reserve capacity is depleted during oxidative stress⁷⁵, and loss of reserve capacity also leads to decreased ability of a cell to respond to cytotoxic insults⁷⁶. The respiratory control ratio (RCR), is the ratio between State 3_u/State4_o. The respiratory control ratio is a very valuable tool, because it takes into account changes in uncoupling and the maximal respiration rate. In short, if mitochondria are dysfunctional from a respiration standpoint RCR will decrease²⁶.

When measuring mitochondrial function in whole cells, glycolytic metabolism is often monitored simultaneously by measuring the rate of extracellular acidification (ECAR). The rate of pH change in the extracellular environment is dependent upon proton and CO₂ efflux from the cell and the buffer capacity of the medium. CO₂ can be produced by the TCA cycle and to a lesser extent (10% of oxidized glucose) the pentose

phosphate pathway^{77,78}. CO₂ can influence extracellular pH because it is a weak acid that can react with carbonate to form bicarbonate and H⁺. For this reason, assays that measure ECAR as a measure of glycolytic flux are performed in the absence of bicarbonate⁷⁹. Since CO₂ has low solubility in water (30μM/torr), it is forced into the atmosphere in the absence of buffering and does not have a significant effect on ECAR⁷⁹.

While almost all metabolic pathways produce protons, including glucose used for respiration, glutamine-dependent respiration, pyruvate-dependent respiration, and fatty acid oxidation, glycolysis produces one proton per molecule of ATP. In comparison, pyruvate dependent respiration produces 0.13 H⁺ per ATP, glutamine respiration produces 0.11 H⁺ per ATP, fatty acid oxidation/respiration produces 0.13 H⁺ per ATP, and glucose-dependent respiration produces 0.17 H⁺ per ATP. These non-glycolytic pathways can be largely taken into consideration by monitoring mitochondrial OCR and ECAR simultaneously. If ECAR increases relative to OCR, it is likely that the cell is more glycolytic. While a high rate of ECAR does not necessarily indicate that the cell is glycolytic due to the ability of aerobic respiration to generate protons, it is an imperfect yet comparable method to measure glycolysis as it generates similar values compared to radioactive tracers⁷⁸⁻⁸⁰.

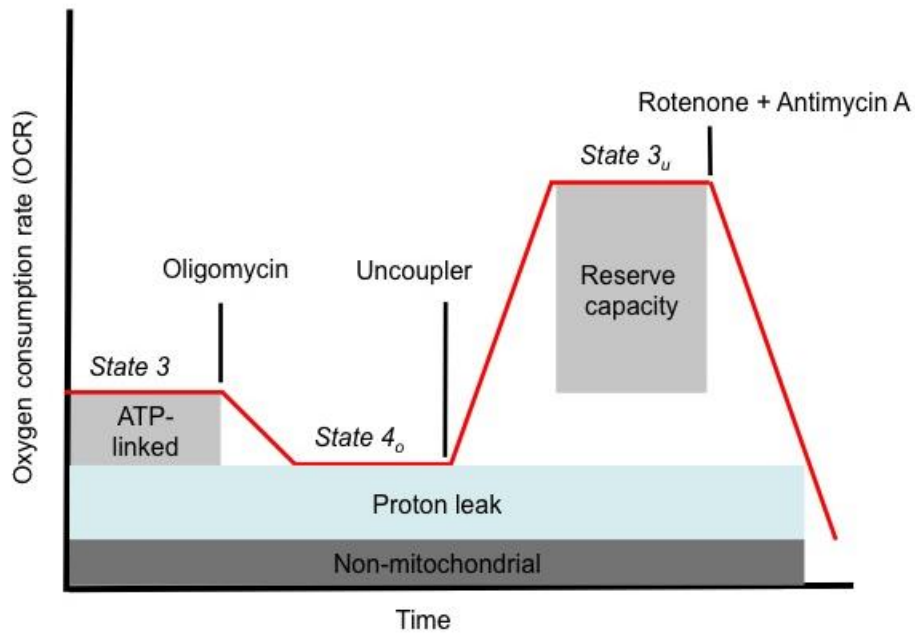


Figure 3: Mitochondrial bioenergetics analysis in whole cells.

Cells begin in State 3 (basal) respiration and are sequentially treated with the ATP synthase inhibitor oligomycin, a mitochondrial uncoupler, and the Complex I and III inhibitors Rotenone and Antimycin A. Coupling efficiency (CE) = ATP-linked/State 3. Respiratory control ratio (RCR) = State 3_u/State 4_o.

1.2 Reactive oxygen species

1.2.1 Overview of reactive oxygen species

As PMF increases, electron flow through the ETC decreases. When PMF increases electrons begin to become exposed to the outside environment, and can be transferred to O_2 to form superoxide (O_2^-). Because of this, PMF must stay within a range that is high enough to allow for sufficient ATP production but low enough to allow for optimal electron flow^{81,82}.

O_2^- production can occur via complexes I, II, and III^{83,84}. Complexes I⁸⁵⁻⁸⁸ and II^{84,89} produce O_2^- to the matrix side of the mitochondria, while complex III can produce O_2^- to both the matrix⁹⁰ and intermembrane space^{85,91}. O_2^- can be reduced to H_2O_2 by superoxide dismutase and spontaneous disproportionation^{92,93}. O_2^- can also oxidize iron-sulfur groups in proteins such as aconitase and fumerase⁹⁴⁻⁹⁶ to form an unstable intermediate which releases Fe(II). Fe(II) can then react with H_2O_2 to form $^{\cdot}OH$, one of the most powerful oxidants in nature⁹⁷. To guard against excessive H_2O_2 production, H_2O_2 can be detoxified by catalase⁹⁸, glutathione peroxidase⁹⁹, or thioredoxin¹⁰⁰ to form water.

Once formed, free radicals can oxidize proteins and lipids. The reaction of free radicals with proteins can form carbonyls and other amino acid modifications such as methionine sulfoxide, valine hydroxides, 2-oxohistadine, protein peroxides, hydroxylation of tyrosine, and conversion of tryptophan to formylkynurenine¹⁰¹. Metal-catalyzed oxidation of proteins is one of the most common protein oxidation methods and occurs when H_2O_2 reacts with metal ion groups within proteins, such as the heme in

NADH oxidase, to form a hydroxyl radical which can then oxidize amino acids near the catalytic site^{102,103}. Protein oxidation is involved in numerous diseases^{103–106} including ischemia-reperfusion injury^{107,108}, in which heme-containing proteins involved in the TCA cycle and electron flow such as aconitase and succinate dehydrogenase can be oxidized and inhibited¹⁰². This can not only decrease ATP production but can cause an accumulation of metabolic intermediates which can increase ROS production, thus initiating a self-amplifying cascade¹⁰⁹.

Free radical-mediated lipid peroxidation occurs via an autoxidation reaction that is predominantly initiated by $\cdot\text{OH}$, and to a lesser extent by $\text{O}_2\cdot^-$ via the reduction of metal ions. This forms a lipid radical that can undergo a variety of propagation reactions to form multiple lipid peroxy radicals¹¹⁰. The nature of these propagation reactions allow for one free radical to induce the formation of many lipid peroxides^{111,112} prior to detoxification. Furthermore, chain propagation by peroxidized lipids occurs independent of the chain-initiating radical¹¹². Lipid peroxidation can disturb the integrity of lipid bilayers and have a myriad of negative biological consequences¹¹² including apoptosis^{113–115}.

To protect from the consequences of high PMF, UCPs 1-3 are activated by $\text{O}_2\cdot^-$ ^{116,117} and ANT can be activated by peroxidized phospholipids¹¹⁸. When ROS are produced UCPs are activated, PMF is lowered, and ROS production is decreased¹¹⁹. Upregulation of UCP1¹²⁰, UCP2^{116,121,122}, UCP3^{123–125}, and UCP4^{54,55} decreases ROS production. Furthermore, mice lacking UCP1¹²⁶ or UCP2¹²⁷ demonstrate increased oxidative stress, and knocking down UCP5 increases ROS production¹²⁸. Thus,

mitochondrial uncoupling can lower PMF and reduce the formation and consequences of O_2^- .

Identification of the sites of O_2^- production and the effects of PMF are largely performed in isolated mitochondria, submitochondrial particles, and isolated ETC complexes. These are used in combination with small molecule inhibitors of specific sites of each ETC complex that allow for a determination of site-specific O_2^- production.

Production of O_2^- in isolated mitochondria is difficult to measure because O_2^- has a very short half-life and cannot pass through the mitochondrial inner membrane. For this reason, cardiac mitochondria are often used because they contain superoxide dismutase but not catalase, which allows the measurement of H_2O_2 as a measure of O_2^- formation in solution^{86,89}. Submitochondrial particles and isolated ETC complexes coupled with MCLA- O_2^- adduct^{89,129} to directly measure O_2^- are also used.

1.2.2 Mitochondrial O_2^- production from complex I

The formation of O_2^- by complex I is thermodynamically favorable and is primarily determined by the concentration of O_2 ¹³⁰ and the proportion of electron carriers that are reactive with O_2 to form O_2^- ⁸². Reduction of O_2 occurs by an outer-sphere mechanism, which requires O_2 and an electron to be in close proximity. To prevent this, electrons are shielded in the ETC from O_2 . However, there are pockets within O_2^- -producing proteins that are accessible by O_2 and allow the reaction to occur¹³¹. Thus, the reactivity of an electron is determined if electrons are freely available to react with O_2 , which occurs if electrons are bound at the periphery of electron-carrying proteins that are not protected^{82,131}. Thus, O_2^- formation increases when the time electrons are exposed to O_2 increases. This can occur when either transfer is increased or electron release from

unprotected regions of the ETC proteins is decreased. When PMF increases, electron flow decreases and occupancy time for electrons in peripheral parts of ETC proteins increases. This increases the probability that an electron will react with O_2 , thus increasing O_2^- production^{82,97}.

Complex I pumps two protons per electron across the mitochondrial inner membrane¹³², which results in complex I accounting for up to 40% of ETC proton translocation¹³³. The crystal structure of complex I was elucidated in early 2013¹³⁴, and is one of the largest known membrane proteins consisting of 14 core subunits used for translocating protons and 31 peripheral subunits that protect and stabilize the hydrophilic core¹³⁵ for a total of 45 different subunits¹³⁶. The entire complex yields a molecular weight of 980 kDa¹³⁷. The electron carriers in complex I are a flavin, six iron-sulfur centers, and an unknown number of semiquinones. The peripheral arm of complex I, known as the NADH dehydrogenase fragment, contains a flavin mononucleotide (FMN) which oxidizes NADH and accepts two electrons. These electrons are transferred individually along a 95Å chain of seven Fe-S clusters²⁰ to the quinone binding site (Q site) and eventually to ubiquinone to form ubiquinol (**Figure 4 A**). The Q site is connected to the membrane-spanning portion of the protein responsible for proton translocation, which consists of four antiporter-like proton channels. The structure of complex I suggests that proton translocation from electron transfer occurs via long-range conformational changes¹³⁴.

Deducing the ability of complex I to produce O_2^- involves pharmacological inhibition of complex I-mediated electron transfer. Potent complex I inhibitors have structural similarity to ubiquinone such that they have a similar cyclic head group to

ubiquinone coupled to a hydrophobic tail¹³⁸. The most common complex I inhibitor, Rotenone, is an isoflavonoid extracted from *Leguminosae* plants¹³⁸ that binds near but not directly to¹³⁹ the ubiquinone binding site of complex I to prevent electron transfer¹⁴⁰ (**Figure 4 A**). Thus, in the presence of Rotenone electron transfer to ubiquinone is blocked but the Fe-S centers and the FML group on complex I can be fully reduced¹⁴¹ and are more likely to donate electrons to O₂. Rotenone treatment in isolated mitochondria¹⁴², submitochondrial particles^{86,143}, and purified complex I¹⁴⁴ utilizing complex I substrates produce higher levels of ROS.

In physiological conditions, complex I-mediated O₂⁻ generation that is enhanced in the presence of Rotenone is determined by the NADH/NAD⁺ ratio. If electron flow is inhibited, NADH concentrations increase, which increases the proportion of reduced complex I FMN groups and the formation of O₂⁻ (**Figure 4 A-B**)^{81,82}. Under these conditions the addition of Rotenone increases O₂⁻ production further due to electrons being unable to release from the FMN group. Thus, inhibition of electron flow downstream of the Q site (such as complex III)¹⁴⁵ or increased PMF will cause O₂⁻ formation from complex I^{82,130,146}. Importantly, decreasing PMF can normalize the NADH/NAD⁺ ratio, which decreases O₂⁻ production¹⁴⁷.

Mitochondrial complex I is reversible¹⁴⁸ and can also form O₂⁻ by reverse electron transfer (RET) as PMF increases⁸¹ (**Figure 4 C**). Succinate can be used to study RET because it can rapidly feed electrons to the ubiquinone pool after being oxidized by succinate dehydrogenase/complex II⁸⁴. Unlike O₂⁻ produced during forward electron transfer, O₂⁻ formation utilizing succinate oxidation is greatly inhibited by Rotenone, which suggests that succinate oxidation contributes to O₂⁻ formation by RET to complex

I^{84,85,142,149}. Similar to forward electron transfer, the formation of O₂⁻ by RET to complex I can also be ameliorated by mitochondrial uncoupling¹⁴⁹, as lowering $\Delta\Psi_m$ can increase ubiquinol oxidation and thus decrease reverse electron supply to complex I¹⁴⁷. Thus, decreasing PMF by mitochondrial uncoupling can decrease ROS production in the forward direction by reducing electron occupancy time in peripheral parts of the protein complex and by oxidizing ubiquinol to reduce RET.

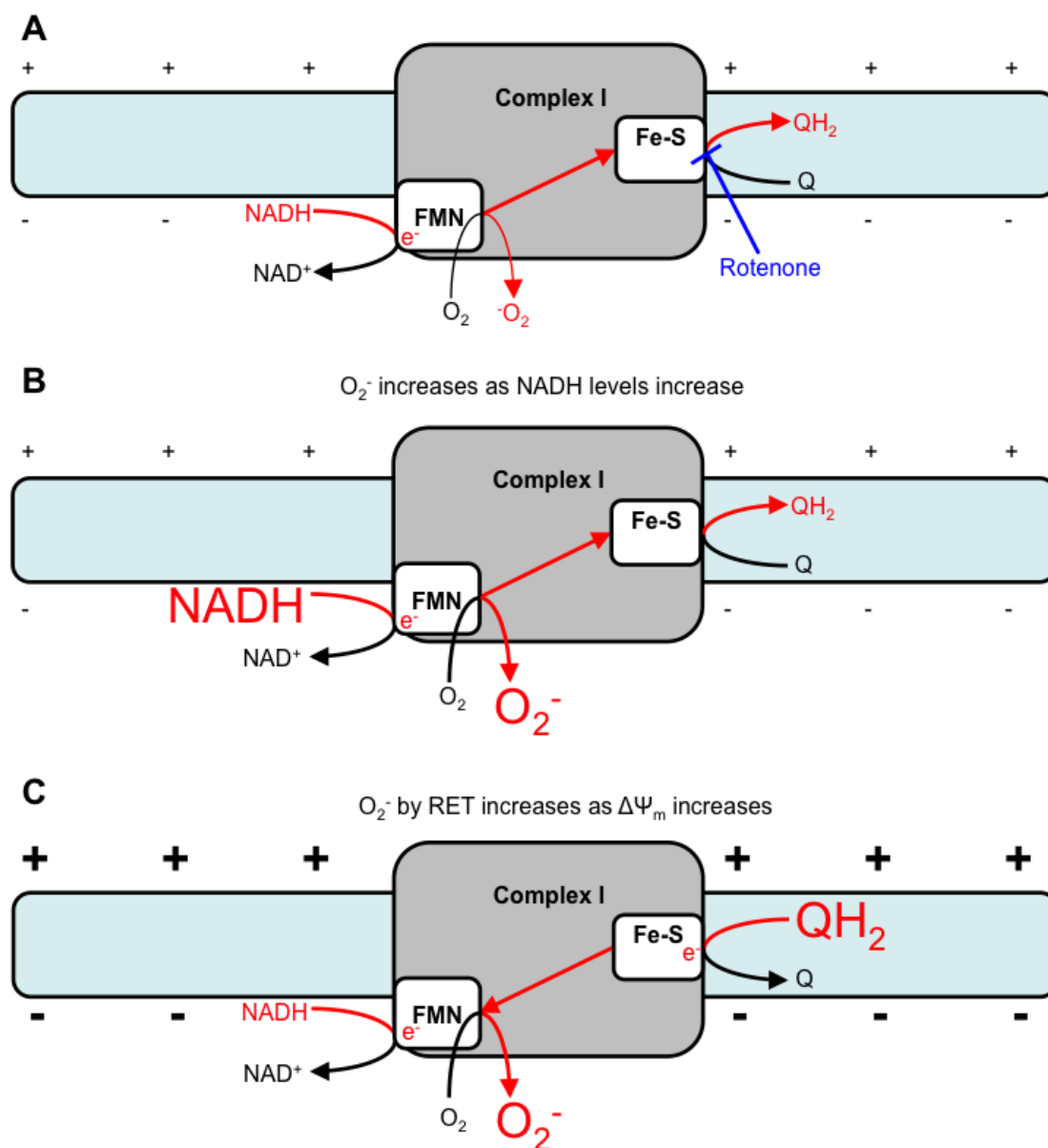


Figure 4: Complex I can generate O_2^- in the forward and reverse direction into the mitochondrial matrix.

A: O_2^- can be generated from the FMN group in the forward direction at the FMN site.

Rotenone inhibits the Q binding site. B: ROS production is increases as NADH

concentrations increase. C: O_2^- production from RET increases as the concentration of ubiquinol (QH_2) increases. This can be caused by hyperpolarization of the mitochondrial inner membrane. Red arrows indicate electron flow.

1.2.3 Mitochondrial O_2^- production by complex II

Complex II consists of four subunits that oxidize succinate to fumarate in the mitochondrial matrix and reduce ubiquinone (**Figure 5 A**). Subunit A contains an FMN group and bound FAD^+ . Subunit B contains a chain of Fe-S clusters, and Subunits C and D are cytochrome b-containing hydrophobic subunits⁸⁴. Following succinate oxidation, the electrons from this reaction are placed on the FMN group that contains covalently bound FAD^+ at site II_F ⁸⁴ and shuttled through the various redox Fe-S clusters until they are used to reduce ubiquinone to ubiquinol at site II_Q in the mitochondrial inner membrane^{84,150}. Electrons do not need to pass through the hemes in Subunits C and D because the proximity between the Fe-S centers and ubiquinone at site II_Q allows for electron tunneling^{84,151}.

Site II_F was recently discovered to generate O_2^- both the forward direction in which electrons are supplied by succinate to FAD^+ and RET from the ubiquinol pool (**Figure 5 B**). This is evidenced by the fact that mitochondria respiring on succinate can generate O_2^- when complexes I and III are inhibited. The addition of atpenin, which inhibits site II_F (**Figure 5 A**), reduces O_2^- formation under these conditions. This is also true if the ubiquinone/ubiquinol pool is fully reduced by the addition of glycerol-3-phosphate (G3P), which is oxidized by G3P dehydrogenase and reduces the ubiquinone/ubiquinol pool. If G3P is added as a substrate when complexes I and III are inhibited the only electron source is from the ubiquinol pool generated by G3P, and any O_2^- production that occurs must be via RET to complex II⁸⁴.

The physiological significance of O_2^- production from complex II is not clear, but it is likely that it is highly influenced by PMF due to the effects of RET. However, because complex II generates the most O_2^- when succinate concentrations are low, it is hypothesized that complex II may be a source of O_2^- during ischemia. In this scenario electron transfer occurs at low rates and the ubiquinone pool demonstrates reduced oxidation⁸⁴.

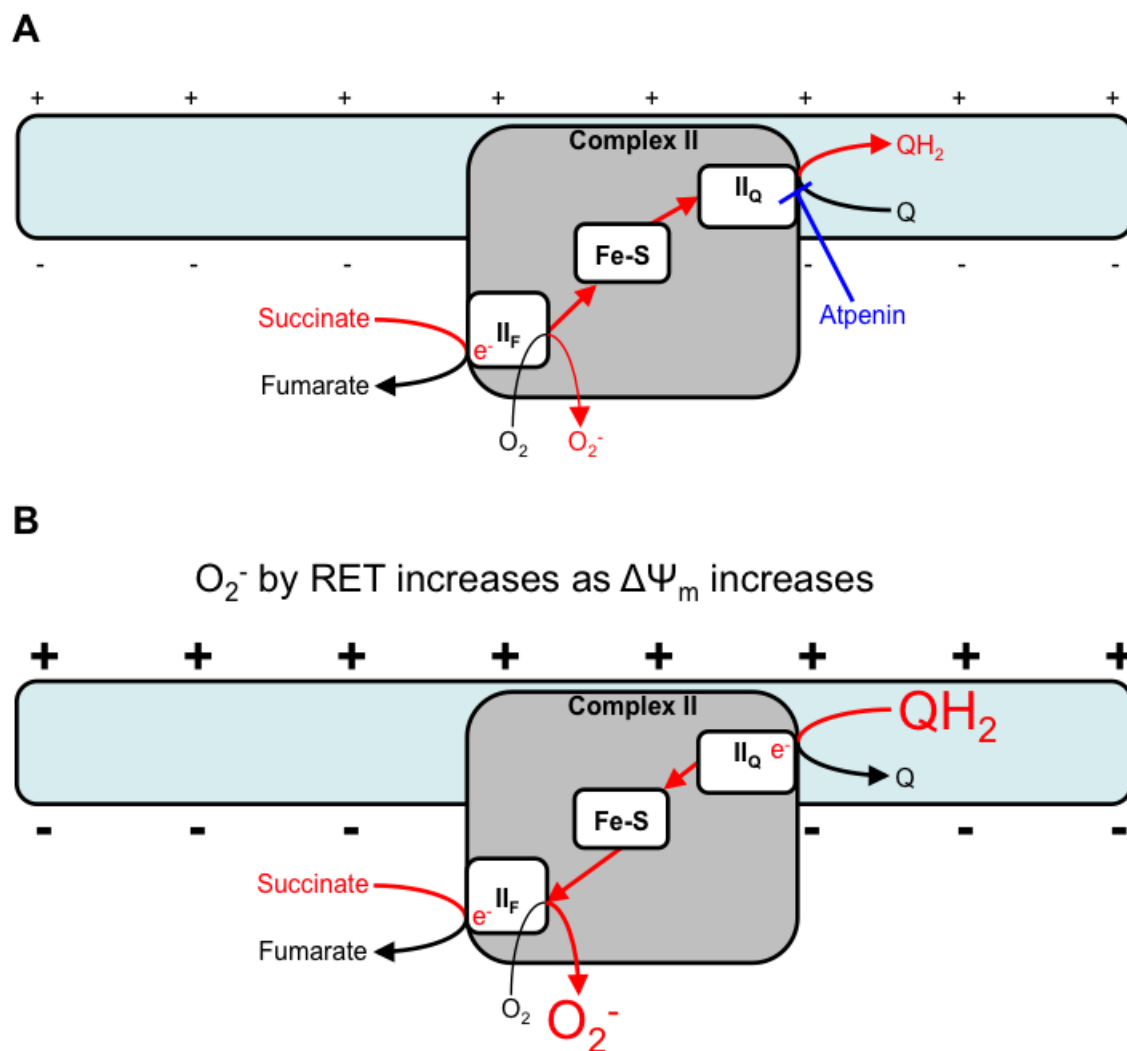


Figure 5: Complex II can generate O_2^- into the matrix in the forward and reverse direction.

A: Complex II generates ROS at the flavin site of Complex II (II_F). B: Complex II generates O_2^- in the reverse direction as ubiquinol concentrations increase relative to ubiquinone. Atpenin inhibits site II_Q . B: Increased ubiquinol concentrations can be caused by mitochondrial hyperpolarization. Red arrows indicate electron flow.

1.2.4 Mitochondrial O_2^- formation by complex III

The generation of O_2^- by complex III is dependent on the delivery of electrons, which occurs by a ubiquinol/ubiquinone cycling mechanism^{44,152} (**Figure 6 A**). Ubiquinol releases one electron to the ubiquinone oxidation site (Q_o) which lies in the intermembrane space¹⁵³. This forms ubisemiquinone and allows for electrons to travel to the Fe-S center to cytochrome c, and eventually complex IV, where two electrons reduce O_2 to form H_2O . Ubisemiquinone then translocates to¹⁵⁴ and donates its second electron to site b_L (cytochrome b566, low potential heme) in the matrix. The electron then travels to site b_H (cytochrome b562, high potential heme)^{153,155} in the mitochondrial inner membrane, to the second ubiquinone reduction site (Q_i) in the matrix¹⁵³. When an electron is in Q_i it can re-reduce ubiquinone one electron at a time, first generating semiquinone and then ubiquinol, thus completing a cycle^{152,156}.

ROS production by complex III is primarily investigated utilizing the complex III inhibitor Antimycin A^{157,158}. Antimycin A was first isolated as a fungicide¹⁵⁹, and inhibits Q_i ¹⁶⁰ without inhibiting other hemes¹⁵⁷. The general chemical structure is an acyl-and alkylsubstituted dilactone ring linked to 3-formamidosalicylic acid via an amide bond, however Antimycin A is a mixture of four different compounds: Antimycin A₁, A₂, A₃, and A₄. Antimycin A is purchased as a mixture of these four compounds, thus the name 'Antimycin A' does not indicate a specific molecule¹⁵⁹.

Antimycin A can increase O_2^- production by binding to the Q_i site, which blocks electron release from the *b* hemes. This decreases ubiquinol oxidation¹⁶¹, which can cause ROS production from complexes I and II by RET. However, complex III can also generate O_2^- via the ubiquinone/ubiquinol pool, and the redox state of the

ubiquinone/ubiquinol pool plays a major role in complex III-mediated O_2^- production^{143,162} at the Q_o site^{163,164}. O_2^- production at the Q_o site is evidenced by the fact that Antimycin A increases O_2^- production on mitochondria respiring on pyruvate/malate or succinate. However, Antimycin A-mediated ROS production is blocked by inhibition of Q_o with myxothiazole and stigmatellin^{145,153,156,165–167}. Complex III can also generate O_2^- at the Q_i site¹⁶⁴.

In addition to a classical forward mechanism, the bulk of complex III-mediated O_2^- production is likely to occur by a mechanism in which semiubiquinone acts as catalyst to shuttle electrons from Q_o ¹⁶⁸ heme b_L to O_2 ^{153,166} (**Figure 6 A**). When ubiquinone and ubiquinol are titrated, O_2^- production increases in isolated mitochondria and purified complex III as the relative amount of ubiquinone compared to ubiquinol increases¹⁶⁶. However, complex III-mediated O_2^- production increases with increasing PMF as long as the ubiquinone/ubiquinol pool is partially oxidized (containing approximately 25% ubiquinone and 75% ubiquinol) (**Figure 6 B**). It is hypothesized that this allows organs such as the lung, brain and heart, where the ubiquinone/ubiquinol pool is normally oxidized, to increase O_2^- production upon small decreases in oxygen that decrease ubiquinol oxidation¹⁶⁶. The dependence of O_2^- production on the oxidation state

of the ubiquinone/ubiquinol pool is significant, because unlike complex I in which increases in $[O_2]$ can increase O_2^- production, the rate-limiting step in O_2^- production in complex III is the oxidation state of the ubiquinone/ubiquinol pool. This is further evidenced by the fact that large increases in O_2 concentrations only lead to modest increases in O_2^- production from complex III¹⁵⁶.

Similar to complexes I and II, PMF has been demonstrated to have direct impact on O_2^- production from complex III via mechanisms in addition to the redox state of the ubiquinone/ubiquinol pool. O_2^- production from isolated complex III has been shown to increase as $\Delta\Psi_m$ increases¹⁶⁹. As PMF increases, electron flow from heme b_L to heme b_H decreases, which promotes a reduced state of heme b_L and increases O_2^- production^{153,169}. Reduction of PMF under these conditions would increase electron flow to site b_H while simultaneously decreasing ubiquinol concentrations, which would decrease O_2^- production.

In sum, O_2^- can be generated from complexes I, II, and III. Increases in PMF can increase O_2^- production from all of these complexes by increasing the availability of electrons to react with O_2 , increasing RET to complexes I and II by reduction of the ubiquinone/ubiquinol pool, and increasing O_2^- production from site b_L . From a therapeutic standpoint, pathological conditions in which PMF is too high, such as ischemia-reperfusion injury may benefit from therapies that decrease PMF by reducing O_2^- production.

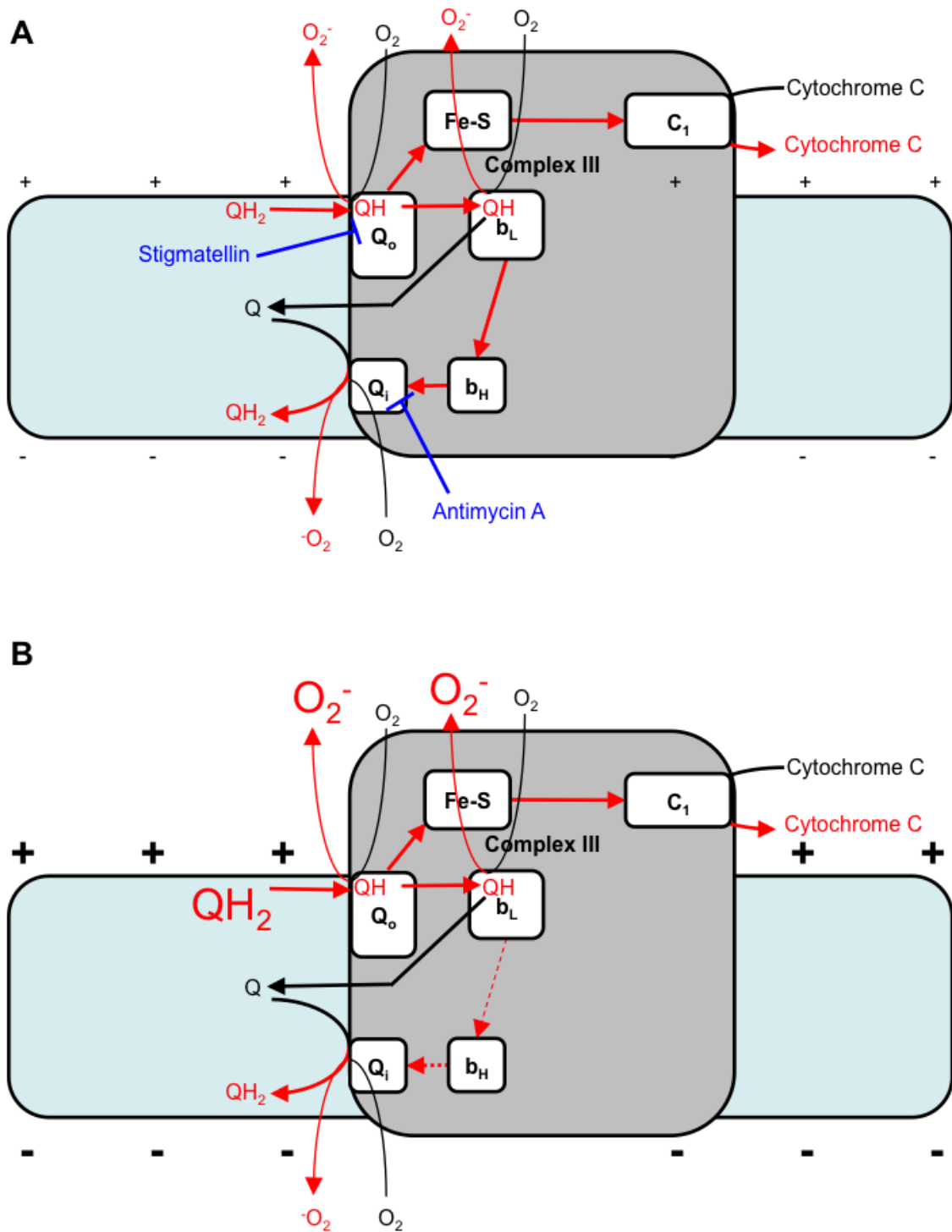


Figure 6: Complex III generates O_2^- into the mitochondrial matrix and intermembrane space.

A: Ubiquinol (QH₂) is oxidized to semiubiquinone (QH) at site Q_o. Semiubiquinone then travels to site b_L and donates another electron. Electrons from Q_o can travel to the Fe-S center to cytochrome C, while electrons at site b_L are then to sites b_H and Q_i, where electrons are added individually to Q to form QH and then QH₂. O₂⁻ can be produced in the matrix from site Q_i and in the intermembrane space at sites b_L and Q_o. O₂⁻ from sites b_L and Q_o requires QH as a mediator of electron transfer. Antimycin A inhibits site Q_i and stigmatellin inhibits site Q_o. B: PMF increases QH₂ concentrations which can increase ROS production from sites b_L and Q_o. Red arrows indicate electron flow.

1.3 Renal Ischemia-reperfusion injury

1.3.1 Overview of renal Ischemia-reperfusion injury

Renal IRI is a serious clinical problem associated with increased morbidity and mortality compared to patients that do not experience renal IRI¹⁷⁰, and is characterized by potentially reversible kidney failure in time duration of a few hours or days. Renal IRI can occur due a decrease in blood pressure, renal artery thrombosis, embolism, or atherosclerosis^{171–173}. It is the primary cause of renal failure in surgeries that require clamping of the renal arteries such as in kidney transplants and cardiac surgery^{174–176}.

Approximately 5.7% of all patients admitted to the intensive care unit^{170,177} and 31% of patients undergoing cardiac surgery¹⁷⁷ will suffer from renal IRI and although only 1-2% will develop full renal failure, the mortality rate is greater than 50%. Patients that experience renal IRI have a post-operative mortality of 63.7% compared to 4.3% of patients without renal IRI, however when other factors involved with increased risk of mortality from cardiac surgery are taken into account it is estimated that approximately 8% of these patients will have postoperative complications directly due to renal IRI, which can include death¹⁷⁷.

Renal IRI causes kidney damage by inducing apoptosis and acute tubular necrosis (ATN). ATN is much more prominent than apoptosis in the post-ischemic kidney due to the ATP requirements of the apoptotic machinery¹⁷⁸. Apoptosis is a mitochondria-dependent signaling pathway which activates a process known as phagocytic clearance^{179,180}. After the cell is broken down by caspases¹⁸¹ a signal is released to neighboring immune cells¹⁸² which promotes the phagocytic clearance of the apoptotic

cell within four hours by macrophages^{182,183}. This process also promotes the proliferation of fibroblasts, epithelial cells, and proximal tubule cells for kidney repair¹⁸⁴⁻¹⁸⁶.

After epithelial proliferation is initiated epithelial precursor cells form in the ischemic area. These cells are flattened and can be seen as a poorly differentiated brush border¹⁸⁵. If the cells recover from the ischemic event these events will resolve and renal function will be normalized¹⁸⁷. Importantly, unlike necrosis, this process suppresses inflammation in surrounding tissues^{181,188} and while it initiates a localized immune response does not cause the long-term surge of immune cells that are associated with ATN^{178,189}.

During the ischemic period, the majority of detrimental effects occur due to ATP depletion in the renal medulla. The renal medulla is highly prone to damage from ischemia because the oxygen concentration is relatively low (5-20 mmHg)¹⁹⁰. The ATP depletion that occurs due to ischemia causes ionic dysregulation due to the inability to maintain transmembrane pumps¹⁹¹⁻¹⁹³, global dephosphorylation¹⁹⁴, and protein aggregation¹⁹⁵ which leads to cellular necrosis¹⁹³. Ischemia in this area also leads to tubular obstruction and backleak which reduces the glomerular filtration rate (GFR) and causes acute renal failure^{196,197}.

One of the major contributors to the pathogenesis of renal IRI is insufficient reperfusion, which can extend the ischemic period and cause necrosis in cells that are unable to regenerate sufficient amounts of ATP¹⁹⁸. Similar to ischemia, the most affected part of the kidney by insufficient reperfusion is the renal medulla. Not only does this area have a high oxygen demand of the tubule segments utilized for glomerular filtration, but there are small blood vessels that are prone to occlusion due to their high density¹⁹⁹⁻²⁰¹

and unique anatomy that renders each nephron dependent on blood from other nephrons^{202,203}. This allows for drastic reduction in nutrient and oxygen delivery and damage particularly in parts of the proximal tubule that cannot convert to glycolytic metabolism to make ATP^{202,204}. Thus, the balance between oxygen delivery and demand is highly influenced by medullary blood flow²⁰⁵.

Decreased ATP concentration causes an influx of calcium and activation of phospholipase A2, degradation of arachidonic acid, and the formation of inflammatory mediators such as leukotrienes and prostaglandins. This results in chemotaxis of leukocytes into the ischemic area^{191,192}, which has been shown to contribute to the pathogenesis of renal IRI^{201,206}. The inflammatory response damages vasculature, which can extend the ischemic period even if the kidney is technically perfused. Because of this, oxygen delivery can be impaired to the medulla despite restoration of blood flow following reperfusion, which can cause further injury^{200,207}. Increased leukocyte-endothelial adhesive interactions, activation of coagulation pathways, and endothelial swelling can all increase ischemia²⁰⁷. Activation and injury of endothelial cells leads to the upregulation of adhesion molecules and endothelial swelling. This combination leads to increased permeability of the endothelial cell barrier, which increases the interaction between leukocytes and platelets. The combination of leukocyte occlusion of small blood vessels and endothelial swelling obstructs blood flow to the medulla after reperfusion and extends the ischemic period^{187,207,208}.

Dendritic cells, macrophages, and neutrophils are the most common leukocytes¹⁹¹ and are thought to be involved in renal IRI^{190,191,209}. The presence of neutrophils and macrophages (innate immune system) following reperfusion indicate pathogenesis^{190,209}.

Neutrophil and macrophage infiltration peaks at 24-48 hours following reperfusion and maintains elevated concentrations for approximately six days²¹⁰. Dendritic cells and macrophages both recruit neutrophil infiltration, which leads to increased tissue damage²¹⁰.

Neutrophils are considered the most important immune cell with regards to inflammatory pathogenesis, and are the predominant cells in the first 6 to 24 hours in acute inflammation¹⁹¹. Coagulation of neutrophils compromises the vasculature and contributes to tissue injury²¹¹. Neutrophils attach to the endothelium and accumulate in the kidney in renal IRI^{210,212} in the capillary network of the medulla as early as 30 minutes after reperfusion. Neutrophils produce proteases, myeloperoxidase, ROS, and cytokines, which increases the activation of apoptotic pathways²¹³, decreases the integrity of endothelial cells, and aggravates kidney injury²¹⁰. Although some interventions have been shown to be protective without having any effect on neutrophil invasion^{206,214-216}, it is clear that they play a central role in the pathogenesis of renal IRI. Activation of neutrophils can exacerbate the pathological effects of renal IRI²¹⁷ and inhibition of neutrophils with antibodies²¹⁸, pharmacological interventions that decrease neutrophils²¹⁹, blockade of neutrophil adhesion to the endothelium, and inhibition of the complement system all decrease renal damage caused by IRI^{210,218,220-223}.

Macrophages and dendritic cells are also highly involved in the early immune response from renal IRI, and depletion of macrophages²²⁴⁻²²⁶ or dendritic cells¹⁹⁰ has shown protective effects. Dendritic cells and macrophages reside in the interstitial extracellular compartment and interact with signaling molecules that are shuttled from the lumen of the tubule into the surrounding vasculature^{190,227}. Following activation by

proinflammatory cytokines¹⁹⁰ dendritic cells and macrophages can potentiate the effects of IRI by recruiting neutrophils¹⁹⁰. Macrophages can also release matrix metalloproteases²²⁸, which exacerbates tissue injury by degrading matrix proteins¹⁹⁰.

1.3.2 Readouts of renal health

Renal function is typically measured using plasma creatinine concentrations, and is a prognostic indicator of mortality, length of stay, and cost of care in admitted hospital patients. Normal serum creatinine concentrations are normally less than 1.5 mg/dL^{229,230}, and even modest increases in serum creatinine above 0.5 mg/dL upon hospital admission is associated with a 6.5-fold increase in risk of death²³¹. Creatinine concentrations are also a prognostic indicator of kidney failure and mortality following cardiac surgery^{174,232,233}.

Despite clinical utility, creatinine concentrations are not an absolute measure of renal function because plasma creatinine concentrations reflect a composite of creatinine production, GFR, and the volume of distribution of creatinine itself. All of these can be drastically altered in renal IRI. Creatinine is excreted by glomerular filtration and tubular secretion, and as GFR decreases during renal IRI and lowers creatinine excretion to such an extent that creatinine clearance can overestimate GFR by 50-100%. Edema can also increase the volume of distribution of creatinine and dilute plasma creatinine concentrations^{234,235}. During renal IRI, the rates of creatinine generation rarely equal the rate of excretion, so plasma creatinine levels can change independent of GFR. The opposite can also be problematic, as GFR can quickly fall without causing significant changes in plasma creatinine because the change in flux between creatinine creation and filtration is small²³⁵. In summary, a variety of markers must be used to determine if renal

function has been disrupted or restored in addition to plasma creatinine to accurately determine the effects of a medical intervention on renal IRI.

ATN can be specifically identified by increased proliferation of proximal tubule and epithelial cells^{184,185}, brush border loss¹⁸⁵, vacuolization, and flattening and dilation of proximal tubules¹⁸⁷ with casts. When ATN occurs the distal tubules are occluded by casts which causes a condition known as cast nephropathy²³⁶. Casts are predominantly made up Tamm-Horsfall protein (THP), a protein that is synthesized and present in the thick ascending limb of kidney tubules^{184,237-240} and is the most abundant protein in urine^{241,242}. THP is normally secreted as a monomer into the urine, but can also become a gel-like polymer material^{243,244}. THP also acts as a ligand that binds neutrophils and potentially stabilizes their recruitment to increase the occlusion of tubules^{245,246}. Thus, cast appearance demonstrates tubular damage by apoptosis or necrosis²⁰².

1.3.3 Current treatments for renal IRI

There are no current effective pharmacological agents to treat renal IRI. Thus, the only treatment options available are dialysis and kidney transplantation¹⁷², and the risks associated with renal IRI have barely changed in the last 65 years^{172,235}. Treatment for renal IRI is limited due to medical interventions that do not take into account the etiology of the disease and are used indiscriminately based on empirical evidence²³⁵. However, a recent therapeutic target of renal IRI has been ROS detoxification. ROS can upregulate chemokine expression and activate immune cells. This causes upregulation of adhesion molecules²⁴⁷. When leukocytes are exposed to cytokines in the infarcted tissue they can become sequestered²⁰⁸ and enhance ROS production. This causes a positive feedback loop that increases ROS, inflammation, and vascular health²⁰¹.

Xanthine oxidase (XO) was long considered a primary producer of reactive oxygen species in ischemic conditions^{248,249}. Type D XO normally uses NAD⁺ as an electron acceptor to oxidize xanthine, but during hypoxic conditions type D XO is converted to type-O XO²⁵⁰, which uses oxygen as an electron acceptor instead of NAD⁺ and generates O₂⁻¹⁸⁷. This theory was further supported by the protective effects of the XO inhibitor allopurinol in hepatic^{251,252} and cardiac^{253,254} ischemia-reperfusion.

XO also appears to play an important role in chronic heart failure, in which XO expression is increased by over two-fold²⁵⁵. Allopurinol administration has been shown to be beneficial to human patients^{256,257} and dogs²⁵⁸ with chronic heart failure. However, acute and chronic allopurinol treatments have different effects. Both dosing regimens increase cardiac output, but only chronic allopurinol treatment has beneficial effects on left ventricular and diastolic pressure. Only acute allopurinol treatment lowers cardiac ROS as measured by electron spin resonance spectroscopy, but both treatments have no effect on lipid peroxidation. The differential effects of chronic versus acute treatment on ROS and cardiac function suggest that allopurinol may have alternative mechanisms that can contribute to improved cardiac function independent of cellular redox status²⁵⁹.

Furthermore, allopurinol treatment in these experiments was performed 8-18 weeks after ischemia, which suggests that allopurinol has effects independent of ROS-induced apoptosis and oxidative damage²⁵⁹. Because of these effects, the beneficial effects of allopurinol are now being attributed to its ability to lower plasma uric acid⁸¹, a recognized prognostic indicator of mortality in heart failure, via xanthine oxidase inhibition⁸². Allopurinol also is only protective against IRI if concentrations are used that

are far above the concentrations required to inhibit XO, which suggests that allopurinol may have protective effects independent of XO²⁶². In sum, XO is likely not the primary source of ROS from renal IRI.

Renal function is closely tied to oxidative phosphorylation. The kidney is less than 1% of total body weight yet consumes 10% of the whole body oxygen supply due to the high ATP demands of renal ion transport^{187,205}. Because of this, oxidant damage to mitochondria following reperfusion can lead to insufficient ATP generation to meet the ATP demands of rescuing the cell^{201,263}.

One of the most efficacious therapies for renal IRI in animal models is ischemic preconditioning. During IRI ROS production can increase by over six-fold^{264–268}. Because of this, ischemic preconditioning dramatically increases mitochondrial superoxide dismutase (MnSOD), which can detoxify ROS during IRI²⁶⁹. In support of the central role of ROS in preconditioning, administration of mitochondrial antioxidants during preconditioning ablates the benefits observed from preconditioning^{270–274}, and treatment with low doses of H₂O₂ in perfused hearts²⁷⁵ or O₂⁻ from xanthine and XO treatment in cardiomyocytes²⁷⁶ increase expression of MnSOD and protects against IRI²⁷⁵. This suggests that the central node of ischemic preconditioning is an upregulation of antioxidant defenses that can last as long as 12 weeks²⁶⁹.

In an attempt to recapitulate the effects of ischemic preconditioning, many experimental therapies in recent years have been focused on antioxidants. Mice overexpressing glutathione peroxidase are protected from renal IRI, and these mice demonstrate decreased neutrophil concentrations, chemokine expression, and tubular necrosis in the kidney following IRI²²¹. The effects of renal IRI can also be ameliorated

by antioxidant administration^{277,278}, but their effects on plasma creatinine levels^{277–279} are modest. Furthermore, when multiple antioxidant agents are combined the effects on serum creatinine and tubular necrosis are not additive²⁷⁸, which indicates that the administration of exogenous antioxidants may have a therapeutic plateau and even become detrimental as doses increase. Overexpression of mitochondria-targeted²⁸⁰ and non-mitochondria-targeted²⁸¹ superoxide dismutase in mammalian tissues can paradoxically increase lipid peroxidation following cardiac IRI. This may be due to the ability of O_2^- to terminate the propagation of lipid peroxidation reactions^{280,282}, as evidenced by the fact that the administration of a lipid peroxidation inhibitor reverses the negative effects of high doses of mitochondrial superoxide dismutase²⁸³. Thus, antioxidant scavengers may be limited because they can only detoxify ROS that have already formed, which can alter the balance of redox-sensitive reactions. Thus, a therapeutic approach that can lower O_2^- production by mitochondria may have high therapeutic potential compared to antioxidants.

ROS formation following reperfusion is primarily due to an increase in PMF following reperfusion²⁷, which has made mitochondrial uncoupling an attractive therapeutic target. Mitochondrial uncouplers have been shown to protect against cardiac^{284,285} and cerebral²⁸⁶ IRI concurrent with decreased ROS production. In addition to MnSOD, ischemic preconditioning upregulates UCPs and induces proton leak^{287,288}. The predominant leak in IRI is mediated by ANT rather than UCPs, as inhibition of UCPs with GDP has minimal effects on preconditioning-induced proton leak while inhibition of ANT with carboxyatractyloside greatly reduces preconditioning-induced leak²⁸⁸. However, UCP2 and UCP3 are upregulated from ischemic preconditioning²⁸⁹,

and upregulation of UCP2 protects from cerebral IRI, reduces ROS production, and preserves $\Delta\Psi_m$ ²⁹⁰.

The role of antioxidant pathways in renal IRI has been studied via the stanniocalcin-1 (STC1) pathway. Following renal IRI, the STC1 pathway causes overexpression of UCP2, mitochondrial depolarization, and reduced ROS production in macrophages^{291,292} and renal epithelial cells¹⁷⁴. Macrophage-dependent clearance of apoptotic cells is also dependent on UCP2¹⁸⁰, which suggests that mitochondrial uncoupling may serve a dual role in preventing ROS production from epithelial cells to prevent immune cell infiltration while stimulating macrophages to clear apoptotic cells that may enhance immune cell infiltration and inhibit the regeneration process.

In sum, mitochondrial uncoupling is an attractive therapeutic target for the treatment of renal IRI. UCPs have already been shown to protect from renal IRI, and reduction of PMF during reperfusion could reduce ROS production, immune cell infiltration, and necrosis. Furthermore, small molecule mitochondrial uncouplers that can prevent PMF from increasing during reperfusion may have therapeutic benefits.

1.4 Mitochondrial uncouplers

1.4.1 The use of uncoupling agents in humans

The first known mitochondrial uncoupler was 2, 4-Dinitrophenol (DNP)²⁹³, which was first utilized in massive quantities in World War I as an additive in explosives²⁹⁴. DNP poisoning was characterized by sweating and fever, while constant exposure caused rapid weight loss²⁹⁵. These notable toxic effects acted as a stimulus for its use amongst the public as a popular anti-obesity agent. However, despite the toxicity of DNP it could

not be removed from the market due to a lack of regulatory control over medicine by the United States Food and Drug Administration (FDA)²⁹⁶⁻³⁰⁰. During this time, the FDA was not granted the legal authority to set strict liability standards, determine what doses of a drug were considered toxic, what kind of tolerance should exist for unavoidable hazards, or to determine what labels were misleading²⁹⁹. While the organization could file lawsuits in an attempt to prosecute for fraudulent claims of pharmaceutical safety, it did not have a means by which to prove that claims or intent were fraudulent²⁹⁷. This made the courts reluctant to convict those that had violated the guidelines set forth by the FDA³⁰¹. Furthermore, the FDA consisted of only 166 professionals located at 18 inspection stations across the country, which made their presence only a minor deterrent to the over 3,000 medicine firms in the late 1910s³⁰¹. Thus, drug makers marketed DNP and other potentially dangerous medicines as safe and effective well into the 1930s³⁰¹.

The popularity of DNP originated when Maurice Tainter, a clinical pharmacist at Stanford University, began to experiment with DNP as an anti-obesity treatment^{295,302}. After nine obese patients treated with DNP lost an average of 20 pounds³⁰³, the popularity of DNP soared²⁹⁵. The balance between efficacy and safety of DNP was said to be dependent on dosing, with the goal of causing weight loss without inducing hyperthermia. It was reported that doses of approximately 5mg/kg induced a 20-30% increase in metabolic rate for approximately 24 hours³⁰³ along with increased perspiration and a feeling of warmth, but not increased body temperature³⁰³⁻³⁰⁶. Increasing the dose of DNP above 5 mg/kg was said to cause profuse sweating but still did not affect body temperature until a dose of 10 mg/kg was reached. Above 10 mg/kg, DNP increased human body temperature and caused an increase in heart and respiration rate³⁰³. After

continuous dosing, DNP was shown to cause a 40% increase in metabolic rate for 10 weeks without any apparent adverse effects³⁰³. In a second study Tainter reported that he treated 170 obese patients that lost an average of 1.5 pounds per week over a course of three months³⁰⁷.

The promising results of these trials and the lack of a national pharmaceutical regulation lead to DNP being used by over 100,000 patients by 1938³⁰⁸. As time progressed, however, the toxic effects of DNP began to emerge such as potential hepatotoxicity³⁰⁹. Tainter refuted many of these initial claims³¹⁰, but it was clear that the effects of DNP were not uniform and in some instances a DNP-induced fever and increased heart rate had been observed at doses of 5mg/kg³¹¹. Furthermore, Cyril MacBryde at the Washington School of Medicine demonstrated that patients treated with DNP had detrimental effects to the liver, skeletal muscle, and heart³¹² along with skin rashes and loss of taste³¹¹.

DNP also became associated with cataracts, and was reported to cause damage to the lens epithelium that progressed unabated until the entire lens became opaque³¹³. Over thirty DNP users developed cataracts in San Francisco alone in patients consuming DNP for as little as three months³¹³, and it was estimated that 2,500 Americans lost vision due to cataracts caused by DNP³¹⁴. MacBryde himself wondered whether the danger of DNP was worth the risk of treating a “relatively benign condition such as obesity”²⁹⁵. However, other physicians advocated DNP because they now believed that obesity was not merely a cosmetic defect, but contributed to other pathologies such as diabetes and heart diseases which made DNP treatment valuable despite the potential risks²⁹⁵.

On February 7, 1934 DNP was sold under the marketing name Formula 281 by advertising guru Harry Gorov, and one year later he released dinitrocresol (DNC), which contained an added amino group resulting in potency five times greater than DNP. The packaging contained testimonials such as “We feel much better and it has shown absolutely no ill effects”, and “proven beyond any question of doubt that the preparation does not affect the heart or other vital organs,” but warned customers of rashes and discoloration of the skin or eyes, which could be remedied with baking soda²⁹⁵. Gorov’s aggressive marketing gave the FDA the ammunition it needed to file a lawsuit against Gorov for his marketing of DNP and DNC. While the FDA could not distinguish efficacy or safety, it could file charges for misrepresenting benefits or safety for anything transported across state lines. Furthermore, Gorov’s advertising suggested that obesity was not a simple cosmetic defect, but an illness curable by DNP. Because of this, the FDA stated that Gorov attempting to misrepresent the known risks of a drug, which was defined as an agent designed to cure a disease. Gorov was charged with interstate transport of a misbranded drug, but due to the FDA’s limited authority Gorov simply pleaded “no contest”, paid a \$50 fine, and continued interstate sale of DNC²⁹⁵.

Deaths from DNP poisoning peaked in 1937 with 37 deaths in one year, mostly due to tachycardia and hyperthermia³¹⁵. However, the downfall of DNP during this time was initiated when the Elixir Sulfanilamide, a microbial drug which contained diethylene glycol as a diluent, was prescribed to 353 patients in four weeks with a 30% fatality rate. This disaster prompted public outrage and drastic changes to FDA power. Soon after in 1938, congress passed the Federal Food, Drug, and Cosmetic Act, which required proof of safety to the FDA before the release of a new treatment. This law changed the focus of

the FDA from a policing agency concerning false claims to a full regulatory agency that monitored safety and formula disclosures with federal power³¹⁶. While the FDA did not yet have the ability to gauge efficacy³¹⁶, this was more than enough power to outlaw DNP.

Shortly after its formation in 1938, the new FDA banned DNP. By 1960 no annual reported deaths occurred by DNP. Recently, however, DNP has made a comeback in the bodybuilding community where it is promoted over the internet as a safe weight loss supplement for those trying to reduce adiposity while maintaining muscle mass³¹⁵. DNP powder can be purchased illegally via bodybuilding websites, which endorse the drug despite the obvious dangers. DNP is considered to be “the most powerful weapon in a bodybuilder’s arsenal”, and users are advised to drink up to 8L of water per day, exercise in the cold, and aim a fan at one’s head while sleeping to avoid brain damage and hyperthermia³¹⁷.

1.4.2 Small molecule mitochondrial uncouplers

Mitochondrial uncouplers fall into two categories: ANT agonists and mitochondrial protonophores such as DNP. ANT agonists such as butylated hydroxytoluene allosterically modulate ANT resulting in channel opening and proton conductance into the matrix³¹⁸. Mitochondrial protonophores such as DNP, trifluorocarbonylcyanide phenylhydrazone (FCCP), and carbonyl cyanide *m*-chlorophenyl hydrazone (CCCP) are lipophilic weak acids that utilize the pH gradient in the mitochondria to shuttle protons from the inner membrane space (pH = 6.8) to the mitochondrial matrix (pH = 8.0)³¹⁹. Both classes of compounds can decrease PMF, but ANT agonists are not used for bioenergetics studies because of reliance on ANT activity

that may be independent bioenergetic function and to a lesser extent the effect of increased nucleotide translocation through ANT such ATP and ADP³¹⁸. A further complexity is the association of ANT with the mitochondrial permeability transition pore (MPTP), a multi-protein complex that, when opened, can cause a range of effects including indiscriminate release of mitochondrial macromolecules such as cytochrome C, which results in apoptosis³²⁰.

Mitochondrial protonophores are lipophilic weak acids, and their uncoupling activity is dependent on the efficiency in which they shuttle protons across the lipid bilayer of the mitochondrial inner membrane³²¹. The anionic form of mitochondrial uncouplers are more membrane soluble than the protonated form, thus the anionic form of FCCP cycles within the membrane³²², and the potency of uncouplers are defined as the rate constants for the movement of the protonated and deprotonated forms of the weak acid and the rate at which protonation and deprotonation occurs at the interface of the mitochondrial inner membrane³²³. For uncouplers in which this occurs, such as FCCP, the conductance increases linearly with protonophore concentration^{323,324}.

Anion diffusion is determined by the energy barrier required to permeate the hydrophobic membrane core³²⁵, while proton dissociation is determined by the pKa of the ionizable proton that is donated in the matrix³²¹. The pKa of FCCP is about 6.4 in aqueous buffer and between 6.1 and 6.4 on the surface of a phospholipid bilayer³²⁶, compared to a pKa of 6.0 of CCCP, a less potent but structurally similar compound³²³.

The maximal respiration rate achievable by an uncoupler in isolated mitochondria is dependent on the pKa of the ionizable proton³²¹, which will change dissociation constants relative to the matrix pH. As protons diffuse into the matrix, the matrix

acidifies and compounds with high pKa values cannot uncouple any further. The potency of uncouplers in isolated mitochondria is equal at low pKa values but decreases dramatically when the pKa is above 7.5³²¹. Theoretically, uncouplers which are close to but not exceeding this value would be the most effective at determining the maximal rates of mitochondrial respiration, since their activity would decrease as the mitochondrial matrix acidifies.

The addition of a weak acid protonophore that varies with the ratio of proton concentrations according to the Nernst equation, however this does not take into account the effects of the membrane potential or the solubility of the anion in the phospholipid bilayer. Mitochondrial protonophores have π electrons located in aromatic rings, which delocalize the charge on the anion and increase membrane solubility³²⁷. Thus, lipophilicity and acidity are not sufficient to account for the protonophoric effects of a small molecule.

DNP is not very lipophilic, with a clogp of 1.82, and should not be able to permeate a phospholipid bilayer in its protonated form³²⁸. Furthermore, the conductance maximum with regards to pH occurs at the pKa of the uncoupler^{324,329}, and DNP has been shown to create a negative charge when bound to neutral lipid membranes³³⁰. This has led to the theory that DNP shuttles a proton via a dimerization reaction^{322,324,327,328,331}. The dimer is a complex of the protonated (HA) and deprotonated (A^-) forms of the uncoupler (HA_2^-)^{327,332}. Both HA and A^- absorb strongly to the lipid-aqueous interface and their concentrations are much greater than in the lipid or aqueous phases^{324,327}. Furthermore, the solubility of an ion inside of a charged membrane increases with the size of the ion³³³, thus the formation of dimers of ions with the opposite charge to form an

ion pair can increase their mass and cancel their charge³³³. The rate of DNP-mediated proton translocation is dependent on the formation of DNP dimers³³⁴. Inside of the membrane HA_2^- is in equilibrium with HA and A^- , and the concentration of HA_2^- increases when a voltage is applied. As A^- levels increase, this pushes the formation of HA and a proton is shuttled into the intermembrane space. On the matrix side of the intermembrane space, HA is driven to form $\text{HA}_2^- + \text{A}^-$, and a proton is deposited into the matrix³³³.

The rate of proton translocation is not only governed by pKa, but largely the rate of influx and efflux from the membrane. This can also be affected by protonophore concentrations and stabilization in the membrane, and not the extraction rate of the ion from the aqueous phase³³⁵. FCCP utilizes a trifluoro substituent to increase potency relative to the unfluorinated compound CCCP. Although this leads to an increase in the pKa of FCCP, fluorination of membrane protonophores has also been shown to decrease lipophilic weak acid translocation across the plasma membrane despite making the compound more soluble in lipid bilayers³³⁶. This is primarily due to the large the atomic mass of fluorine compared to carbon, oxygen, or nitrogen as larger ions require less energy to bring them from an aqueous environment with high dielectric constant into the lipid bilayer³³⁷. Because FCCP translocates protons via a cycling mechanism, this would increase the time FCCP is in the membrane and able to perform acid-base proton translocation across the mitochondrial inner membrane, thus increasing potency by a mechanism independent of pKa.

Hydrophobicity can govern the partitioning of uncouplers into a phospholipid bilayer, but it is not the sole determining factor of uncoupling activity of small molecule

uncouplers. Charge distribution within the molecule can also affect uncoupling activity by small molecule uncouplers³³⁴. Because of this, the addition of fluorine can also have the opposite effect on lipophilic protonophores. The larger size of fluorine compared to hydrogen or carbon and dense electron cloud can generate a repellent sheath over the molecule. This increases the rate constant by which the anion diffuses out of a phospholipid bilayer and decreases the concentration of the molecule in the lipid membrane^{337,338}. For uncouplers that require cyclical protonophore activity, the addition of fluorines can decrease activity at membranes in which the anion simply diffuses through the phospholipid bilayer without cycling protons.

This phenomenon has been observed with the plasma membrane protonophore triphenylcyanoborate (TPCB). The addition of one fluorine on the phenyl ring of TPCB increases membrane translocation of TPCB by 20-fold. The addition of three fluorines increases anion translocation by five orders of magnitude. Anion translocation rates also vary by two orders of magnitude depending on the lipid composition of the membrane³³⁹. Interestingly, the translocation of fluorinated anions across the plasma membrane does not appear to change as concentrations increase, indicating that the PM can become fully saturated with fluorinated anions at low concentrations³³⁶. Thus, fluorination of lipophilic anions can decrease protonophore activity in membranes. This occurs by lowering protonophore concentrations in membranes by decreasing protonophore influx and increasing protonophore efflux from the phospholipid bilayer.

In summary, the potency of a mitochondrial protonophore in a specific membrane may depend on numerous factors including pKa of the ionizable protons, possible dimerization reactions, and the solubility of the protonated and deprotonated form of the

protonophore in the phospholipid bilayer. These reactions can also be governed by the dielectric constant and applied voltage of a given environment. Thus, protonophore activity of a given molecule may be membrane or organelle-specific.

1.4.3 Limitations of mitochondrial protonophores

Mitochondrial uncouplers have secondary effects independent of their protonophore activity on mitochondria. For example, proton translocation alone cannot account for all of the uncoupling activity of DNP, as pH has an independent effect on uncoupling activity independent of membrane voltage. This suggests an alternative mode of proton leak, which is attributed to disruption of phospholipid bilayers³³⁰. The protonated form of DNP increases K^+ and Na^+ permeability, which is demonstrated by the fact that DNP-induced ion permeability decreases by approximately 100-fold when extracellular pH is increased from 5 to 7³⁴⁰. DNP also increases K^+ conductance independent of oxidative phosphorylation³⁴¹, by activating ATP-sensitive K^+ channels (K^+_{ATP} channels) independent of ATP concentrations or oxidative phosphorylation^{342, 343}. K^+_{ATP} channels also exist in the mitochondria³⁴⁴, and can change $\Delta\Psi_m$ independent of proton conductance³⁴⁴. Thus, due to both the low solubility of DNP and the ability to activate ion channels, DNP is not recommended for mechanistic bioenergetics studies.

To complicate bioenergetics further, FCCP and DNP have been shown to bind to mitochondrial proteins using photoaffinity labeling, and the K_d for these binding interactions correlates with uncoupler activity. However, whether or not uncoupler binding to these sites is necessary for uncoupling activity is unknown^{345,346}. CCCP has been shown to bind to bacterial cytochrome oxidase³⁴⁷, and DNP has been shown to bind mitochondrial proteins including ATP synthase³⁴⁸. Thus, a major limitation of analyzing

the effects of mitochondrial uncoupling is potential off-target protein binding interactions by current mitochondrial uncouplers. To study the effects of uncoupling, it may be necessary to utilize control compounds that have similar structure to the uncoupler being utilized but do not contain an ionizable proton.

The protonophore activity of FCCP and DNP are also not specific for mitochondria and have protonophoric capabilities across all membranes, which acidifies the cytoplasm^{349,350} and disrupts the function of other pH-sensitive organelles such as endosomes. Extramitochondrial effects can decrease the metabolic rate of the cell as uncoupler concentrations increase, which results in an artifactual assessment of State 3_u²⁶ (**Figure 7**).

FCCP depolarizes the plasma membrane^{349,351–354} and causes intracellular acidification that is partially reversible when the plasma membrane is depolarized with glutamate or 50 mM K⁺, suggesting that PM proton flux mediated by FCCP causes intracellular acidification³⁴⁹. This is further supported by the fact that the PM current³⁵² and intracellular acidification^{353,354} induced by FCCP is dependent on extracellular pH.

Na⁺ currents are also observed following FCCP treatment, however in bovine epithelial cells FCCP-induced Na⁺ transport is dependent on extracellular pH, but FCCP-mediated proton transport across the PM is not affected by extracellular Na⁺ concentrations³⁵². Furthermore, in hepatocytes FCCP-induced current does not change Na⁺ conductance at the PM³⁵³, which provides further evidence that uncouplers transport protons across the plasma membrane. The inward current seen by FCCP treatment is also independent of Ca²⁺, as replacing Ca²⁺ with Ba²⁺ does not alter FCCP-induced inward current³⁵³. FCCP and DNP have also been found to activate Cl⁻ currents in astrocytes, and

these effects do not occur with oligomycin or cyanide, which suggests that these effects are independent of mitochondria³⁵⁵.

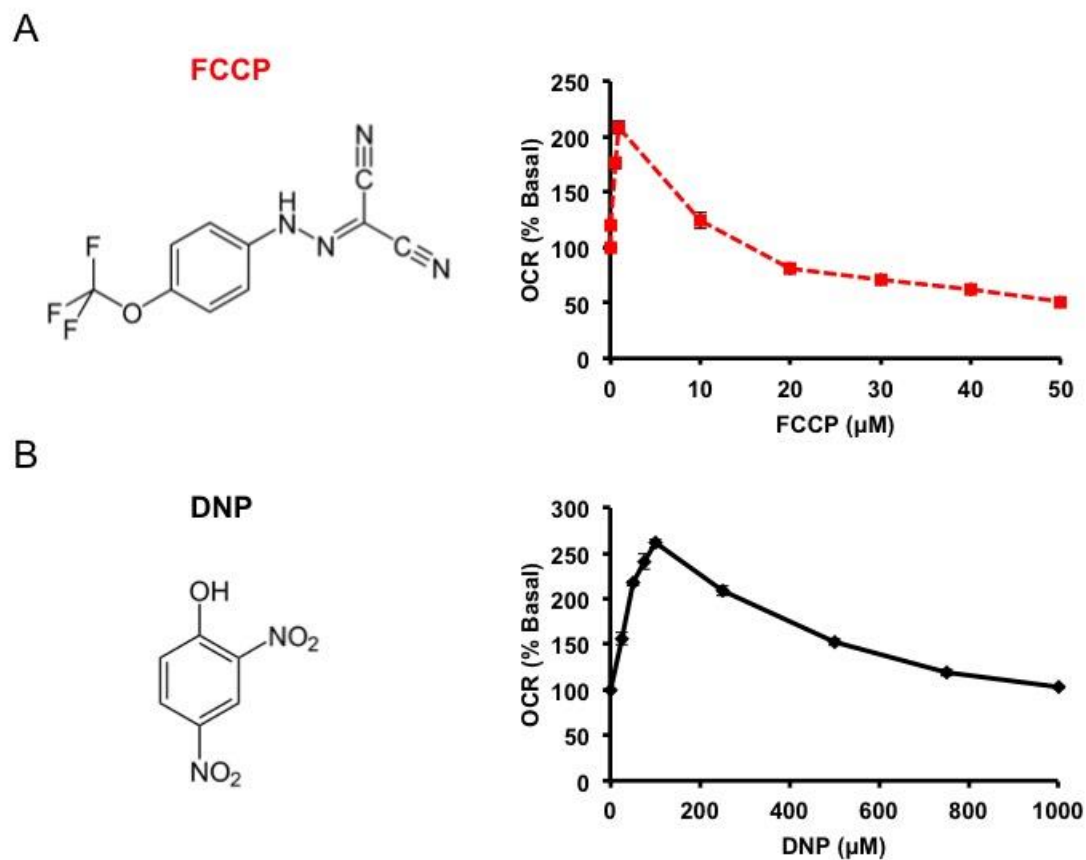


Figure 7: Mitochondrial uncouplers cause mitochondrial failure.

Oxygen consumption rate (OCR) was measured in L6 cells treated with increasing concentrations of FCCP (A) and DNP (B). Following the induction of the maximal rate of mitochondrial respiration, both compounds rapidly decrease OCR as uncoupler concentrations increase. Data is expressed as a percentage of basal respiration. Error bars indicate SEM. $N = 6$.

1.4.4 Toxicity of mitochondrial protonophores

The toxicity of uncouplers is often centered on ATP concentrations, however toxic doses of uncoupler treatment causes an initial drop in ATP levels followed by a slow increase that rises over normal ATP concentrations³⁵⁶. The initial effects of FCCP on cell viability are rapid, as genes involved in cell cycle arrest are upregulated. As time progresses, however, ATP levels increase steadily due to the upregulation of glycolytic enzymes such as pyruvate dehydrogenase, which results in ATP levels that are paradoxically higher than untreated cells. The switch to an overcompensation of glycolytic metabolism is further supported by the fact that lactate production increases over time³⁵⁶. This suggests that although the transcriptional changes induced by FCCP are due to ATP depletion, it may not be the only method of cytotoxicity. However, this is likely dependent on a cell's glycolytic reserve capacity. Further evidence that mitochondrial depolarization is not the only mode of uncoupler-induced effects on cell viability is that FCCP can decrease cell viability at doses that do not depolarize mitochondria³⁵⁷.

1.5 Concluding remarks

Mitochondrial uncouplers are valuable chemical tools that are used to assess the maximum rate of mitochondrial respiration, and they have potential clinical applications in diseases that are caused by decreased energy expenditure or increased ROS production. The potential clinical applications for uncouplers were first discovered when the effects of DNP on energy expenditure and adiposity were first recognized. Despite the dangers of DNP, it was clear that uncouplers had beneficial clinical applications if their

safety profile could be improved. The field of mitochondrial bioenergetics first utilized DNP, but slowly transitioned to the more potent and soluble FCCP. Both compounds, however, are limited in their ability to assess mitochondrial function in whole cells due to their off-target activities at other membranes. While both FCCP and DNP have been valuable in pioneering the manipulation of mitochondrial metabolism for both therapeutic and experimental purposes they remain limited in their ability to answer scientific questions about mitochondrial bioenergetics in whole cells.

Uncouplers can be modified to change activity based on their pKa and rate constants that govern their concentration within a membrane. Other reaction rate constants may also affect uncoupling activity, such as the ability of DNP to dimerize. Thus, mitochondrial uncouplers may favor specific membrane environments over others for reasons largely independent of pKa. Symmetrical fluorocarbons, for example, can shield charge in membranes, and can produce very little uncoupling because they cannot accumulate within a phospholipid bilayer. While uncouplers have been shown to have membrane selectivity, uncouplers have not been developed which target mitochondria without having protonophore activity at other membranes such as the plasma membrane. The identification of a protonophore that can have uncoupling activity in the mitochondrial membrane would be a significant advance in mitochondrial bioenergetics.

Another possible use for mitochondrial uncouplers is the prevention of ischemia-reperfusion injury. Unlike the use of DNP to treat obesity, only small amounts of proton leak are required to induce a therapeutic benefit, as small reduction in PMF can result in dramatic decreases in ROS production. This could reduce apoptosis, immune cell invasion, blood vessel occlusion, and ATN. Thus, Renal IRI represents a possible avenue

for the use of an uncoupling agent for clinical benefit. The effects of mitochondrial uncouplers have not been evaluated in renal IRI and the mechanism by which uncouplers could potentially ameliorate this condition are also unknown. Furthermore, acute uncoupler treatment to treat IRI would likely have a lower chance of long-term consequences compared to the chronic dosing regimen used for the treatment of obesity.

**CHAPTER 2: IDENTIFICATION AND VALIDATION OF A NOVEL
MITOCHONDRIAL UNCOUPLER THAT DOES NOT DEPOLARIZE THE
PLASMA MEMBRANE**

2.1 Introduction

Pharmacological uncouplers enable protons to enter the mitochondrial matrix along their concentration and electrochemical gradient. FCCP is often used for analysis of mitochondrial function in living cells, tissues, and isolated mitochondrial preparations due to its relatively high potency compared to other uncouplers. However, the protonophore activity of mitochondrial uncouplers such as FCCP is not restricted to mitochondria, and their use for mitochondrial bioenergetics studies is limited by plasma membrane depolarization (**Section 1.4.3**).

Mitochondrial uncouplers can induce mitochondrial failure in whole cells as uncoupler concentrations increase; however this phenomena is not seen in isolated mitochondria. Thus, we hypothesized that the narrow dosing range of mitochondrial protonophores in whole cells is due to off-target effects of mitochondrial protonophores, rather than mitochondrial depolarization alone. Our goal was to identify a novel mitochondrial uncoupler that was specific for mitochondria and therefore could be used as a better tool to assay mitochondrial bioenergetics.

We screened a diverse chemical library to find new mitochondrial uncouplers. The first screen was a non-quantitative medium-throughput assay to find compounds that increased oxygen consumption. The second screen was to eliminate compounds that increased ROS formation as they increased oxygen consumption. The remaining compounds were evaluated for their ability to increase OCR and ECAR in a Seahorse XF Analyzer across a broad dosing range. This screening process identified one molecule, BAM15, (2-fluorophenyl){6-[(2-fluorophenyl)amino](1,2,5-oxadiazolo[3,4-e]pyrazin-5-yl)}amine which had a broad dosing range. We then performed a rigorous series of

functional assays to validate that BAM15 was a bona-fide mitochondrial protonophore uncoupler. From this study it can be concluded that BAM15 is a mitochondrial protonophore that does not depolarize the plasma membrane, and that the narrow dosing range that mitochondrial protonophores (including FCCP and DNP) demonstrate are due to off-target effects at other membranes in whole cells.

2.2 Materials and methods

2.2.1 Non-quantitative oxygen consumption assay

L6 myoblasts were grown to confluence, washed with PBS, trypsinized and then seeded into a 96-well plate in cell culture media wherein an O₂-sensitive fluorophore tris 1,7-diphenyl-1,10 phenanthroline ruthenium (II) chloride is embedded in silicone at the base of each well of a 96-well plate (BD-OBS microplate, BD Biosensor). This system takes advantage of Fick's law, which stipulates that as oxygen consumption is increased the amount of dissolved oxygen in the media will also increase due to increased diffusion. The reporter dye is quenched by O₂, thus fluorescence intensity increases as the rate of oxygen consumption of the cells increases³⁵⁸. Cells were incubated with 0.5% (v/v) library compound or vehicle control (DMSO) and fluorescence intensity recorded over 45–90 min (1 read/min) at 37 °C by a SpectraMax M5 dual-monochromator microplate reader (Molecular Devices, CA) using a bottom-read configuration and with the excitation and emission filters set at 485 nm and 630 nm, respectively. The mitochondrial uncoupling agent FCCP was used as positive control increase oxygen consumption. Fluorescence data were recorded on SoftMax Pro (version 4.8) software. Fluorescence tracers were evaluated

manually and the top 25 ‘hits’ that increased oxygen consumption over DMSO control were selected for secondary screening.

2.2.2 ROS production assay

L6 myoblasts were seeded into black-walled clear-bottom 96-well microplates in L6 growth media and grown to confluence. Cells were then washed twice with PBS and co-incubated with 7.5 μM CM-H₂DCFDA (Molecular Probes, Invitrogen, Carlsbad, CA) and 0.5 ng/ μL of each hit compound or vehicle control (DMSO) in Krebs-Ringer phosphate buffer (136 mM NaCl, 4.7 mM KCl, 10 mM NaPO₄, 0.9 mM MgSO₄, 0.9 mM CaCl₂, pH 7.4) supplemented with 25 mM D-glucose at 37 °C in 5% CO₂/95% air for 1 h. 100 nM H₂O₂ was used as a positive control for ROS production. Following incubation, cells were washed three times with PBS to remove excess probe. Cells were then covered with 100 μL /well PBS and fluorescence intensity measured by a Tecan Infinite[®] M200 microplate reader (Tecan Group Ltd., Switzerland) using a top-read configuration and with the excitation and emission filters set at 495 \pm 9 nm and 530 \pm 20 nm, respectively. Fluorescence data were recorded on Magellan (version 6.4) software and exported to Microsoft Excel for subsequent analysis. Having subtracted the background fluorescence (that emitted from a well which did not receive the CM-H₂DCFDA probe) from each well, ROS production was expressed in terms of percentage fluorescence of the vehicle control for each condition. Compounds which increased ROS levels by greater than 20% were eliminated.

2.2.4 Measurements of OCR and ECAR in whole cells

Oxygen consumption rate (OCR) and extracellular acidification rate (ECAR) were measured using a Seahorse XF-24 Flux Analyzer (Seahorse Biosciences, North Billerica, MA). NMuLi, C2C12, and L6 cells were seeded in a Seahorse 24-well tissue culture plate at a density of 3.5×10^4 cells/well, isolated cardiomyocytes at a density of 4×10^4 cells/well, and human primary fibroblasts at a density of 1.1×10^4 cells/well. The cells were then allowed to adhere for 24 h. Prior to the assay, the media was changed to unbuffered DMEM containing pyruvate and glutamine (Gibco #12800-017, pH=7.4 at 37 °C) and the cells were equilibrated for 30 mins at 37 °C. Compounds were injected during the assay and OCR and ECAR were measured using 2 min measurement periods.

2.2.5 Mitochondria isolation from mouse liver

Mitochondria were isolated from the livers of male C57BL/6 mice. Mice were euthanized by CO₂ inhalation and cervical dislocation. Livers were removed, minced with scissors, and immediately placed in 1 mL ice-cold isolation medium (250 mM sucrose, 10 mM Tris-HCl, 1 mM EGTA, 1% fatty acid free BSA, pH 7.4). The tissue was homogenized using four strokes of a custom automated Potter-Elvehjem tissue homogenizer. After adding 4 mL of isolation medium the homogenate was centrifuged at $800 \times g$ for 10 min at 4 °C. The supernatant was then divided into four 2 mL Eppendorf tubes and centrifuged at $12,000 \times g$ for 10 min at 4 °C. The supernatant was removed and any white debris was aspirated from the brown mitochondria pellet. The pellets were then combined in 1 mL isolation medium and centrifuged at $10,000 \times g$ for 10 min. The supernatant and any white debris were removed and the mitochondria were resuspended in 1 mL mitochondrial assay solution (MAS, 70 mM sucrose, 220 mM mannitol, 10 mM KH₂PO₄, 5 mM MgCl₂, 2 mM HEPES, 1 mM EGTA, 0.2% fatty acid free BSA, pH 7.2).

2.2.6 Electron flow assay

Electron flow assays were performed using the methods described in Rogers et al.³⁵⁹. Briefly, 5 μg of mitochondrial protein in MAS was loaded into a Seahorse 24-well tissue culture plate and centrifuged at $2000\times g$ for 15 min at 4 °C. Prior to the assay, mitochondria were incubated at 37 °C for 10 mins in MAS containing 10 mM pyruvate, 2 mM malate, and 5 μM BAM15 or FCCP. Rotenone (2 μM), succinate (10 mM), antimycin A (4 μM), and N,N,N',N'-tetramethyl-p-phenylenediamine (TMPD, 100 μM) plus ascorbate (10 mM) were added sequentially as indicated in the figure. $N=3$ wells/plate of a representative of 3 plates.

2.2.7 Mitochondrial titration assays

Mouse liver mitochondria were isolated and respiration was measured according to Rogers et al.³⁵⁹. Oxygen consumption was measured using a Seahorse XF96 Flux Analyzer on mitochondria respiring on pyruvate (10 mM) and malate (2 mM) or succinate (10 mM) and rotenone (2 μM).

2.2.8 $\Delta\Psi_m$ in whole cells

L6 cells were incubated with the fluorescent indicator of $\Delta\Psi_m$ tetramethylrhodamine (TMRM, 125 nM) or DMSO (1%) control for 30 min. The cells were then centrifuged for 5 min at $700\times g$ and resuspended in unbuffered DMEM at a concentration of 1×10^5 cells/mL. The cells were then treated with BAM15/FCCP or DMSO (0.1%) for 10 min prior to flow cytometric analysis.

2.2.9 ANT-independence assay

C2C12 cells (ATCC) were plated in XF96 tissue culture plates (15,000 cells/well) and cultured overnight as recommended by the supplier. Just before initiation of the XF assay (XF96, Seahorse Bioscience), cells were washed twice with 200 μ l/well MAS buffer, permeabilized with 1.0 nM XF PMP (Seahorse Bioscience), and simultaneously provided 4 mM ADP, 10 mM succinate, and 10 μ M cyclosporin A (Sigma-Aldrich) to obtain State 3 respiration as described [20]. The plate was immediately placed into the XF96 instrument and assay initiated. Respiration (State 3) was recorded, followed by sequential injections of 3 μ g/mL oligomycin or carboxyatractyloside (CAT, Sigma) and then 1.0 μ M BAM15 or FCCP with measurements taken after each injection.

2.2.10 Mitochondrial swelling assay

Mitochondrial swelling was calculated as previously described by Shchepinova et al. [21]. Briefly, isolated liver mitochondria from female WT FVB mice were added to 1 mL isotonic acetate buffer (145 mM potassium acetate, 5 mM Tris-HCl, 0.5 mM EDTA, 3 μ M valinomycin, and 1 μ M rotenone, pH 7.4) in a cuvette at a final concentration of 0.25 mg/mL mitochondrial protein. Absorbance at 600 nm of the mitochondrial suspension was measured at a rate of 30 measurements/min using a SpectraMax M5 dual-monochromator microplate reader (Molecular Devices, CA) using a cuvette-read configuration for 60 s before the addition of 10 μ M uncouplers. Data was recorded on SoftMax Pro (version 4.8) software.

2.2.11. $\Delta\Psi_m$ in isolated mitochondria

Isolated liver mitochondria from male WT FVB mice incubated with 200 nM TMRM in MAS_{SRO} buffer (MAS buffer supplemented with 10 mM succinate, 1 μ M rotenone, and

1 μM oligomycin) for 20 min at 25 °C. The mitochondria were then centrifuged for 5 min at 3000 $\times g$ and resuspended in MAS_{SRO} . Mitochondria were then added to MAS_{SRO} containing the indicated concentrations of uncouplers and incubated at room temperature for 20 min. The mitochondria were then centrifuged for 5 min at 3000 $\times g$. The supernatant was then removed and placed into a black clear bottom 96-well plate (100 μL /well). TMRM fluorescence was determined using an excitation emission of 545_{ex}/580_{em}. Fluorescence data were recorded on Magellan (version 6.4) software and exported to Microsoft Excel for subsequent analysis. Having subtracted the background fluorescence (that emitted from a well which did not receive the TMRM probe) from each well, TMRM fluorescence was expressed in terms of percentage fluorescence of the vehicle control for each condition.

2.2.12. Plasma membrane electrophysiology

In preparation for recording, L6 cells were plated onto poly-L-lysine-coated glass coverslips and returned to the incubator to adhere for at least 1 h prior to use. Cells were used within 1 day of plating. Whole cell recordings were performed at room temperature with 3–5 M Ω Sylgard-coated borosilicate glass patch pipettes and an Axopatch 200B amplifier (Molecular Devices). The internal solution contained 120 mM KCH_3SO_3 , 4 mM NaCl, 1 mM MgCl_2 , 0.5 mM CaCl_2 , 10 mM HEPES, 10 mM EGTA, 3 mM ATP-Mg and 0.3 mM GTP-Tris (pH 7.2). The bath solution was composed of 140 mM NaCl, 3 mM KCl, 2 mM MgCl_2 , 2 mM CaCl_2 , 10 mM HEPES and 10 mM glucose (pH 7.3) and was flowed over the cells at approximately 2 mL/min. For voltage clamp experiments, cells were held at -70 mV and a 750 ms ramp from -150 mV to $+80$ mV was applied at 10 s intervals using pCLAMP software and a Digidata 1322A digitizer (Molecular Devices).

Conductance measurements were taken between -130 mV and -60 mV. For current clamp experiments, cells were recorded at the resting membrane potential.

2.2.13 Cytotoxicity assays

Cells were seeded into 96 well plates at a density of 5000 cells/well for NMuLi, L6 and C2C12 cells and 10,000 cells/well for primary rat left ventricular cardiomyocytes. Cells were incubated overnight at 37 °C prior to drug treatment. Drugs were diluted in cell culture medium (10% fetal calf serum in Dulbecco's Modified Eagle Medium) (Gibco Life Technologies, Grand Island, NY, USA) and added to each well at the indicated concentrations. Cell viability was measured 48 h later using 3-(4,5-dimethylthiazol-2-yl)-2,5-diphenyltetrazolium bromide solution (MTT) (Amresco, Solon, Ohio, USA) or crystal violet staining (0.5% w/v in 50% methanol). Absorbance was measured using a SpectraMax M5 dual-monochromator microplate reader (Molecular Devices, CA). Cell viability of drug-treated cells is displayed as a percentage of control cells i.e. cells with equivalent concentrations of the vehicle, dimethylsulfoxide (DMSO). The final concentration of DMSO exposed to the cells was no more than 0.1% (v/v) for the duration of the experiment.

2.2.14 ATP Assay

L6 cells were seeded into 96-well plates. Cells were washed 3x with PBS and placed into serum-free DMEM supplemented with 1 mM pyruvate for 30 min. Cells were then treated with the indicated concentrations of BAM15, FCCP, and 0.1% DMSO for six hours. ATP was measured using ATPlite Luminescence ATP Detection Assay System (PerkinElmer).

Luminescence was measured using a SpectraMax M5 dual-monochromator microplate reader (Molecular Devices, CA).

2.3 Results

2.3.1 A biochemical screen to search for new uncouplers

Enhanced O₂ consumption is a consequence of mitochondrial uncoupling; therefore, we measured cellular O₂ consumption as a primary screen to identify novel uncouplers using a non-quantitative assay. Rat L6 myoblasts were chosen for this screen because they are fast growing, have abundant mitochondria, and have spare mitochondrial reserve capacity. L6 cell number was optimized such that 500,000 cells per well produced a reliable 2-fold increase in fluorescence over background across a time course of up to 50 min. Using FCCP as a positive control for increased O₂ consumption and DMSO as a vehicle control, we screened a small molecule diversity library of 5040 compounds at a concentration of 5 µg/mL (TimTec Apex Screen). Hits were identified as those that increased O₂ consumption over DMSO control. Compounds that increased O₂ consumption were subjected to a secondary screen to identify, and eliminate, compounds that increased ROS production.

To measure ROS production, cells were coincubated with 2',7'-dichlorodihydrofluorescein diacetate (H₂DCFDA), an H₂O₂-sensitive fluorophore that is distributed in the cytoplasm. O₂⁻-sensitive fluorophores that are targeted to mitochondria, such as MitoSox Red, were not used because their mitochondrial concentration is reliant upon ΔΨ_m. These dyes utilize a positively-charged triphenylphosphene group which utilizes the negative potential to cause localization.

The addition of FCCP at concentrations that depolarize mitochondrial more than 30mV, or approximately 250 nM FCCP, will cause significant redistribution of MitoSox Red from the mitochondrial matrix into the cytoplasm where it can be oxidized by O₂⁻. The

resulting molecule, Mitoethidium, can then enter the nucleus and have its fluorescence enhanced even further by nuclear DNA intercalation,³⁶⁰ which can be problematic considering the fluorescence of ethidium is forty times higher when bound to DNA³⁶¹. To further complicate matters, MitoSox Red and Mitoethidium are oxidized by H₂O₂, O₂⁻, and ferryl radicals. While oxidation by H₂O₂ is approximately 15 times slower than O₂⁻, ferryl radicals (as generated by FeSO₄ and H₂O₂) cause greater oxidation of mitoethidium on a molar scale³⁶². Thus, MitoSox Red can be used to measure mitochondrial O₂⁻ in settings that do not cause a mitochondrial depolarization of more than approximately 30 mV, but these types of dyes are not suitable to measure the effects of uncoupler treatment.

In muscle cells, approximately 96% of cytosolic H₂O₂ is generated by mitochondria³⁶³. For this reason we used H₂DCFDA, which is a cytosolic fluorophore that fluoresces when oxidized by O₂⁻ and H₂O₂. Although it can be oxidized by other redox-sensitive compounds³⁶⁴ and peroxynitrite species, which include NO⁻ and the oxidizing agents it forms such as CO₃⁻ and ⁻OH^{365,366}, these species are increased as a result of increased intracellular H₂O₂, which lessens the chance of one of these species leading to misinterpretation of ROS production compared to MitoSox Red.

This algorithm identified BAM15 as a compound that increased oxygen consumption (**Figure 8 A**) without increasing ROS production (**Figure 8 B**). BAM15 is not structurally related to FCCP (**Figure 9 A**), and we observed that BAM15 had nearly identical potency to FCCP (**Figure 9 B**). Therefore, we continued to use FCCP as a control throughout this study. Low doses of BAM15 from 100 nM to 1 μM increased cellular OCR to a similar degree as FCCP, but higher concentrations from 10 μM to 50 μM revealed that BAM15 was able to maintain uncoupled respiration at a high rate whereas FCCP caused

mitochondrial failure at these doses (**Figure 9 B**). This was observed in a range of additional cell lines including primary rat neonatal ventricular cardiomyocytes, mouse C2C12 myoblasts, normal murine liver cells, and human primary fibroblasts (**Figure 9 C-F**). Similarly, we found that ECAR was maintained at a higher level in BAM15-treated cells (**Figure 10**). This indicates that although the mitochondria are depolarized, cells treated with BAM15 are more metabolically active compared to cells treated with FCCP.

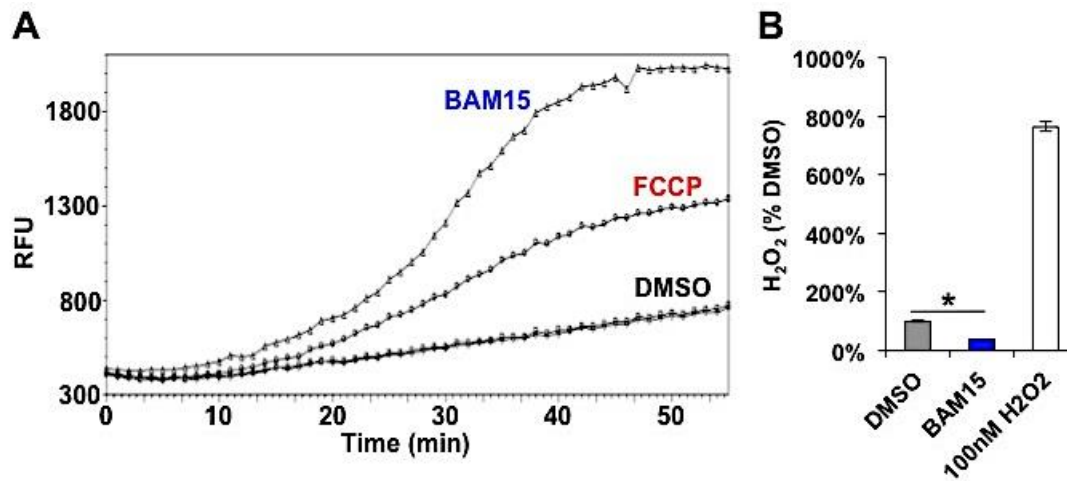


Figure 8: A biochemical screen identifies BAM15 as an oxygen consumption agonist that does not increase intracellular ROS in whole cells.

A: L6 cells were seeded into a 96-well BD-Biosensor plate. Cells were treated with BAM15 or FCCP and the fluorescence signal was monitored over time. Increased fluorescence indicates increased oxygen consumption. B: Intracellular H₂O₂ concentrations were measured in L6 cells treated with 5 μg/mL BAM15. 100 mM H₂O₂ was used as a positive control. Error bars indicate SEM. * indicates $p > 0.05$ by Student's T-test. For (A) $N =$ one representative of two experiments. For (B), $N = 3$ wells/group.

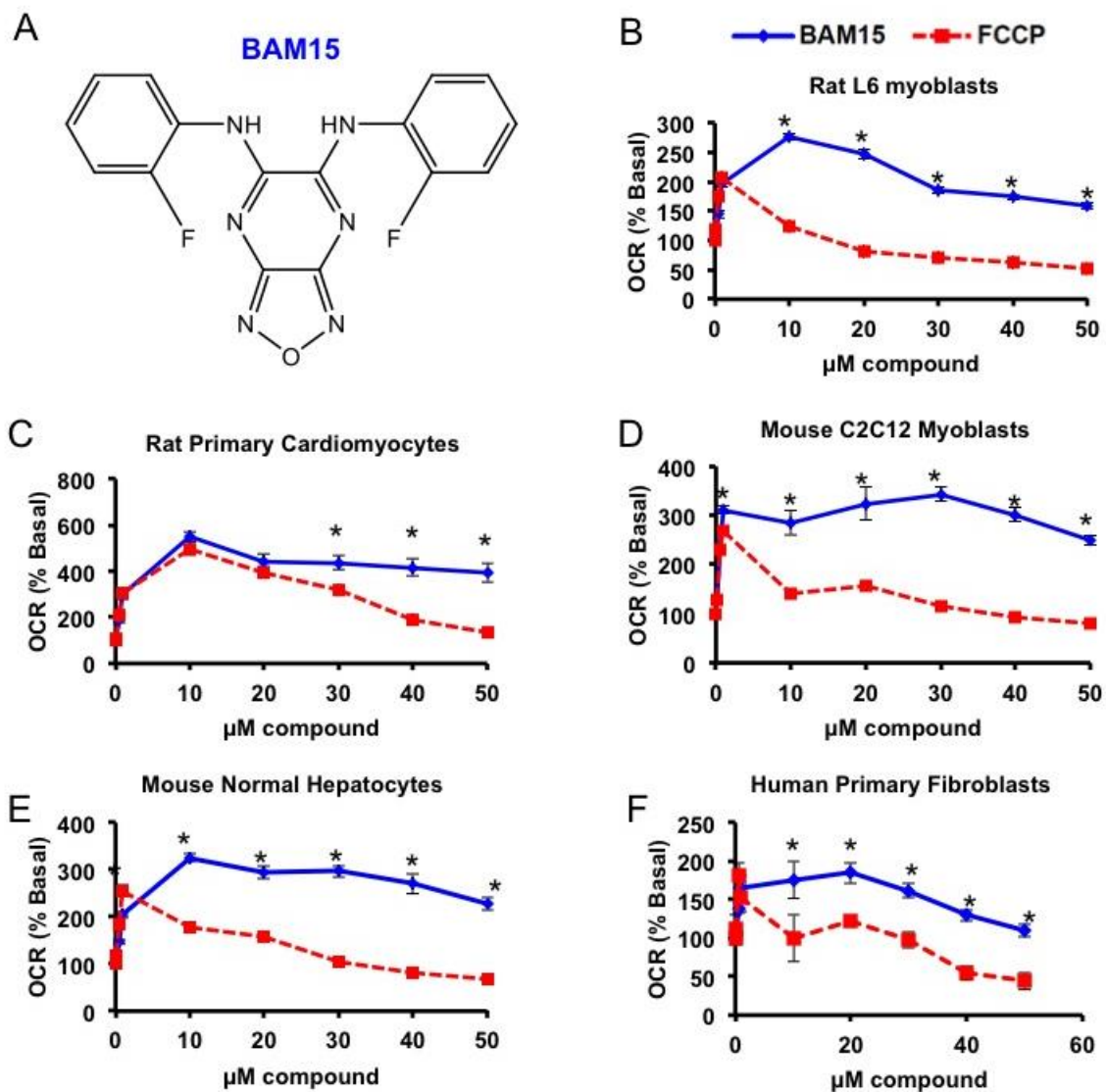


Figure 9: BAM15 increases OCR in whole cells across a broad dosing range.

A: Structure of BAM15. B–F: FCCP- and BAM15-stimulated oxygen consumption rate (OCR) in L6 myoblasts, rat primary cardiomyocytes, mouse C2C12 myoblasts, mouse normal hepatocytes, and human primary fibroblasts at the indicated concentrations. Error bars indicate SEM. For (B–F), * indicates $p < 0.05$ by two-way ANOVA with Bonferroni's posttest and $N = 6$ –8 wells per condition from three separate experiments.

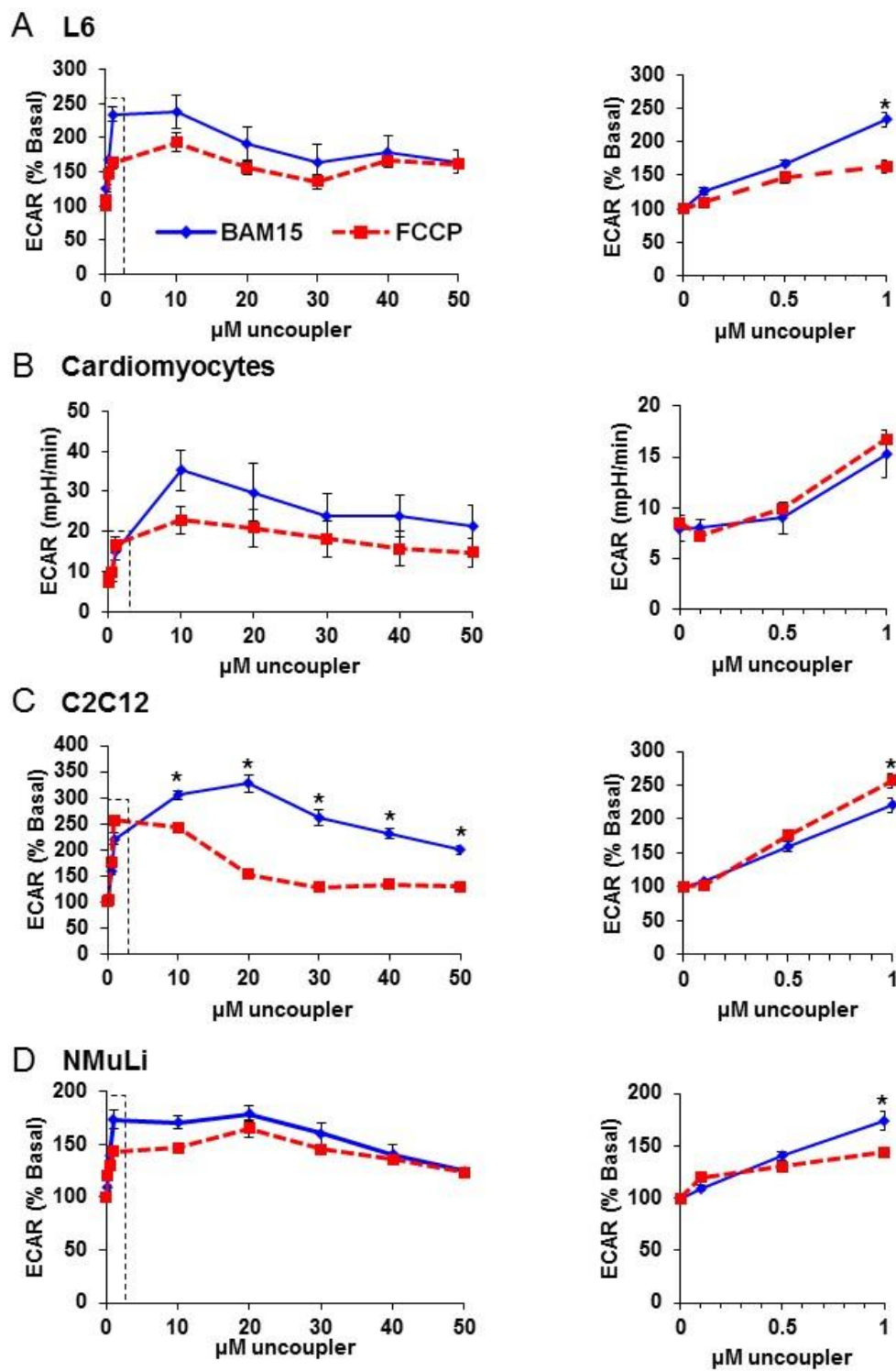


Figure 10: BAM15 increases ECAR.

Extracellular acidification rates were measured in L6 myoblasts (A), neonatal rat ventricular cardiomyocytes (B), C2C12 myoblasts (C), and NmuLi hepatocytes (D)

treated with increasing concentrations of BAM15 versus FCCP, as indicated. Error bars indicate SEM. * indicates $p < 0.05$ by two-way ANOVA with Bonferroni's posttest. $N = 6-8$ wells per condition from three separate experiments.

2.3.2. BAM15 uncouples mitochondria in whole cells

We next sought to determine whether BAM15 was a bona-fide mitochondrial uncoupler. The ATP synthase is the major pathway whereby protons enter the mitochondrial matrix; therefore, we investigated whether BAM15 could increase OCR in the presence of oligomycin. Using FCCP as an equipotent positive control, we found that BAM15 was fully capable of increasing mitochondrial respiration in the presence of oligomycin and did so across a broader concentration range than FCCP in both myoblasts (**Figure 11 A**) and hepatocytes (**Figure 11 B**).

The broad dosing range of BAM15 may be explained either by its effects on $\Delta\Psi_m$ or non-mitochondrial activity. To test the effects of each protonophore on $\Delta\Psi_m$ in intact cells, changes in $\Delta\Psi_m$ was measured using the fluorescent cationic dye TMRM. TMRM is positively charged and accumulates in mitochondria based on $\Delta\Psi_m$, and when $\Delta\Psi_m$ decreases the dye is released and fluorescence decreases. We observed that BAM15 and FCCP had similar effects on TMRM fluorescence on TMRM fluorescence in L6 myoblasts treated with concentrations of each uncoupler at 1 μM and 10 μM (**Figure 12**), despite FCCP causing respiratory failure at 10 μM .

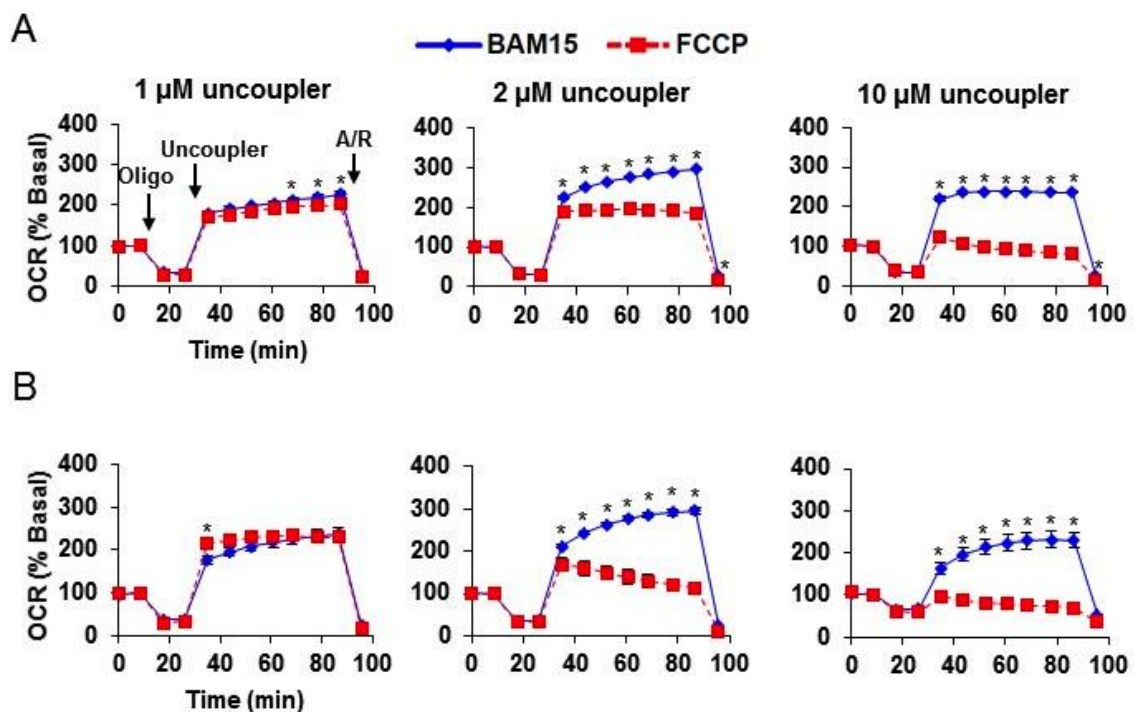


Figure 11: BAM15 causes mitochondrial uncoupling in whole cells.

L6 cells (A) and NmuLi cells (B) were sequentially treated with oligomycin (Oligo), 1 μ M), the indicated concentration of BAM15 or FCCP (Uncoupler), and antimycin A (10 μ M) plus rotenone (1 μ M) (A/R) as indicated by arrows. Error bars indicate SEM. * indicates $p < 0.05$ by two-way ANOVA with Bonferroni's posttest. $N = 5$ wells per condition.

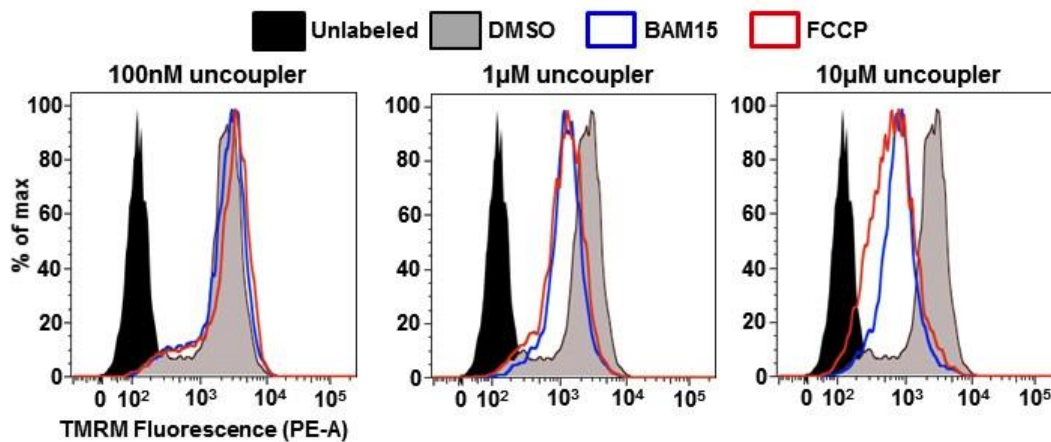


Figure 12: BAM15 depolarizes mitochondria in intact cells.

TMRM-loaded L6 cells were treated with the indicated concentrations of BAM15 or FCCP for 10 min prior to FACS analysis in the phycoerythrin (PE) channel. Uncoupler-treated cells are left-shifted, indicating loss of $\Delta\Psi_m$. $N =$ one representative from three separate experiments.

2.3.3 BAM15 stimulates respiration by acting directly on isolated mitochondria

To determine whether BAM15 stimulated respiration by acting directly on mitochondria, we isolated rat liver mitochondria and treated them with increasing concentrations (1–64 μM) of BAM15 and FCCP. As shown in **Figure 13**, we found that BAM15 and FCCP had comparable effects on the stimulation of OCR on mitochondria respiring on pyruvate and malate (complex I substrates), or succinate (a complex II substrate) in the presence of the complex I inhibitor rotenone. BAM15 was able to stimulate respiration on isolated mitochondria respiring under both substrates in a dose dependent manner, however high doses of FCCP caused slight decreases in respiration. These effects may be attributed to the pKa of FCCP versus BAM15. FCCP has a pKa of approximately 6.4, while BAM15 has a measured pKa of 7.4. This would cause BAM15's weak acid activity to decrease as the mitochondrial matrix acidifies, thus making BAM15 self-limiting at high doses.

To test if BAM15 depolarizes mitochondria directly, isolated mitochondria respiring on succinate in the presence of rotenone were loaded with TMRM. Mitochondrial depolarization was assessed by measuring TMRM release into the extramitochondrial media. BAM15 and FCCP both depolarized isolated mitochondria as indicated by TMRM release in a dose-dependent manner (**Figure 14 A**) and caused complete depolarization at 20 μM . To demonstrate that these effects were independent of ATP synthase, TMRM release was measured in the presence of oligomycin (**Figure 14 B**). Oligomycin increased the amount of TMRM released by both uncouplers, which is expected because TMRM accumulation in mitochondria is caused by the positively charged TMRM molecule

accumulating in negatively-charged mitochondria. The inhibition of ATP synthase increases $\Delta\Psi_m$ and thus increases the concentration of TMRM inside the mitochondria prior to uncoupler treatment.

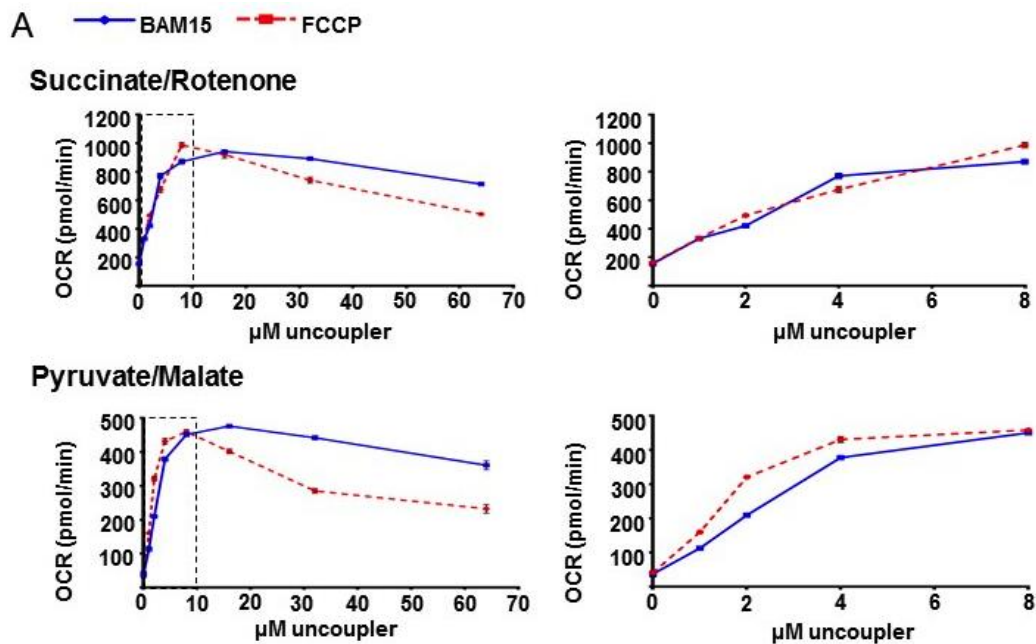


Figure 13: BAM15 stimulates respiration in isolated mitochondria.

Oxygen consumption rate (OCR) of isolated mouse liver mitochondria respiring on succinate in the presence of rotenone and pyruvate/malate was measured following treatment with increasing concentrations of BAM15 or FCCP. Right graphs expand the area that is indicated by the dotted box in the left graph. $N = 6-9$ wells per condition over three separate experiments.

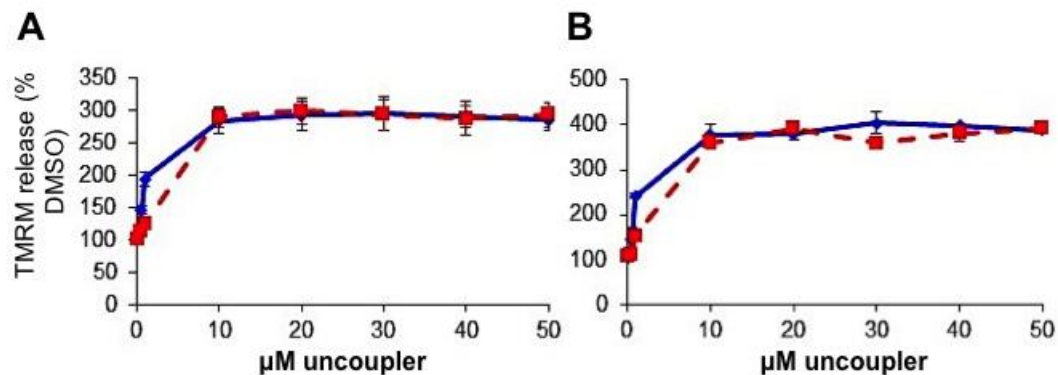


Figure 14: BAM15 depolarizes isolated mitochondria.

TMRM release in isolated mitochondria respiring on succinate (10 mM) in the presence of rotenone (1 µM) was measured following treatment with increasing concentrations of BAM15 and FCCP in the presence (A) or absence (B) of oligomycin. Data is expressed as a percentage of fluorescence from DMSO (0.1%)-treated mitochondria. Error bars indicate SEM. $N = 3$ wells/group.

2.3.4 BAM15 is a mitochondrial protonophore

PMF can be affected by ions other than H^+ , most notably K^+ . To determine whether BAM15 was transporting protons across the mitochondrial inner membrane, we measured proton-dependent mitochondrial swelling³⁶⁷. Isolated mitochondria were incubated in isotonic potassium acetate buffer supplemented with the potassium ionophore valinomycin, which dissipates $\Delta\Psi_m$. Acetate is used as a solute in this assay because the dissociated acetate anion is membrane impermeable and causes the mitochondria to swell when trapped inside the matrix. Under these conditions, only the protonated form of acetate can enter the mitochondria, but the accumulation of protons inside the matrix limits further acetate entry. In this system the only means by which more acetate accumulation into the mitochondria is if protons are released from the matrix, which can only be achieved by proton cycling by a protonophore. If the proton gradient is relieved more acetate accumulates in the mitochondrial matrix and swelling occurs³⁶⁷. As shown in **Figure 15**, both FCCP and BAM15 induced mitochondrial swelling, demonstrating that BAM15 is a protonophore.

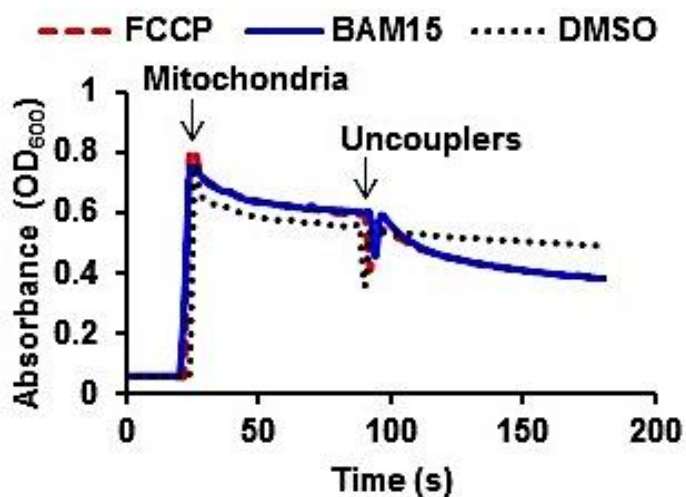


Figure 15: BAM15 induces proton-dependent mitochondrial swelling.

Absorbance at 600 nm was read over time following the addition of isolated mouse liver mitochondria respiring on succinate (10 mM) in the presence of rotenone (1 μ M) and valinomycin. Mitochondria and 10 μ M uncouplers were added at the indicated time points. N = one representative of three separate experiments.

2.3.5 BAM15's effect on respiration is not complex-specific and independent of ANT

Compounds that donate electrons to the ETC will increase oxygen consumption, therefore we tested if BAM15 had electron-donating activity. To determine whether BAM15 was altering mitochondrial electron flow at each complex we measured mitochondrial respiration in isolated mitochondria respiring on pyruvate and malate in the presence of FCCP or BAM15 (5 μ M). As previously observed, minimal differences in respiration were observed at this dose. When complex I was inhibited with Rotenone, BAM15 and FCCP-stimulated respiration were both depleted, which indicates that both compounds do not donate electrons downstream of complex I. To determine if complex II-mediated respiration was equal between the two compounds, the mitochondria were treated with Rotenone and succinate, which feeds electrons to complex II and causes complex-II dependent respiration. Both compounds enabled complex II mediated respiration, and this was inhibited by blocking complex III with Antimycin A. Since both BAM15 and FCCP-mediated respiration was inhibited by Antimycin A, these data demonstrate that neither molecule can donate electrons from succinate to cytochrome c or complex IV. Finally, the addition of the electron donor system of N,N,N',N'-tetramethyl-p-phenylenediamine dihydrochloride (TMPD) and ascorbate was able to fully rescue respiration at complex IV in the presence of both BAM15 and FCCP (**Figure 16**). These data demonstrate that BAM15 does not donate electrons to any of the ETC complexes.

Some non-protonophore uncouplers increase proton transport into the matrix via interaction with the mitochondrial inner membrane adenine nucleotide translocase (ANT)³¹⁸. To determine whether the ANT was necessary for BAM15-mediated respiration we treated permeabilized cells with the ANT inhibitor carboxyatractyloside

prior to BAM15 or FCCP treatment (**Figure 17**). BAM15 and FCCP were both able to stimulate respiration independent of the adenine nucleotide translocase in permeabilized cells. These data demonstrated that both BAM15 and FCCP did not require the ANT to increase mitochondrial respiration.

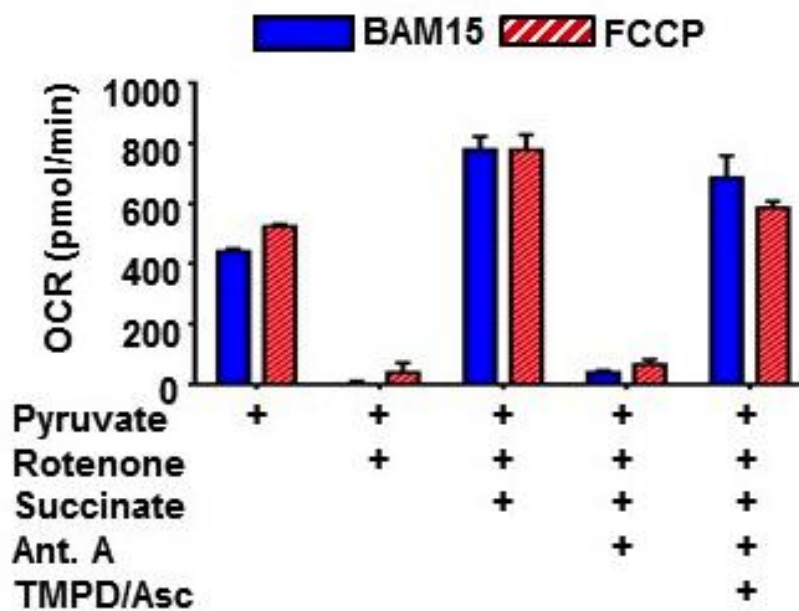


Figure 16: BAM15-mediated respiration is not complex-specific and is not due to electron donation.

Isolated mouse liver mitochondria respiring on pyruvate and malate in the presence of FCCP (5 μ M) or BAM15 (5 μ M) were treated sequentially with rotenone (4 μ M), succinate (10 mM), Antimycin A (4 μ M), and the electron donors TMPD (100 μ M) and ascorbate (10 mM). $N = 3$ wells/condition.

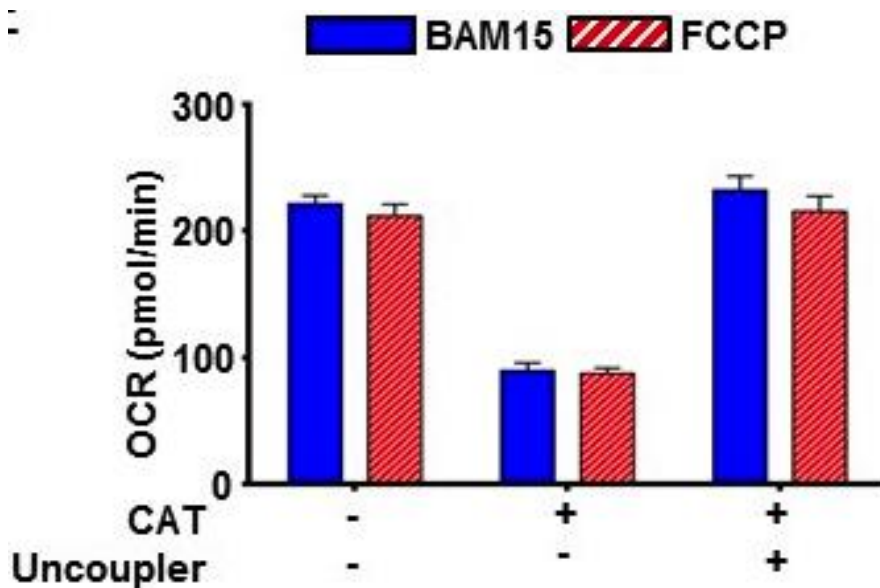


Figure 17: BAM15 increases oxygen consumption independent of the adenine nucleotide translocase.

Oxygen consumption rate (OCR) was measured on permeabilized C2C12 cells respiring on succinate (10 mM) and treated with rotenone (2 μ M) and ADP (4 mM). Mitochondria were then treated with carboxyatractyloside (CAT, 3 μ g/mL), followed by FCCP or BAM15 (1 μ M). $N = 6-9$ per condition over three separate experiments.

2.3.6 BAM15 does not depolarize the plasma membrane

Since FCCP is known to have off-target effects on the plasma membrane, which results in PM depolarization, we measured the effects of BAM15 *versus* FCCP on plasma membrane electrophysiology in L6 cells using whole cell voltage and current clamp recordings. As expected, under voltage clamp conditions at a holding potential of -70 mV, FCCP induced an inward current (**Figure 18 A-E**) that was dose-dependent and associated with an increase in conductance (**Figure 18 F**). In contrast, BAM15 elicited no appreciable change in current in the same cells. Under current clamp conditions, FCCP caused reversible and repeatable plasma membrane depolarization (**Figure 18 G-H**), whereas BAM15 had no effect. The differential effects of BAM15 and FCCP on plasma membrane properties were independent of the order of uncoupler application (not shown).

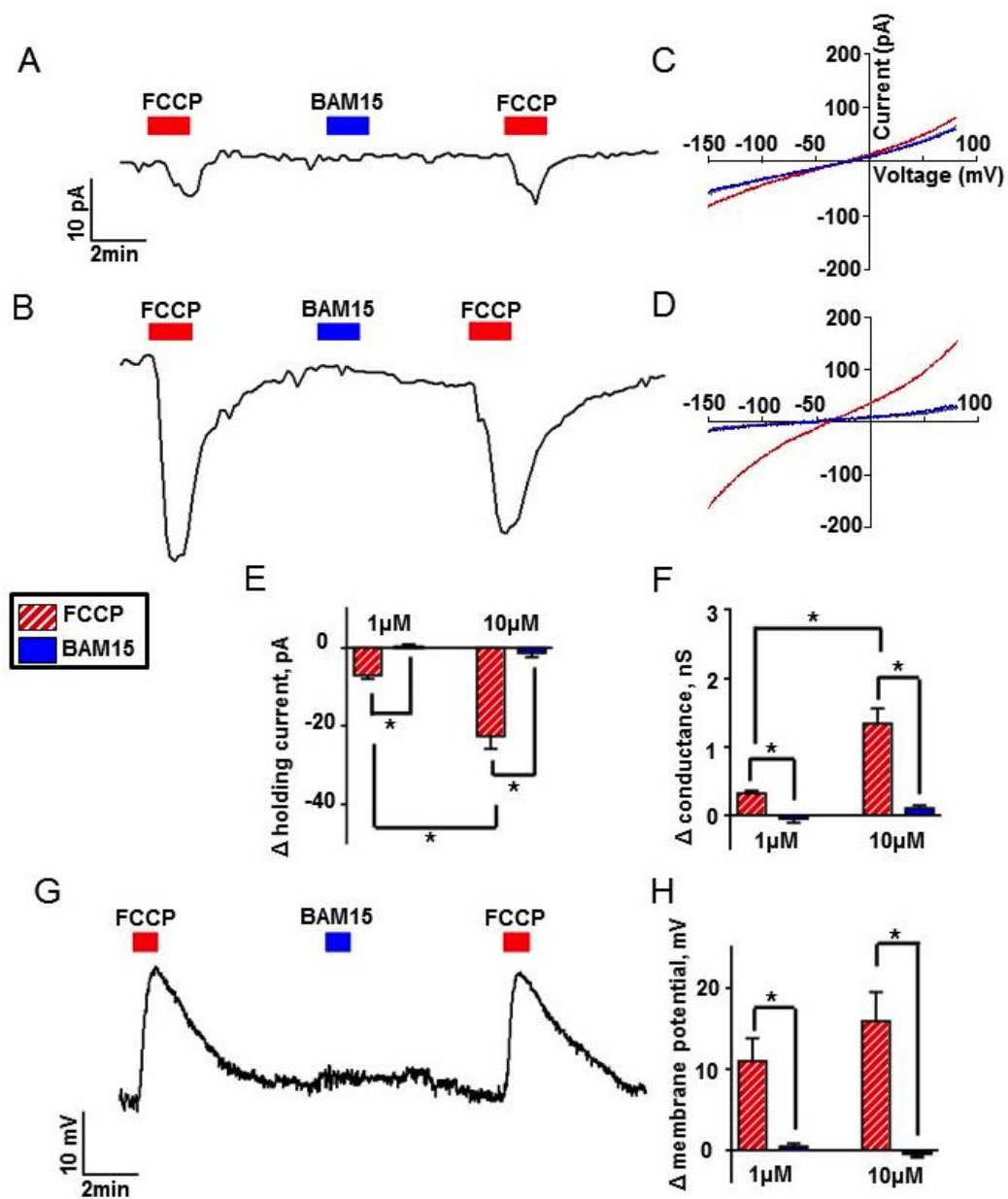


Figure 18: BAM15 does not alter plasma membrane electrophysiology.

(A) Representative whole cell voltage clamp recording from a L6 cell showing the holding current (at -70 mV) during exposure to FCCP and BAM15 (both 1 μ M). (B) Voltage clamp with 10 μ M FCCP and BAM15. (C and D) Currents were elicited with a voltage ramp from -150 mV to $+80$ mV using 1 μ M uncouplers in (C) and 10 μ M uncouplers in (D); I - V relationships are plotted under control conditions and in the

presence of the uncouplers. (E) Average data comparing the change in holding current caused by FCCP and BAM15 at 1 μM and 10 μM . (F) Average data comparing the change in conductance generated by either drug in the range of -130 mV to -60 mV. (G) Representative whole cell current clamp recording at concentrations of 10 μM for FCCP and BAM15. (H) Average data comparing the change in membrane potential by both drugs. Error bars indicate SEM. For (E)–(H), * indicates $p < 0.05$ by two-way ANOVA with Bonferroni's posttest, $N = 7$ – 9 cells per condition.

2.3.7 BAM15 demonstrates significantly less intracellular acidification than FCCP

Depolarization of the plasma membrane causes proton influx into the cell. This, along with the sharp increase in glycolysis and the hydration of CO₂ to form H⁺ decreases intracellular pH³⁶⁸. The sharp decrease in intracellular pH is hypothesized to be responsible for mitochondrial failure by limiting the ability of metabolic enzymes to fuel mitochondria²⁶. Since mitochondrial failure occurs quickly, we measured intracellular pH after two minutes of uncoupler treatment to be able to measure the initial decrease in intracellular pH caused by the increase glycolytic flux. Following two minutes of uncoupler treatment, BAM15 and FCCP both caused nearly equal decreases in intracellular pH at 1 μM (**Figure 19**). When cells were treated with 10 μM uncouplers, the dose in which mitochondrial failure was observed in whole cells with FCCP but not BAM15, intracellular pH decreased further with FCCP but not BAM15 despite BAM15 demonstrating increased respiration and ECAR at these doses. This suggests that the intracellular acidification observed with FCCP is not related to increased nutrient oxidation, and is likely caused by proton influx into the cell at the plasma membrane.

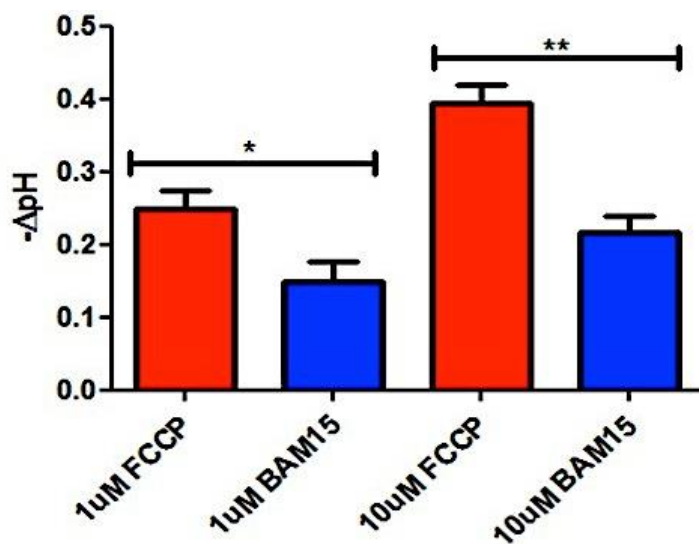


Figure 19: BAM15 causes less intracellular acidification compared to FCCP.

L6 cells were loaded with SNARF-1 were treated for 2 min with the indicated doses of uncouplers prior to measurements of intracellular pH. Error bars indicate SEM. * indicates $p < 0.05$ by Student's t-test comparing each dose. $N = 3$.

2.3.8 BAM15 is less cytotoxic than FCCP

Chronic ATP depletion caused by mitochondrial uncouplers can lead to cell cycle arrest and apoptosis. Thus, we measured cellular ATP concentrations in L6 cells with 1 μM and 10 μM BAM15 and FCCP for six hours. Despite decreasing $\Delta\Psi_m$, BAM15 treated cells showed no significant change in cellular ATP concentrations compared to vehicle-treated cells after six hours of treatment (**Figure 20**). FCCP treated cells, however, contained significantly less ATP. Furthermore, BAM15-treated cells were more viable after 48 hours than FCCP-treated cells when administered across a broad dosing range up to 50 μM (**Figure 21**). These data indicate that cultured cells can generate sufficient ATP when mitochondria are uncoupled, and that BAM15 does not share the adverse nonmitochondrial effects of other uncouplers that may decrease ATP concentrations and contribute to cytotoxicity.

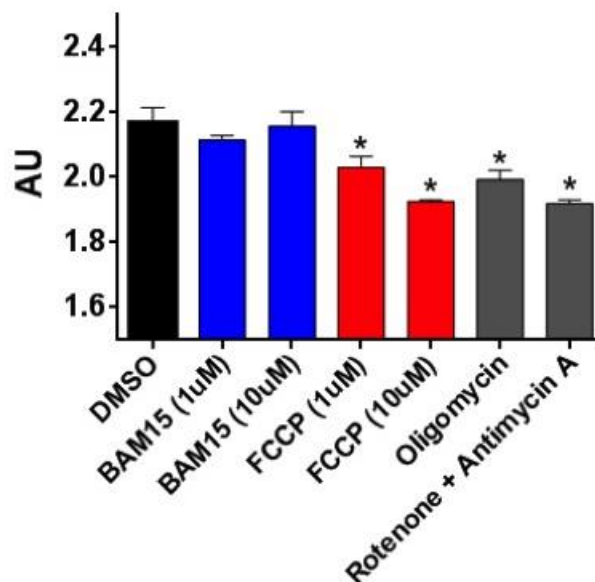


Figure 20: BAM15 does not decrease ATP concentrations.

ATP concentrations were measured in L6 cells treated with the indicated concentrations of BAM15, FCCP, oligomycin, or Rotenone and Antimycin A for six hours. * indicates statistical significance compared to DMSO as determined by one-way ANOVA with Dunnett's posttest. Error bars indicate SEM. $N = 3$ wells/condition.

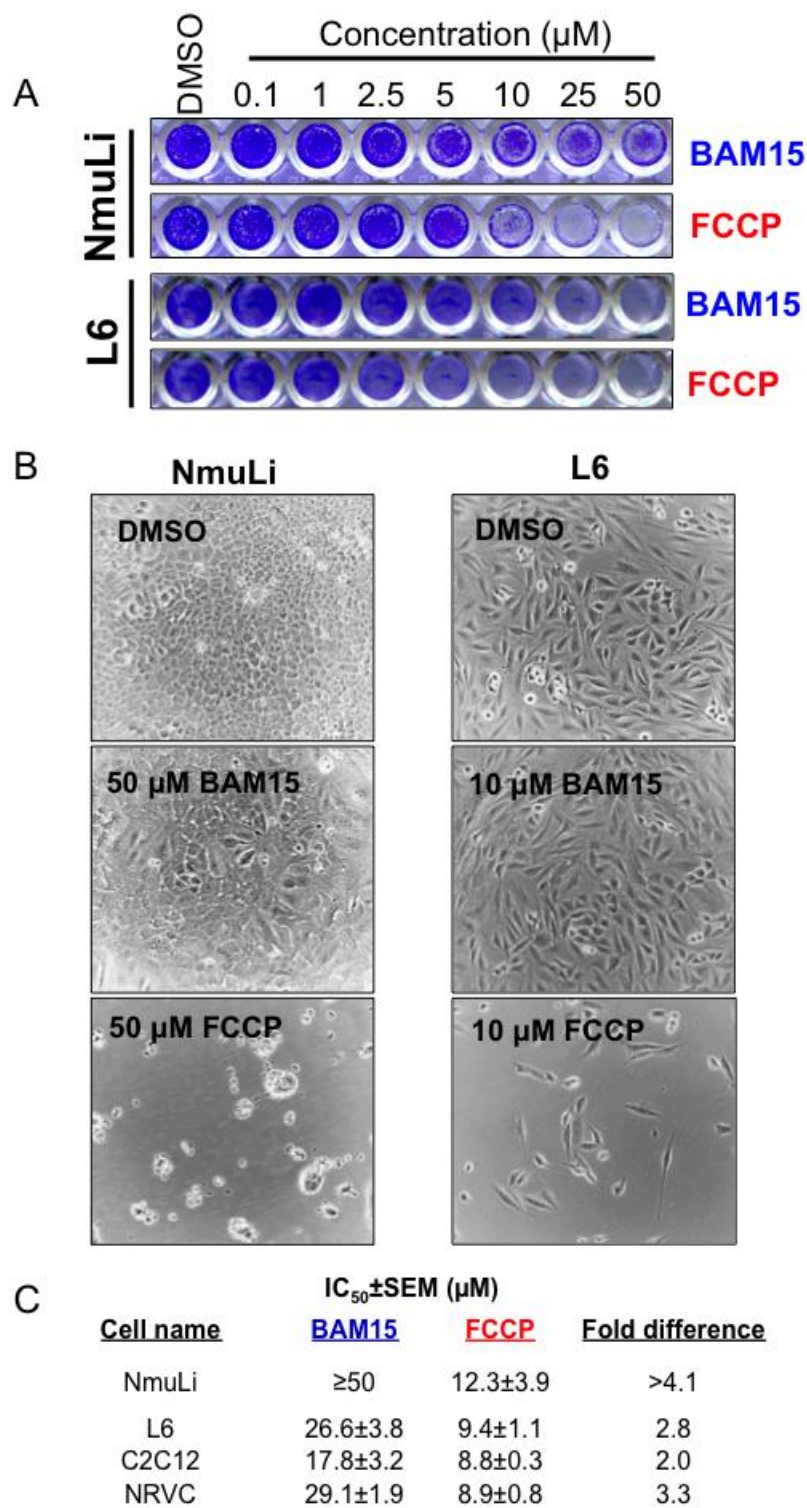


Figure 21: BAM15 is less cytotoxic than FCCP.

A: L6 and NMuLi cells were treated with increasing concentrations of BAM15 or FCCP for 48 hours and stained with crystal violet. B: L6 and NMuLi cells were treated with FCCP or BAM15 for 48 hours and viewed with phase microscopy. C: IC50 values of C2C12, NRVCs, L6, and NMuLi cells were calculated via MTT assay or crystal violet staining.

2.4 Discussion

Synthetic mitochondrial uncouplers are invaluable tools for the analysis of mitochondrial function and they represent possible therapeutics for diabetes, obesity, neurodegeneration, cancer, ischemia-reperfusion injury, and other disorders linked to mitochondrial dysfunction. However, a possible factor limiting the use of available protonophore uncouplers is their unwanted activity at the plasma membrane, which causes intracellular acidification independent of metabolic flux. The overarching goal of this study was to identify new mitochondrial uncouplers that lack activity at the plasma membrane with the goal of generating an uncoupler with broader dynamic range. We identified BAM15 as a bona-fide mitochondrial uncoupler that does not affect plasma membrane conductance, causes significantly less intracellular acidification, and has a broad effective range. The mechanism by which BAM15 has a preference for protonophore activity at mitochondria but not the plasma membrane is unclear, but may be due to a pKa of its ionizable protons, which has been measured to be 7.4. However, other alternative explanations exist and include the possibility that BAM15 may have a structural preference for the unique lipid composition of the mitochondrial inner membrane, or that either the protonated or deprotonated form of BAM15 is membrane impermeable. BAM15 may also undergo dimerization reactions similar to DNP in the mitochondrial inner membrane, which may be due to lipid composition or be driven by the relatively high (approximately 180 mV)³⁶⁹ membrane potential of the mitochondrial inner membrane compared to the plasma membrane of an L6 cell (-40-50 mV)³⁷⁰.

The initial characterization of BAM15 has answered several important questions concerning the effects of pharmacological mitochondrial uncoupling on cellular function.

For example, since some metabolic substrates utilize the pH gradient to enter mitochondria, it is thought that mitochondrial depolarization is a limiting factor for mitochondrial respiration²⁶. Indeed, FCCP-induced mitochondrial failure coincides with the loss of $\Delta\Psi_m$; however, we observed that BAM15 was fully capable of stimulating maximal mitochondrial respiration at concentrations above 10 μM where the mitochondria were fully depolarized. These data suggest that FCCP-induced mitochondrial failure is not due to mitochondrial depolarization and instead may be caused by off-target effects, such as plasma membrane depolarization. Furthermore, when BAM15 and FCCP were used at high concentrations (20–60 μM) in isolated mitochondria, BAM15 was able to continuously drive a greater rate of respiration than FCCP. The FCCP-induced decline in mitochondrial respiration was less pronounced in isolated mitochondria than the decline observed in whole cells, which indicates that the deleterious effects of FCCP are most likely due to its extra-mitochondrial actions. Consistent with this notion, BAM15 was significantly less cytotoxic than FCCP. Finally, BAM15 treatment stimulated ECAR to a greater rate than FCCP. Since ECAR is a correlative measure of glycolysis (proton co-transport with lactate out of the cell), these data demonstrate that FCCP is not able to maximally drive the metabolic capacity of the cell. Although FCCP has been used for more than 50 years to assay maximal mitochondrial function, these data demonstrate that FCCP underestimates maximal mitochondrial and cellular metabolic capacity. Therefore, BAM15 is a more reliable chemical tool for the study of mitochondrial function, particularly in living cells.

**CHAPTER 3: MECHANISTIC DETERMINATION OF THE PROTONOPHORE
ACTIVITY OF BAM15**

3.1 Introduction

We have identified a novel mitochondrial protonophore, named BAM15, which does not depolarize the plasma membrane. While we have validated that BAM15 is a proton transporter, the exact mechanism by which BAM15 translocates protons into the mitochondrial matrix is not known. The goal of this study was to determine the structural properties of BAM15 that allow protonophoric activity in mitochondria, to elucidate which parts of the molecule are transporting protons, and to determine if BAM15 can be modified to increase or decrease potency. We have determined that BAM15 acts through acid-base proton translocation of two ionizable protons, and that the pKa of these ionizable protons can be modified to adjust potency. We have also determined which parts of the BAM15 molecule are essential for uncoupling activity, which allows for full customization of the BAM15 ‘core’ for proton translocating properties across lipid bilayers.

3.2 Results

3.2.1 The lipophilic furazano ‘core’ of BAM15 is required for activity

Mitochondrial protonophores are typically hydrophobic weak acids. Because FCCP is known to ‘cycle’ within the lipid bilayer, we hypothesized that BAM15 demonstrated a similar mechanism of action. If this were the case, we hypothesized that the furazano core of BAM15 (**Figure 22 A**) would be required for membrane implantation and proton transport. To test this, two BAM15 derivatives, SHC121007 (**Figure 22 B**) and SHC121009 (**Figure 22 C**), were synthesized. SHC121007 contains a pyrazine group in place of the furazano group, with the only difference being the

elimination of the oxadiazole in the furazano core. SHC121009 contains the oxadiazole only, and does not have the pyrazine component of the furazano core. As expected, both of these compounds failed to stimulate respiration in L6 cells up to a concentration of 10 μM (not shown). This demonstrates that the hydrophobic core, which is most likely required for membrane implantation, is necessary for protonophore activity.

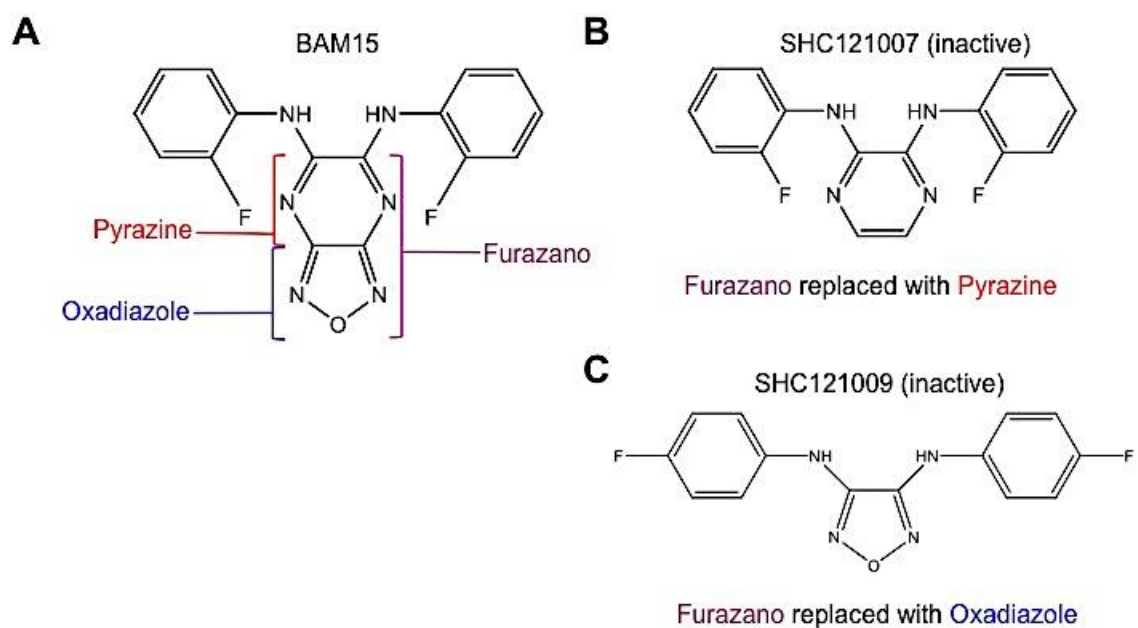


Figure 22: The furazano core of BAM15 is required for uncoupling activity.

Structures of SHC121007 (top) and SHC121009 (bottom). SHC121007 lacks the oxadiazole portion of the furazano core, and SHC121009 lacks the pyrazine group in the furazano core. Both compounds do not stimulate OCR or ECAR at doses from 0.01-10 μM in L6 cells. $N = 6$ wells/condition

3.2.2 Determination of the ionizable proton location of BAM15

FCCP is a hydrophobic weak acid that contains one ionizable proton which utilizes the pH gradient across the mitochondrial inner membrane to shuttle protons into the matrix. The location of BAM15's ionizable protons were hypothesized to be attached to one of three pairs of nitrogen atoms located in the compound. There are two pairs of nitrogen groups in the furazano ring, with one pair in the pyrazine and the other in the oxadiazole component. Elimination of either of these groups ablated BAM15 activity, but it was likely this was due to a lack of membrane implantation. The last pair of potential ionizable protons rests in the aniline group attached to the furazano core (**Figure 23**). To test if these protons were required for activity, oxygen was used as a replacement for nitrogen, which would not coordinate an ionizable proton (**Figure 23**). N to O substitution at these locations resulted in a complete loss of activity with respect to OCR and ECAR, suggesting that these sites contained the ionizable protons of BAM15.

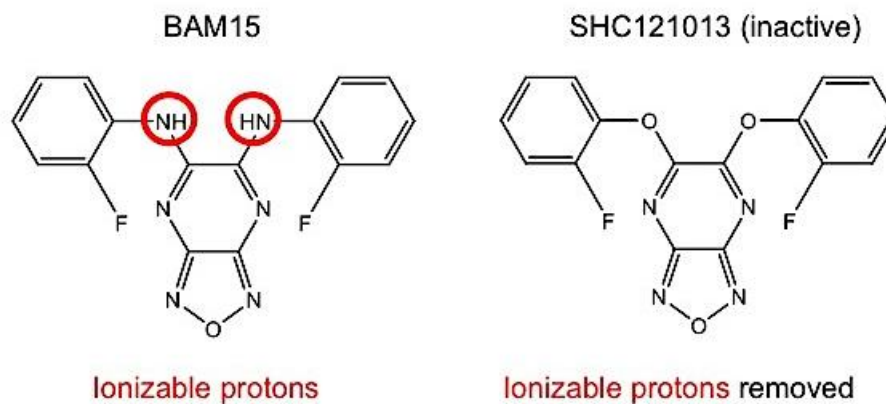


Figure 23: Identification of ionizable protons of BAM15.

BAM15 contains two ionizable protons (left) that are necessary for uncoupling activity.

When the ionizable protons are removed by substituting the amine with an ether

(SHC121013, right) the compound is inactive with respect to OCR and ECAR from a

dose of 1-10 μM in L6 cells. $N = 6$ wells/condition.

3.2.3 The potency of BAM15 is dependent on the electron withdrawing groups

FCCP is a lipophilic weak acid, and the potency can be modified by the addition or subtraction of electron-withdrawing groups (**Section 1.4.2**). BAM15 has two fluorines located on the ortho position on benzyl rings that do not contain a potential ionizable proton (**Figure 24 A**). To test if BAM15 had acid-base mitochondrial protonophore activity, we generated multiple derivatives that contained different electron-withdrawing groups on the benzyl rings away from the potential sites of ionizable protons. Changing the position of halogen electron withdrawing groups from the ortho position to the meta (SHC121005) and para (SHC121003) positions had little effect on potency or dynamic range with respect to OCR (**Figure 24 B-C**). While SHC121005 caused similar changes to ECAR compared to BAM15 (**Figure 25 A**), SHC121003 demonstrated significantly less ECAR despite stimulating OCR at a similar rate (**Figure 25 B**). This indicates that the sharp increases in glycolytic flux seen from BAM15 and SHC121005 may not be a requirement to maintain mitochondrial function when mitochondria are uncoupled.

Removal of halogen groups from the benzyl rings resulted in a more than ten-fold decrease in potency with regard to OCR (**Figure 26 B**) and ECAR (**Figure 27 A**). To decrease electron density around potential ionizable protons a second fluorine was added to each fluorobenzyl ring in the para position. This resulted in an increase in activity by approximately ten-fold with respect to OCR (**Figure 26 C**) and ECAR (**Figure 27 B**). These data demonstrate that BAM15 contains two ionizable protons that translocate across the mitochondrial inner membrane via an acid-base reaction into the mitochondrial matrix. These data suggest that either BAM15's molecular mass or the

pKa of the ionizable protons govern protonophore potency. Furthermore, this data suggests that fluorine-mediated charge shielding does not decrease the potency of BAM15 as observed with other fluorinated protonophores.

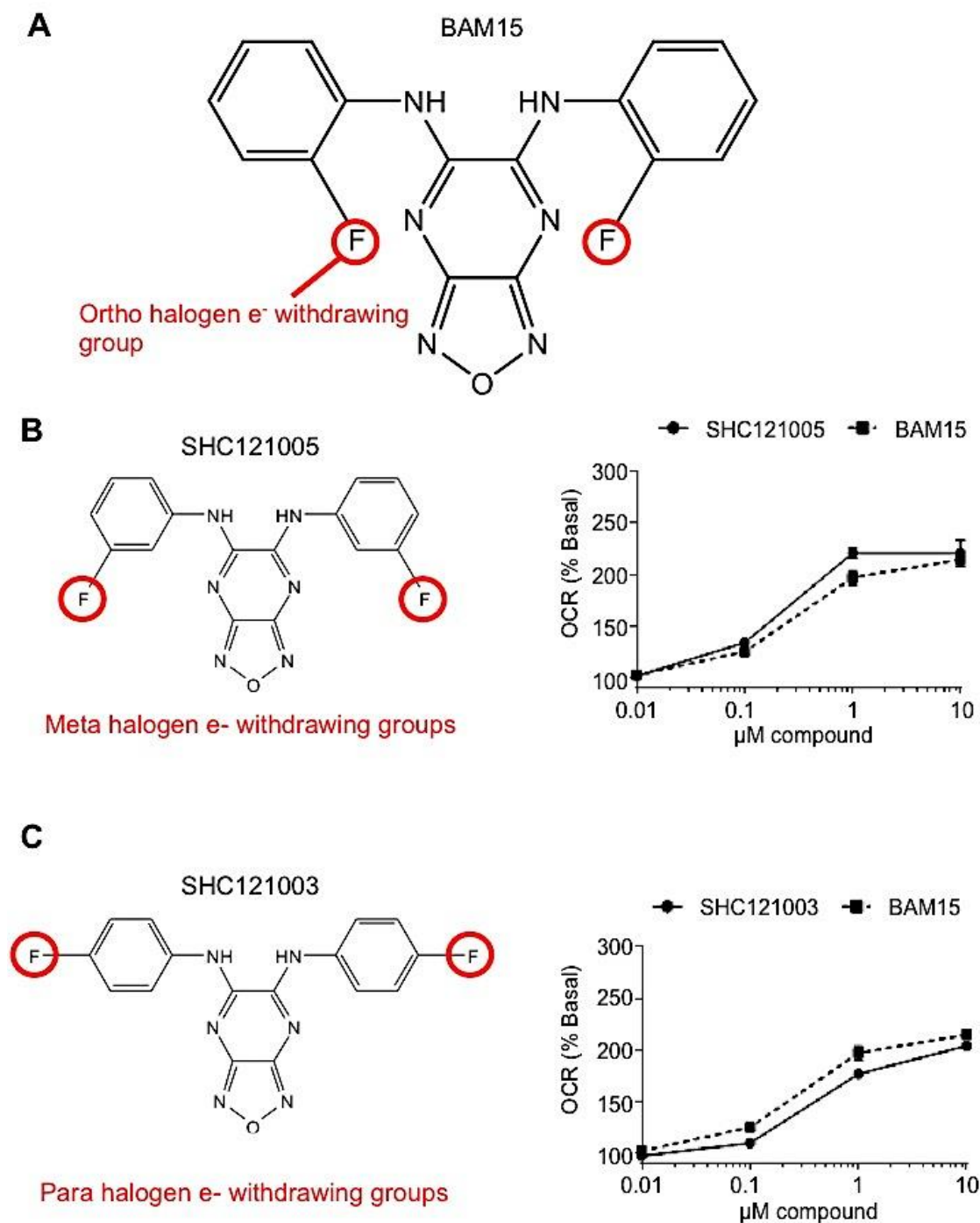


Figure 24: Alterations of halogen positioning have little effect on potency or dynamic range.

A: BAM15 contains an electron withdrawing fluorine in the ortho position. Substitution of a fluorine in the meta (B, left) and para (C, left) have no effect on potency or dynamic

range with respect to OCR (right) in L6 cells. Error bars indicate SEM. $N = 6$ wells/group.

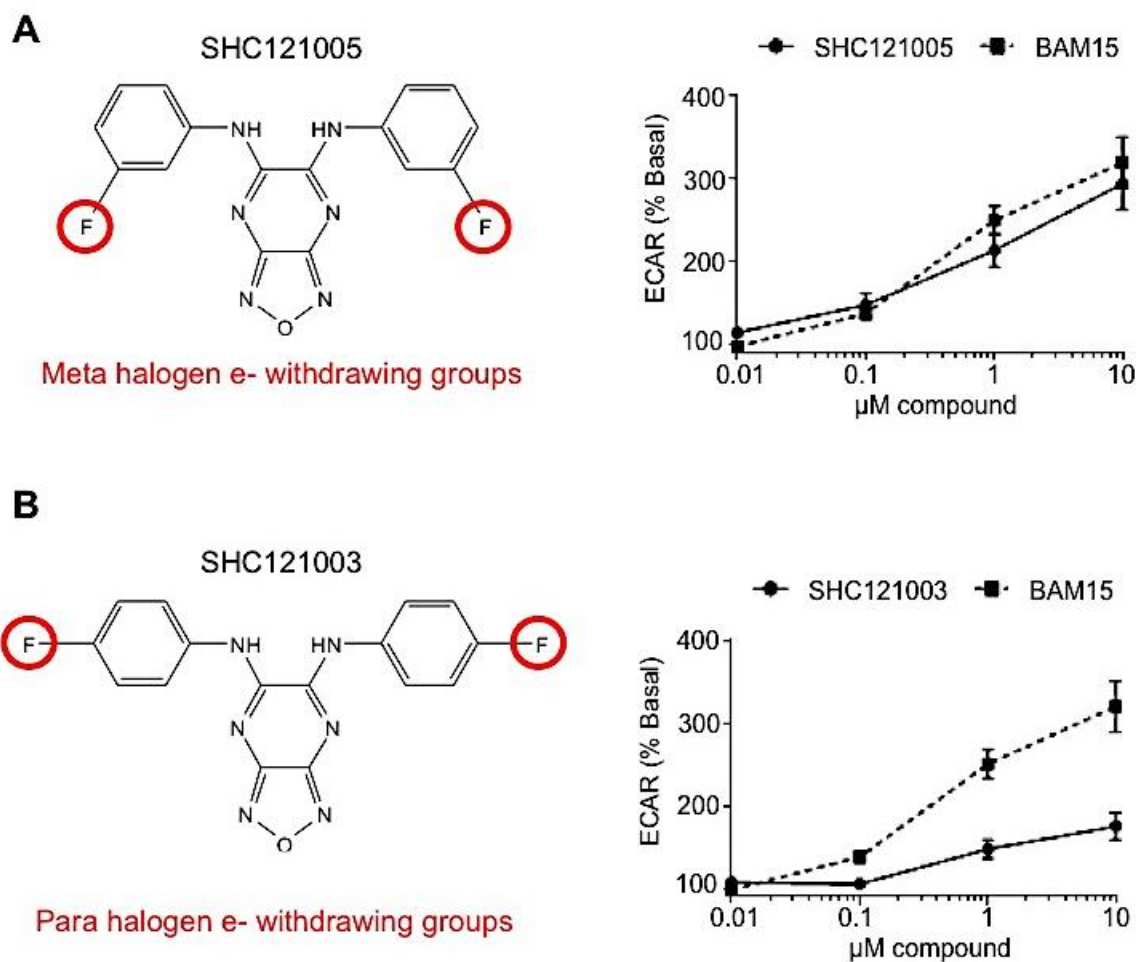


Figure 25: Para, but not meta halogen positioning decreases ECAR compared to BAM15.

A: Substitution of fluorine in the meta position (left) has little effect on ECAR in L6 cells (right). B: Substitution of fluorine in the para position (left) decreases ECAR compared to BAM15 in L6 cells (right). Error bars indicate SEM. $N = 6$ wells/group.

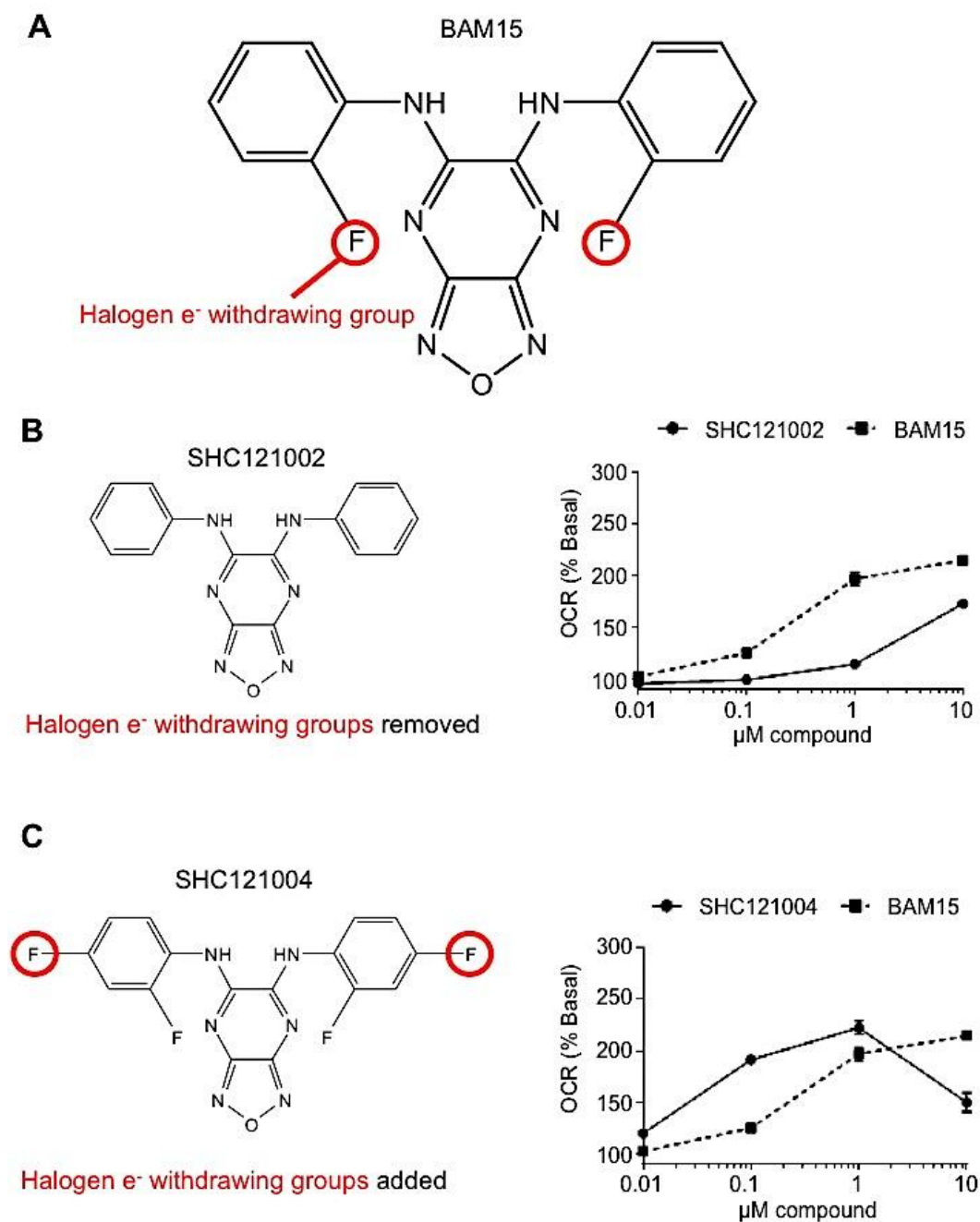


Figure 26: Modification of electron density alters potency of the BAM15 family of uncouplers.

A: BAM15 contains halogen electron withdrawing groups. B: SHC121002 lacks halogen electron withdrawing groups (left) and is less potent than BAM15 with respect to OCR in L6 cells (right). C: SHC121004 contains additional fluorines in the para position (left),

which increases potency with respect to OCR in L6 cells (right). Error bars indicate SEM.

$N = 6$ wells/condition.

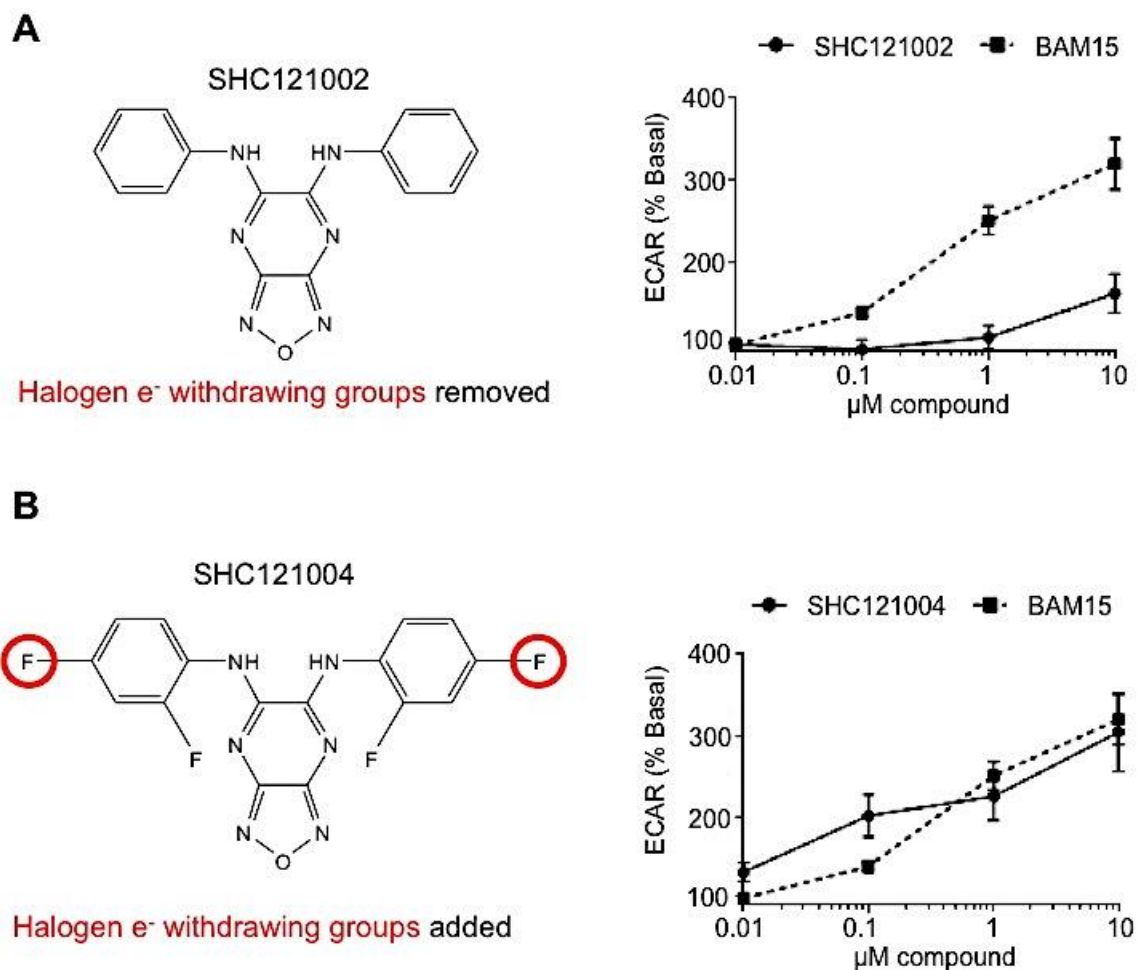


Figure 27: Modification of electron density alters potency of the BAM15 family of uncouplers with respect to ECAR.

A: SHC121002 lacks halogen electron withdrawing groups (left) and is less potent than BAM15 with respect to ECAR in L6 cells (right). C: SHC121004 contains additional fluorines in the para position (left), which increases potency with respect to ECAR in L6 cells (right). Error bars indicate SEM. $N = 6$ wells/condition

3.2.4 The dynamic range of BAM15 is dependent on symmetric fluorination

The ability of BAM15 to selectively target mitochondrial membranes and avoid mitochondrial failure may be due to specific protonophore activity at the mitochondria. BAM15 is a fluorinated symmetric anion, which indicates that fluorine substituents may shield charge in specific membrane environments, thus confining cyclic acid-base protonophore activity to specific environments. To test if fluorination was critical for BAM15's dynamic range, the fluorobenzyl groups of BAM15 were replaced with chlorobenzyl groups (BAM8, **Figure 28 A**). Although chlorine has similar electronegativity and molecular mass, unlike fluorine the addition of chlorine has little effect on lipophilic anion membrane translocation³³⁹. As expected, this modification had little effect on potency with respect to OCR (**Figure 28 B**) and ECAR (**Figure 28 C**). However, BAM8 demonstrated a similar dynamic range to FCCP with respect to OCR (**Figure 28 B**) and ECAR (**Figure 28 C**), which suggests that a combination fluorine-mediated charge shielding only seen in symmetrical lipophilic anions and a pKa that falls within a narrow window is critical to broad dynamic range of BAM15.

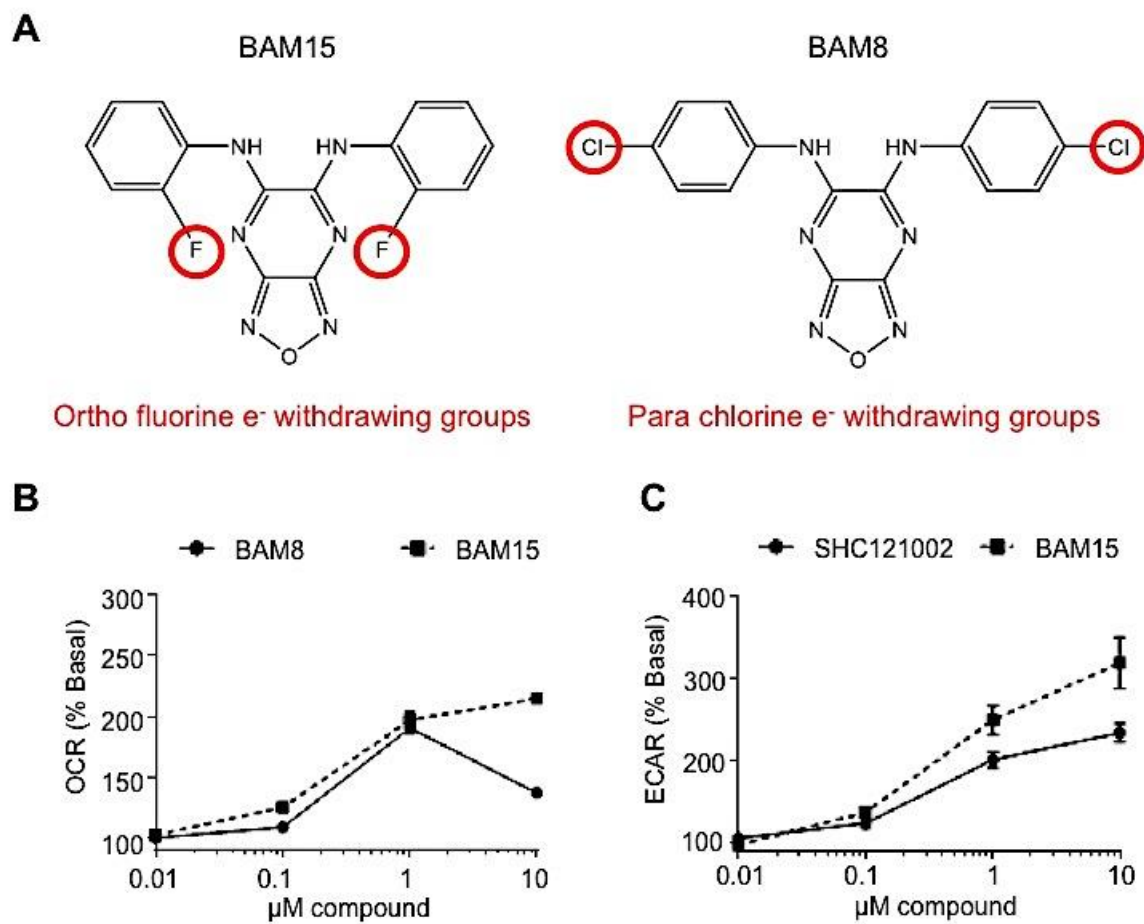


Figure 28: Electron-withdrawing fluorines are critical for dynamic range

A: BAM8 contains a chlorine in the para position (right) instead of a fluorine in the ortho position (left). B: BAM8 does not have broad dynamic range with respect to OCR (left) and stimulates less ECAR (right) in L6 cells.

3.2.5 Alkyl chains can be utilized as a source of electron density

For further structure-activity analysis of BAM15, we determined if the benzyl rings were required for protonophore activity. To test this, we replaced these groups with alkyl chains of increasing length to progressively draw electron density away from the ionizable proton and increase potency (**Figure 29**). As predicted, the potency was dependent on the length of the alkyl chain with respect to OCR (**Figure 29 B-D**) and ECAR (**Figure 30 A-C**). Elimination of the amide containing the ionizable proton in these molecules (**Figure 31 B**) ablated activity even if electronegativity was increased with a trifluoro substituent (**Figure 31 C**), suggesting that these compounds acted as protonophores similar to BAM15.

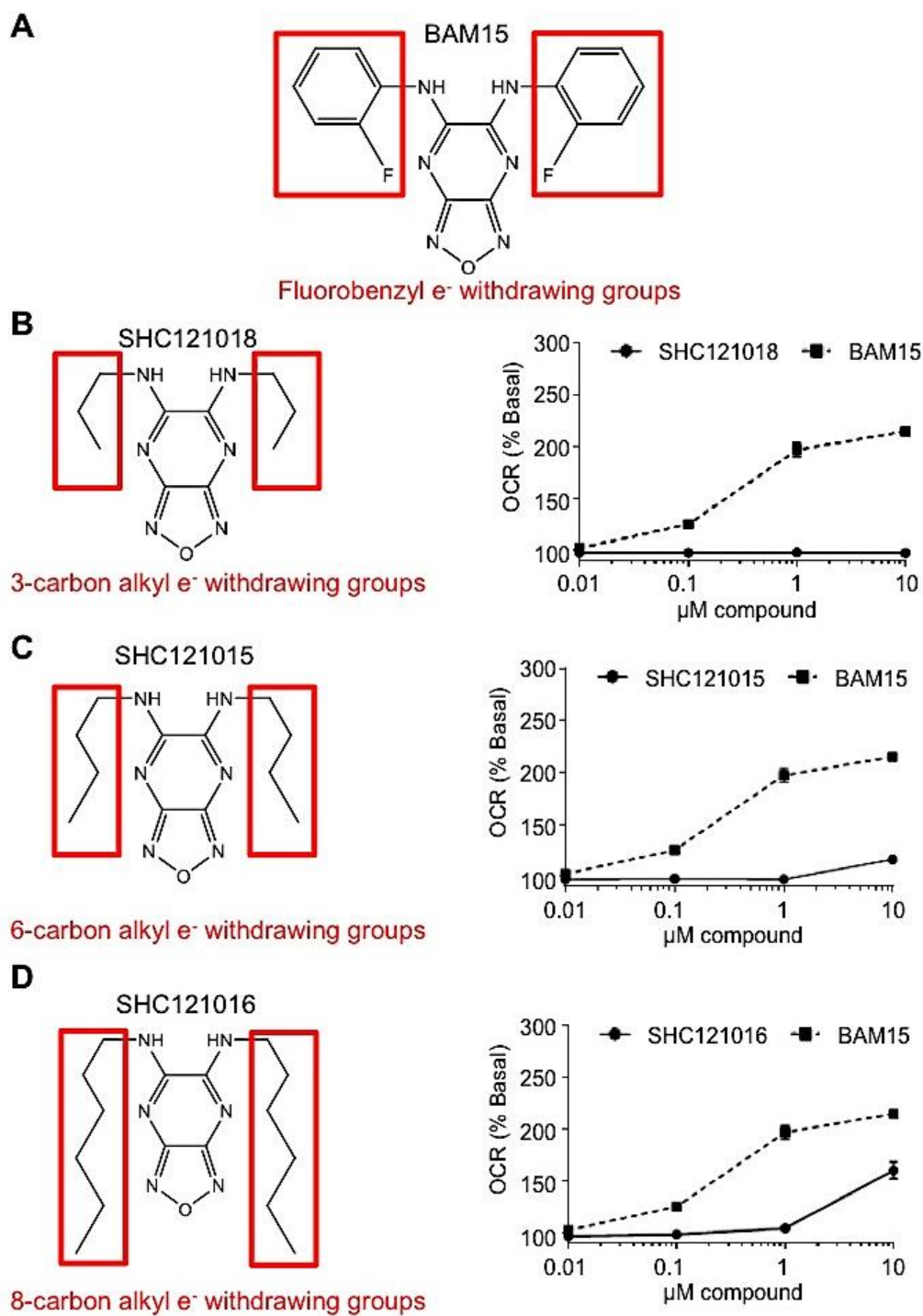


Figure 29: Alkyl chains can be utilized as electron withdrawing groups.

A: BAM15 contains fluorobenzyl electron withdrawing groups. B: 3-carbon alkyl chains (left) are not sufficient to promote uncoupling activity from a dosing of 0.1-10 μM (right). The addition of four-carbon (C, left) and eight-carbon (D, left) alkyl chains

increase potency with respect to OCR in L6 cells (C and D, right). Error bars indicate SEM. $N = 6$ wells/group.

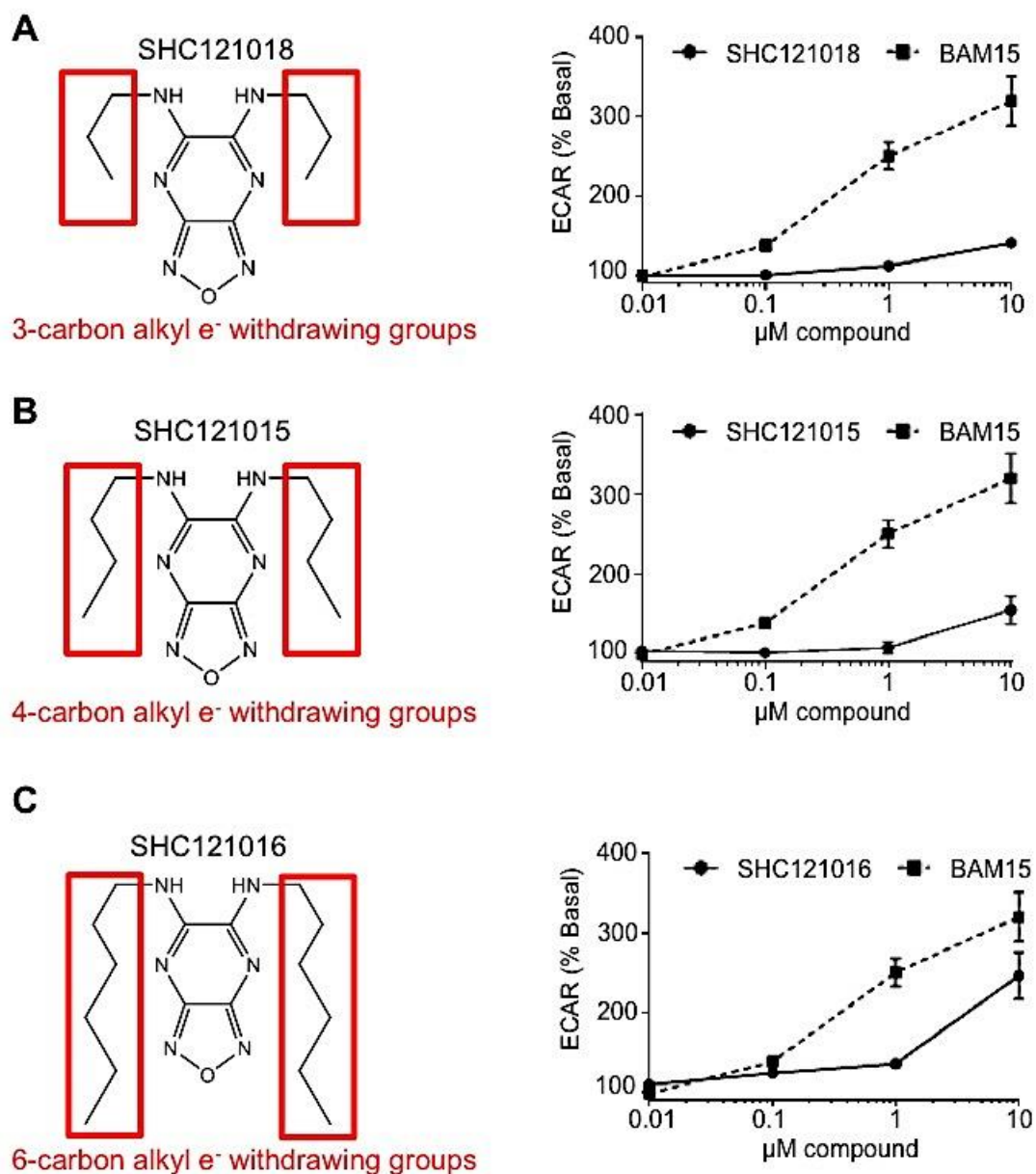


Figure 30: Effects of utilizing alkyl chains as electron withdrawing groups on ECAR are similar to OCR.

A: 3-carbon alkyl chains (left) increases ECAR (right). The addition of four-carbon (B, left) and eight-carbon (C, left) alkyl chains increase potency with respect to ECAR (C and D, right) in L6 cells. Error bars indicate SEM. $N = 6$ wells/group.

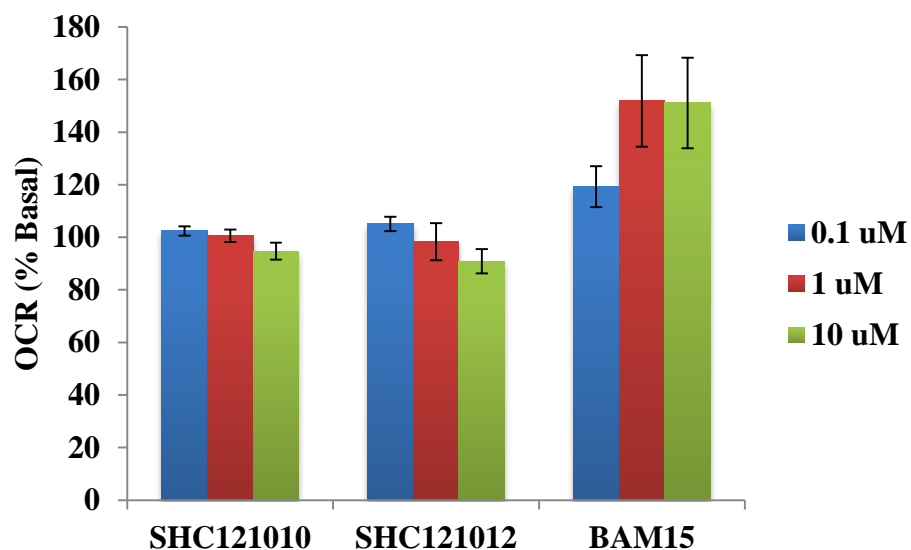
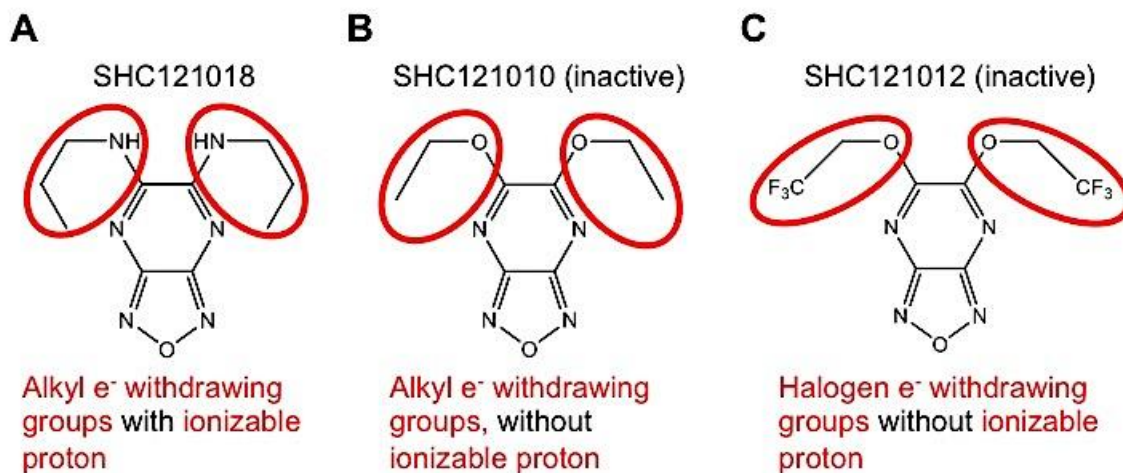


Figure 31: BAM15 derivatives that do not contain benzyl electron withdrawing groups utilize the same ionizable proton as BAM15.

A: BAM15 derivative containing alkyl electron withdrawing groups. B: Removal of ionizable proton in BAM15 derivative lacking benzyl electron withdrawing groups eliminates uncoupling activity tested using a dosing range of 0.1-10 μ M in L6 cells. C: Addition of highly electronegative trifluoro group without an ionizable proton does not rescue uncoupling activity using a dosing range of 0.1-10 μ M in L6 cells. $N = 4-6$ wells/group.

3.3 Discussion

BAM15 was characterized as a mitochondrial protonophore that does not depolarize the plasma membrane, but the exact mechanisms of how BAM15 translocates protons into the mitochondrial matrix remained unclear. The goal of this study was to determine which parts of the BAM15 molecule were required for uncoupling activity, if the potency of the molecule could be customized, and if fluorine-mediated charge shielding was critical for dynamic range. We conclude that BAM15 contains ionizable protons linked to amide groups linked to the pyrazine in the furazano core. Eliminating fluorine-mediated charge shielding greatly decreases the dynamic range of BAM15, which suggests that shielding of the ionizable proton is critical for broad dynamic range. Importantly, the uncoupling activity of BAM15 can be achieved so long as the furazano core and associated amide groups remain intact.

The BAM15 backbone allows for a considerable lipophilic acid customization, which can allow for highly specific pKa values that allow for proton transport across membranes that contain aqueous environments of specific pH values. In conclusion, this study provides a mechanism by which BAM15 translocates protons across lipid bilayers and identifies a novel scaffold for which other protonophores can be synthesized. This will allow for customized electrophysiological studies across membrane bilayers of other organelles, which cannot be achieved using traditional protonophores. For example, lowering the pKa by the addition of electron withdrawing groups would provide a stronger acid which could be used to evaluate proton transport activity across organelles that have highly acidic lumens, such as lysosomes. Removal of electron withdrawing

groups and increasing the pKa would not allow BAM15 to transport protons into alkaline environment of the mitochondrial matrix.

The structure-activity relationships outlined may also be used to generate an uncoupler that induces 'mild' uncoupling and is self-limited by the acidification of mitochondria. A molecule with a pKa greater than the pH of the mitochondrial inner membrane would not dissociate an ionizable proton as the mitochondrial matrix acidified, which would allow for a self-limiting uncoupler. This would be advantageous for the use of uncouplers in obesity, where the goal is to induce the futile oxidation of nutrients but to maintain a broad dosing range that does not induce hyperthermia. This would also be advantageous for diseases in which 'mild' uncoupling could be valuable such as ischemia-reperfusion injury, in that only small amounts of proton leak would be generated over broad dosing ranges. In sum, the structure activity relationships described outline the BAM15 'core', which allows for a fully customizable protonophore with a broad range of potential applications both for the study of bioenergetics in multiple organelles and potential therapeutic applications in which uncoupling is beneficial but currently unsafe due to narrow dosing ranges.

Increasing the potency of BAM15 with respect to OCR increased the potency with respect to ECAR, which suggests that that two are directly related to one another. Elimination of uncoupling activity was concomitant with an elimination of ECAR, which demonstrates that the oxidative and glycolytic relationships that the BAM15 family of uncoupling agents demonstrates are not due to off-target effects of the molecule. This is a significant finding because it validates the use of BAM15 to study the relationship between glycolysis and oxidative phosphorylation by modifying $\Delta\Psi_m$. The structure of

BAM15 can also be modified to maintain uncoupling activity without the use of halogen groups. This allows for further customization of BAM15. The effects on OCR utilizing carbon chains as electron withdrawing groups mirrored that of ECAR, which demonstrates that these derivatives can also be utilized for metabolic studies.

Alteration of the furazano core eliminates the functional ability of BAM15 to uncouple mitochondria. This suggests that the development of a hydrophobic weak acid is not sufficient for the uncoupling activity of these molecules, and that the hydrophobic core must be large enough to implant itself within the membrane similar to FCCP. It is not clear, however, if the alterations of the furazano core of BAM15 eliminates its ability to enter the cell or mitochondria. The ability to eliminate the uncoupling activity of BAM15 and the necessity for fluorobenzyl groups suggests that BAM15 may be selective for the mitochondrial inner membrane, or modifiable to target specific membranes within the cell to initiate proton leak across membranes that have lipid compositions that allow BAM15 translocation.

We observed that moving the ortho fluorine substituents on BAM15 to the meta position (SHC121005) had little effect on OCR and ECAR, but moving fluorine to the para position (SHC121003) had little effect on OCR but strangely decreased ECAR compared to BAM15. The reason for this is unknown, but future studies may determine if SHC121003 affects intracellular acidification or perhaps inhibits cellular proton/lactate efflux at the plasma membrane. Measuring lactic acid production in the presence of SHC121003 may present a clearer representation of how much extracellular acidification can be attributed to increases in aerobic metabolic flux in our experimental system.

Substituting the fluorine substituents of BAM15 with chlorine (BAM8) had little effect on potency but decreased the dynamic range of the compound. It is not known if this occurs due to the pKa of the ionizable proton of BAM8 compared to BAM15, or if BAM8 has different rates of anion diffusion or dimerization in the mitochondrial inner membrane or other membranes compared to BAM15. Because a difference in potency was not observed it is possible that fluorine substituents are required to shield charge of BAM15 in non-mitochondrial membranes or when the mitochondria is depolarized. Future studies utilizing charged liposomes and pKa measurements will be necessary to determine the role of fluorine on BAM15-mediated proton transfer across charged phospholipid bilayers of different lipid compositions.

**CHAPTER 4: BAM15 PROTECTS FROM RENAL ISCHEMIA-REPERFUSION
INJURY**

4.1 Introduction

Mitochondrial uncouplers have beneficial antioxidant effects that are a consequence of reducing PMF (**Section 1.2**), and genetic and pharmacologic uncoupling have favorable effects on disorders that are linked to mitochondrial oxidative stress including ischemic-reperfusion injury (**Section 1.3.3**). Renal ischemia-reperfusion injury has been linked to oxidative stress, but uncoupling agents have not been demonstrated to be efficacious at protecting from renal IRI. The pathogenesis of renal IRI is centered on ROS-mediated apoptosis and immune cell recruitment, which occludes the vasculature and extends the ischemic period (**Section 1.3**). In this study we hypothesized that BAM15 could protect from renal IRI by reducing immune cell recruitment into the vasculature and decreasing tubular necrosis. The goal of this study was to first develop a means of utilizing BAM15 *in vivo*. A method for measuring BAM15 in plasma was developed, which allowed the development of a drug vehicle that provided a suitable half-life for BAM15. Second, we sought to determine BAM15-induced mitochondrial uncoupling could protect from renal IRI.

4.2 Materials and methods

4.2.1 BAM15 mass spec analysis

Analyses were performed using a triple quadrupole mass spectrometer (AB-Sciex 4000 Q-Trap) coupled to a Shimadzu LC-20AD LC system equipped with a Supelco Discovery C18 column (50 mm × 2.1 mm × 5 μm bead size). A binary solvent system (total flow 1 ml/min) was used that consisted of the following solvents; Solvent A: 79.9% H₂O, 20% methanol, 0.1% formic acid; Solvent B: 99.9% methanol, 0.1% formic acid.

Chromatographic runs started at 100% A for 0.5 min, a linear gradient to reach 100 % at 5.6 min, then 100% B for 4.4 min, and finally 100% solvent A for 1 min (11 min total). Measurements were carried out in positive mode using the following transition m/z 341.1 \rightarrow m/z 122.0, and the following settings (in volts): DP: 91, EP: 10; CE:55 ; CXP: 8. Quantification was carried out by measuring peak areas using the software Analyst 1.5.1. Retention time for BAM15 was 4.5 min.

4.2.2 Pharmacokinetics

BAM15 was prepared in 50% PEG + 3% DMSO and was injected ip. Blood was taken via tail vein at the indicated time points and collected in heparinized Microtainer blood collection tubes. The samples were centrifuged 16,000 x g for 3 min at 4°C to isolate plasma. 10 μ L of plasma was added to 200 μ L 9:1 acetonitrile:methanol to precipitate protein. The samples were centrifuged 16,000 x g for 15 min to pellet protein and the supernatant was used for mass spectrometry analysis.

4.2.3 Renal ischemic reperfusion injury

All animals were handled and procedures were performed in adherence to the National Institutes of Health Guide for the Care and Use of Laboratory Animals, and all protocols were approved by the University of Virginia Institutional Animal Care and Use Committee. Male mice (8-week old, C57BL/6, from the National Cancer Institute, Frederick, MD) were anesthetized with a mixture (i.p.) of ketamine (120 mg/kg), xylazine (12 mg/kg), and atropine (0.324 mg/kg) and were subjected to bilateral ischemic reperfusion injury (26 min ischemia, then 24 h or 48 h reperfusion) as previously described³⁷¹. During the surgery, mouse core temperature was maintained at 34–36 °C with a heating pad; during the

recovery and reperfusion period, mice were housed in a warming incubator with ambient temperature at 30–32 °C. Control, sham-operated mice underwent a similar procedure, but the renal pedicles were not clamped. Mice were i.p. injected with BAM15 at 1 or 5 mg/kg, 1 h before kidney IR. Vehicle mice were also injected with the same solution BAM15 was prepared with (3% DMSO in 50% PEG400).

4.2.4. Assessment of kidney function and histology

Plasma creatinine, as a measure of kidney function, was determined using a colorimetric assay according to the manufacturer's protocol (Sigma-Aldrich). For histology, kidneys were fixed overnight in 0.2% sodium periodate/1.4% DL-lysine/4% paraformaldehyde in 0.1 M phosphate buffer (pH 7.4) and embedded in paraffin. Kidneys were prepared for H&E staining and viewed by light microscopy (Zeiss Axioskop). Photographs were taken and brightness/contrast adjustment was made with a SPOT RT camera (software version 3.3; Diagnostic Instruments). Acute tubular necrosis was assessed as previously described [23]. Stained kidney sections were scored in a blinded manner. The score was based on the percentage of outer medulla tubules with pink casts on the inside, which is a marker of tubular necrosis. The scoring system was as follows: 1 (<10%), 2 (10–25%), 3 (25–75%), and 4 (>75%).

4.2.5. Kidney FACS analysis

Flow cytometry was used to analyze kidney leukocyte content. In brief, kidneys were extracted, minced, digested, and passed through a filter and a cotton column as described³⁷². After blocking non-specific Fc binding with anti-mouse CD16/32 (2.4G2), fresh kidney suspensions were incubated with fluorophore-tagged anti-mouse CD45 (30-

F11) to determine total leukocyte cell numbers. CD45-labeled samples were further used for labeling with different combinations of anti-mouse F4/80 (BM8), GR-1 (Ly6G), CD11b, CD11c, IA (MHCII). 7-Aminoactinomycin D (7-AAD; BD Biosciences) was added 15 min before analyzing the sample to separate live from dead cells. Flow cytometry data acquisition was performed on a FACSCalibur (Becton Dickinson). Data were analyzed by FlowJo software 9.0 (Tree Star).

4.3 Results

4.3.1 BAM15 can be measured via LC-MS/MS

To measure BAM15 in plasma, we generated a method to measure BAM15 by liquid chromatography coupled to mass spectrometry. To measure a compound via mass spectrometry it must ionize by electrospray ionization (ESI) and fragment into ions of predictable mass/charge (m/z) ratios. As shown in **Figure 32**, BAM15 ionized in the mass spectrometer as indicated by a peak at 341.4. The ability to ionize allowed us to perform a precursor ion scan (PIS), which resulted in fragmentation into three major ions at m/z 122, 162, and 120. Utilizing the m/z of 122, we determined that BAM15 was split into a positive ion of m/z 122 and a neutral fragment with a mass of 219 amu (**Figure 33**). To determine if BAM15 loses any chemical groups that cannot be accounted for, we performed neutral loss scanning. Neutral loss scanning determined that BAM15 did not lose any chemical groups during mass spec due to ionization (**Figure 34**), which confirmed that we could reliably measure the compound using the fragmentation pattern from the PIS. A standard curve with BAM15 added to plasma confirmed that the signal

intensity from the parent ions in the PIS demonstrated a linear relationship with molar concentration of BAM15 (**Figure 35**).

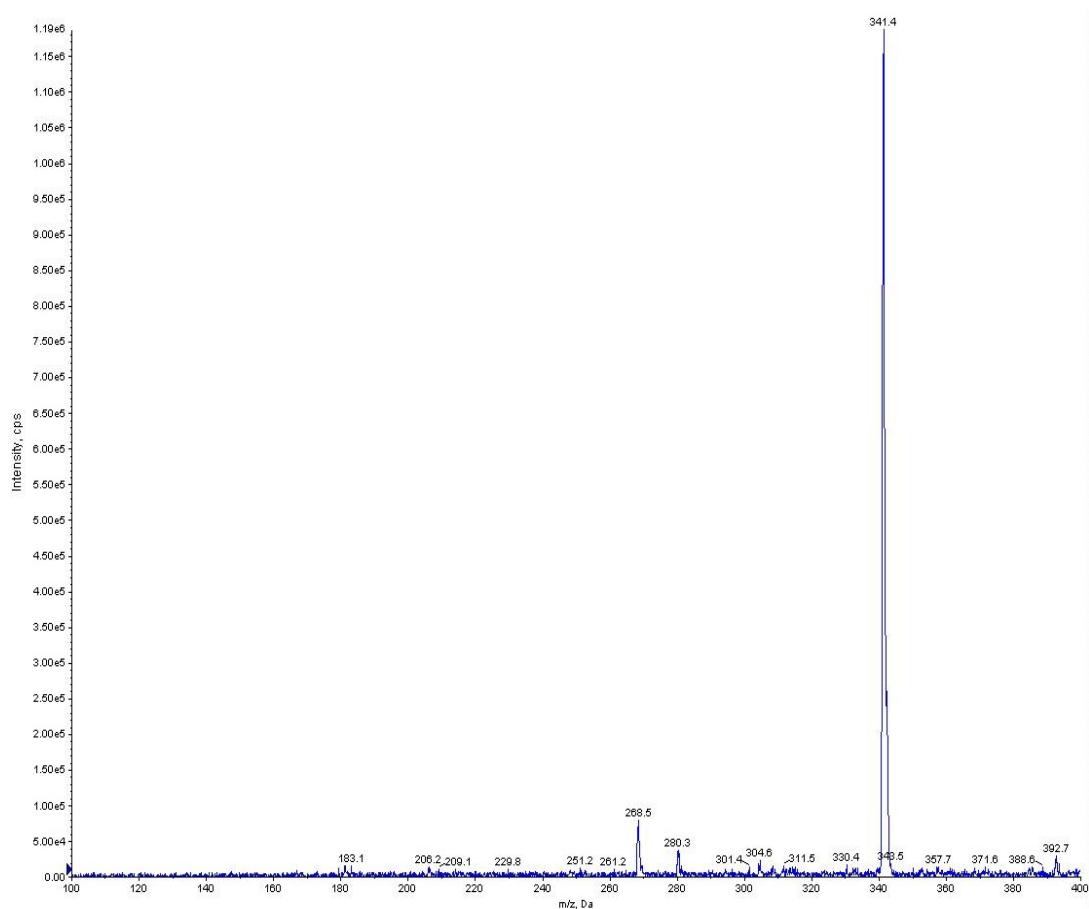


Figure 32: Precursor ion scan following direct injection of BAM15.

Precursor ion scanning of BAM15 demonstrates that BAM15 can ionize via ESI/Turbospray ionization. BAM15 shows an m/z of 341.4 which was used for further studies.

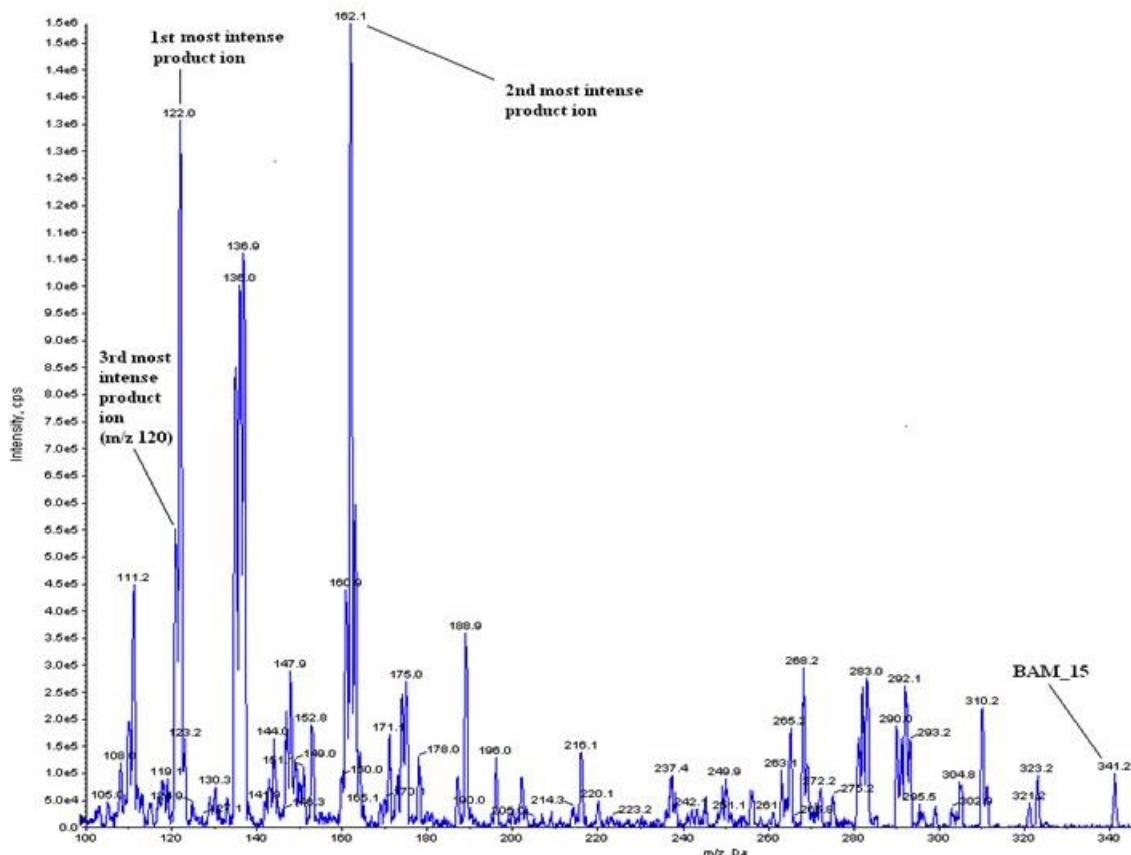


Figure 33: Fragmentation of BAM15 following collision.

BAM15 generates three product ions at m/z 122.0, 162.1, and 120.0. The most intense positive ion of m/z 122.0 can be used along with a neutral fragment of $m = 219$. These transitions can be used to measure BAM15.

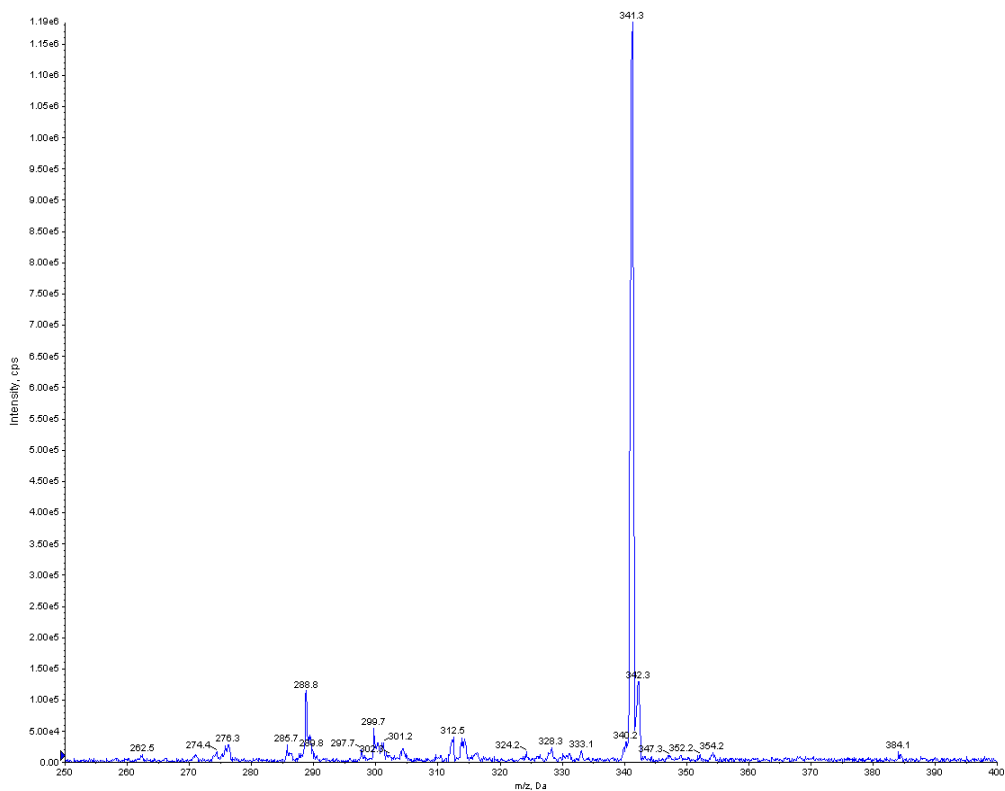


Figure 34: Neutral loss scan of BAM15 using the most abundant product ion.

BAM15 was directly injected into a mass spectrometer and neutral loss scanning was performed using the product ion m/z of 122.0. A signal was observed at a neutral loss of $m = 219$ which was equal to the m/z of BAM15.

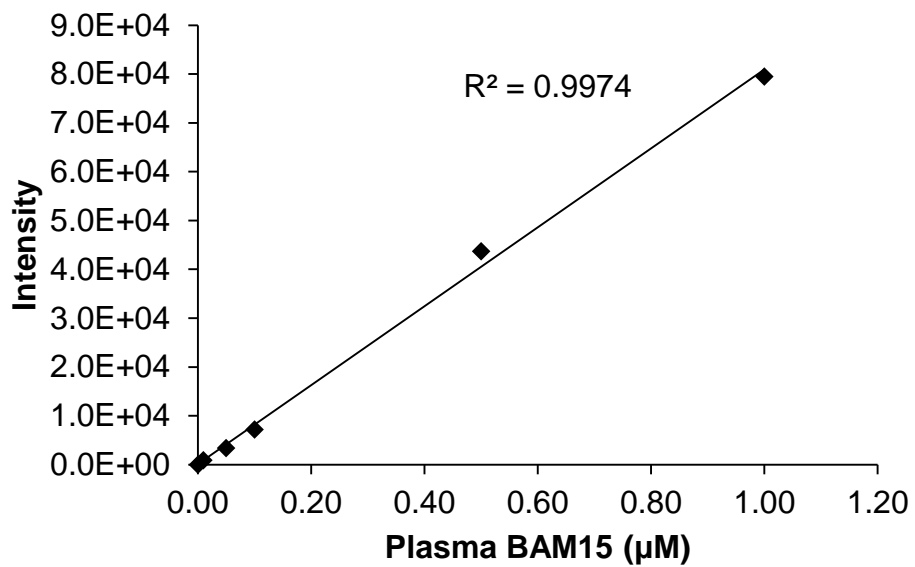


Figure 35: Standard curve of BAM15 as measured via LC-MS/MS.

Standard curve of BAM15 measured via LC-MS/MS demonstrating 0, 0.01, 0.05, 0.1, 0.5, and 1 µM BAM15 extracted from plasma.

4.3.2 Pharmacokinetic profile of BAM15

To determine the pharmacokinetic profile of BAM15, we injected 3mg/kg BAM15 ip in a vehicle of 50% polyethylene glycol 400 (PEG400) and 3% dimethyl sulfoxide into C57/B6 mice. This method was used because pegylation of compounds increases the half-life by reducing renal clearance and slowing the rate of absorption of small molecules^{373,374}. As shown in **Figure 36**, BAM15 had a half-life of approximately 30 min. To test if BAM15 was orally available, PEG was not used as a vehicle because it irritates the stomach³⁷⁵ and small intestine³⁷⁶. To administer BAM15 orally it was complexed to beta-hydroxypropylcyclodextrine (HPCD). By administering BAM15 orally in this vehicle we determined that BAM15 was orally available as demonstrated by measurable concentrations of BAM15 in plasma (**Figure 37**). This also indicated that BAM15 can pass through hepatic circulation without being modified, as the parent ions of BAM15 were still detectable by mass spectrometry.

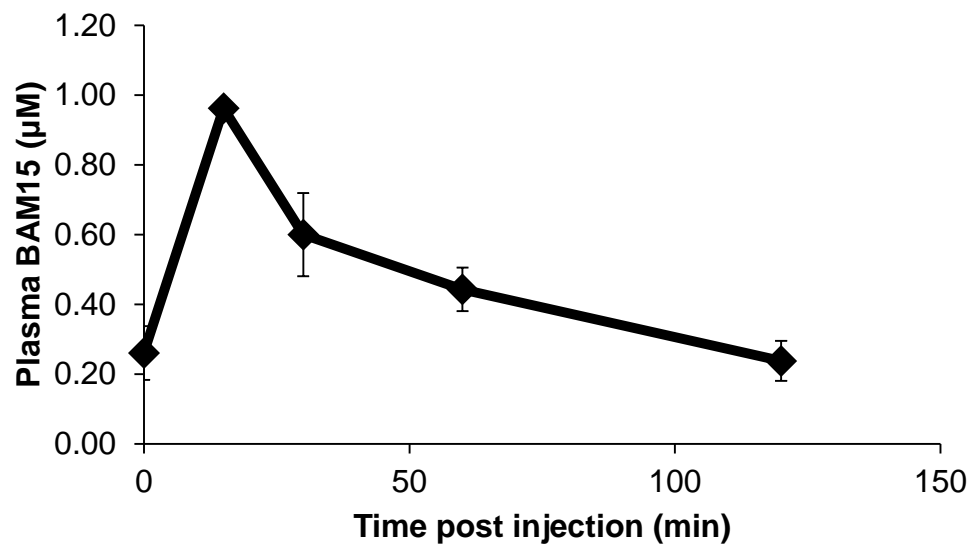


Figure 36: Pharmacokinetics of BAM15.

BAM15 (3mg/kg in 50% PEG400 and 3% DMSO) was injected into C57BL/6 mice and plasma concentrations were measured over time. T₀ indicates the plasma drug concentration immediately following injection. Error bars indicate SEM. *N* = 3.

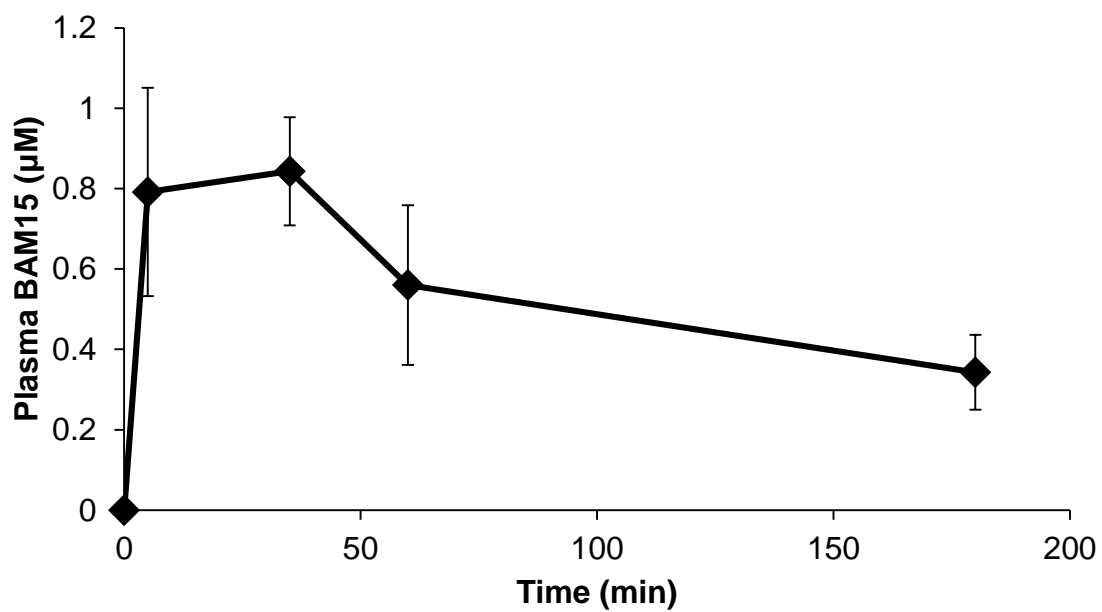


Figure 37: BAM15 is orally available.

BAM15 (5mg/kg in 2% HPCD, 50 mM glycine, pH 10.0) was administered via oral gavage. T_0 indicates the plasma concentration of BAM15 immediately following administration. Error bars indicate SEM. $N = 3$.

4.3.3. BAM15 decreases immune cell infiltration and protects from renal IRI

Mitochondrial uncoupling, both pharmacological and endogenous, is protective in preclinical models of ischemia-reperfusion injury^{284,377,378}. To determine whether BAM15 treatment could protect mice from ischemic reperfusion injury we administered BAM15 as a single intraperitoneal bolus at 1 or 5 mg/kg 1 h prior to 26 min of bilateral renal ischemia. We hypothesized that mitochondrial uncoupling by BAM15 would decrease tubular necrosis by decreasing immune cell infiltration into the renal medulla. 48 hours after reperfusion, we observed significantly less infiltration of all leukocytes (**Figure 38 A**) and macrophages (**Figure 38 B**) in a dose-dependent manner. Importantly, we observed significantly less infiltration of neutrophils (**Figure 38 C**), the immune cell type most responsible for occluding the vasculature and inducing further necrosis. Interestingly, we did not observe any significant changes in dendritic cell populations from IRI or BAM15, suggesting that these cells do not play a significant role in our models.

At 24 and 48 h following reperfusion, plasma creatinine levels were measured. Compared to vehicle-treated mice, animals that received BAM15 were protected from kidney injury as indicated by lower plasma creatinine levels at 24 and 48 h post-ischemia (**Figure 39**), reduced tubular necrosis (**Figure 40 A-B**), less depletion of brush border villi, less obstruction of proximal tubules (**Figure 40 B**).

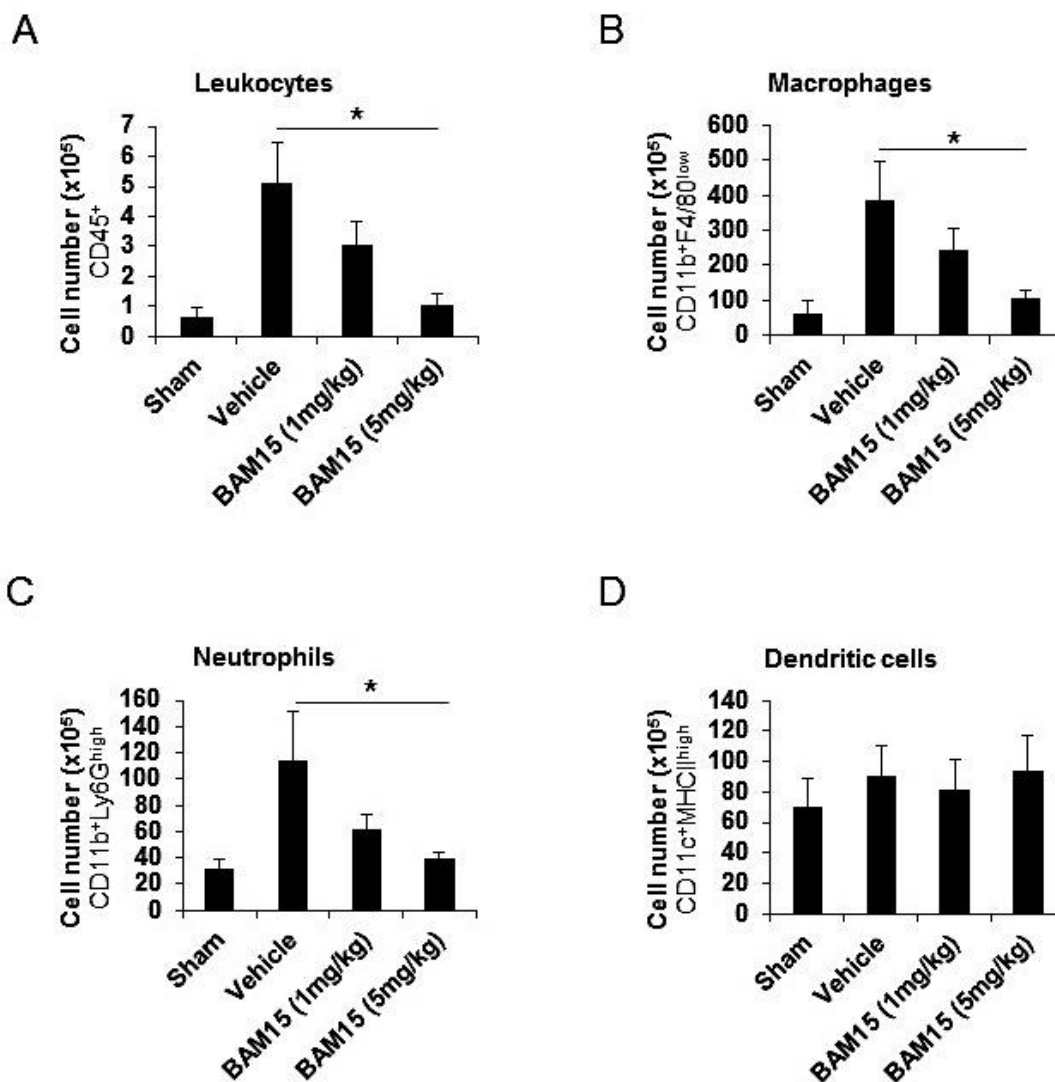


Figure 38: BAM15 decreases immune cell invasion following renal IRI.

Male mice (8-week old, C57BL/6) were treated with vehicle control (VC) or BAM15 at 1 or 5 mg/kg 1 h prior to bilateral ischemia for 26 min followed by 48 h of reperfusion. Sham-operated mice underwent an identical surgical procedure, but the renal pedicles were not clamped. BAM15 pretreatment reduced the concentration of Leukocytes (A), Macrophages (B), and Neutrophils (C). BAM15 did not affect the concentration of Dendritic cells (D). * indicates a statistically significant ($p > 0.05$) difference between

vehicle and BAM15-treated groups by one-way ANOVA with Dunnett's posttest. $N = 3-6$ mice.

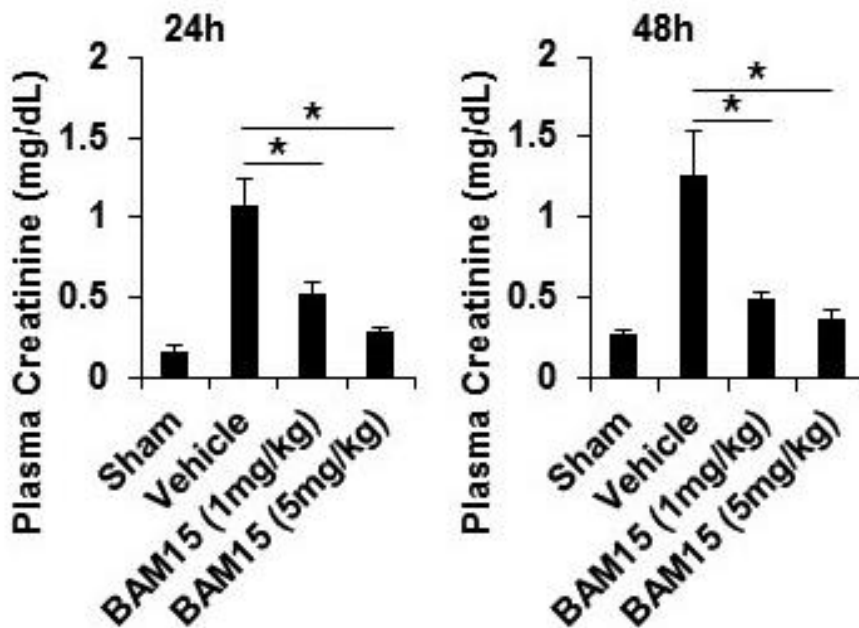


Figure 39: BAM15 protects against kidney ischemic-reperfusion injury.

Male mice (8-week old, C57BL/6) were treated with vehicle control (VC) or BAM15 at 1 or 5 mg/kg 1 h prior to bilateral ischemia for 26 min followed by 48 h of reperfusion. Sham-operated mice underwent an identical surgical procedure, but the renal pedicles were not clamped. BAM15 pretreatment dose-dependently protected from kidney damage, as indicated by the decreased plasma creatinine levels at 24 and 48 h following reperfusion, compared to VC. Error bars indicate SEM. * indicates $p < 0.05$ compared to vehicle control by one- way ANOVA with Dunnett's posttest. N = 3-6 mice per group.

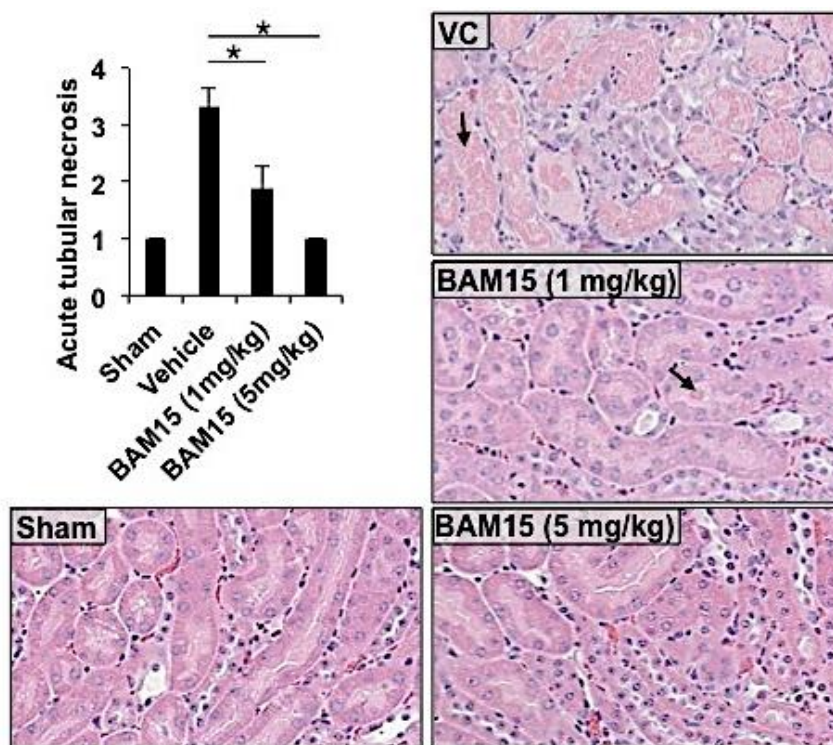


Figure 40: BAM15 pretreatment decreased acute proximal tubular necrosis of the kidney medulla 48 h following reperfusion.

Male mice (8-week old, C57BL/6) were treated with vehicle control (VC) or BAM15 at 1 or 5 mg/kg 1 h prior to bilateral ischemia for 26 min followed by 48 h of reperfusion.

Sham-operated mice underwent an identical surgical procedure, but the renal pedicles were not clamped. BAM15 decreased ATN as shown by numerical scoring (top left) and histological analysis. Arrows indicate sites of tubular cell death (VC) and casts (BAM15 1mg/kg). Error bars indicate SEM. * indicates a statistically significant ($p > 0.05$) difference between vehicle and BAM15-treated groups by one-way ANOVA with Dunnett's posttest. $N = 3-6$ mice.

4.4 Discussion

Mitochondrial uncoupling is an attractive drug target due to its ability to lower mitochondrial ROS production. Low concentrations of uncouplers are demonstrated to have beneficial effects in cell culture and animal models of insulin resistance³⁷⁹, obesity³⁸⁰, protect from neurodegeneration^{381–384}, traumatic brain injury³⁸⁴, and cardiovascular disease^{385,386}. Our data demonstrated that BAM15 treatment dose-dependently protected from renal ischemia-reperfusion injury, indicating that BAM15 is bioactive *in vivo*.

The protective effects of BAM15 from renal ischemia-reperfusion were seen by several readouts. BAM15 reduced plasma creatinine levels, which suggests improved GFR and an amelioration of renal damage. However, creatinine levels alone are not a definitive measure of renal function since it is a summation of creatinine production and excretion. Because of this, we measured other parameters of renal health to determine if the changes in plasma creatinine reflected renal health. Administration of BAM15 prior to renal IRI significantly reduced ATN, which suggests that mitochondrial uncoupling has protective effects against IRI by preventing necrosis. This is a significant finding because much of the damage caused by renal IRI is caused via oxygen and nutrient deprivation, which leads to a lack of ATP production and eventual necrosis.

How mitochondrial uncoupling protects against renal IRI is not entirely clear. Following reperfusion, mitochondrial uncoupling prevents ROS formation and oxidative damage, which can have two primary effects. Uncoupling can have a direct effect on preventing apoptosis and necrosis by reducing cellular oxidative damage. Apoptosis can

be prevented by lowering ROS, and necrosis may be prevented by decreasing oxidative damage to mitochondria which allows them to more easily generate ATP following reperfusion. ROS reduction and a reduction in apoptotic cells may also decrease immune cell recruitment following reperfusion, which can decrease blood vessel occlusion by immune cells and thus decreases the ischemic period (see **Section 1.3.1**).

In support of this, histological analysis of renal tubules showed decreased casts, which are known to obstruct blood flow during or after renal IRI due to immune cell invasion (see **Section 1.3.2**). Decreased cast formation suggests that the immune response that can obstruct blood flow to the renal medulla following IRI was ameliorated by mitochondrial uncoupling. Specifically, neutrophil infiltration was significantly reduced. Because reduction of neutrophil infiltration has been shown to protect from renal IRI, mitochondrial uncoupling may be a method of reducing ROS formation during IRI, which decreases the production of inflammatory cytokines and reduces the infiltration of neutrophils. The reduced infiltration of neutrophils prevents neutrophil-mediated occlusion of blood vessels, which may decrease the ischemic period and the necrosis caused by IRI.

A possible mechanism by which mitochondrial uncoupling reduces neutrophil infiltration is by reducing the recruitment of dendritic cells, but the concentration of dendritic cells was unchanged at doses of BAM15 that decreased neutrophil infiltration. However, BAM15 decreased the recruitment of macrophages, which indicates a lesser response of the innate immune system to clear apoptotic cells following uncoupler treatment. Given all of the available data, it is likely that reduced ROS production and apoptosis during reperfusion decreases macrophage infiltration, which lowers neutrophil

infiltration and decreases cast formation. The increased blood flow caused by uncoupling reduces the ischemic period, decreases ATN, and normalizes GFR to maintain normal plasma creatinine concentrations.

Mitochondrial uncoupling can prevent ROS production and apoptosis from IRI, which may explain why decreased immune cell invasion is observed. However, it is not clear if BAM15-mediated prevention of necrosis and immune cell invasion are a direct result of uncoupling or if uncoupling prevents immune cell invasion, which results in increased blood flow, and decreases necrosis. Future studies utilizing immune-cell depleted mice may determine which, if any, immune cells are responsible for BAM15-mediated renal protection.

While it is likely that the actions of mitochondrial uncouplers are beneficial during reperfusion, it is not clear if uncoupling could have protective effects during the ischemic period. During ischemia $\Delta\Psi_m$ decreases and ATP production is decreased, so it is unlikely that increasing proton leak would have any beneficial effects during this time. However, clinical application of BAM15 should include the optimization of dosing periods, specifically if BAM15 can be administered during reperfusion in clinical settings where an uncoupler could not be used prophylactically.

The doses of BAM15 required for renal IRI were 1 and 5 mg/kg, and this was administered one hour prior to 26 min of IRI. The relative concentration of BAM15 after 90 minutes is relatively low, which indicates that much lower doses of BAM15 can be used to protect from renal IRI if administration times were optimized. After this period, BAM15 would have plasma concentrations in the nanomolar range, which would give little risk for clinical complications of uncoupling such as excessive heat production.

Further studies and vehicle optimization to improve the pharmacokinetic properties of BAM15 will be necessary to administer low doses that maintain a small amount of proton leak that is necessary to safely lower ROS production. Further studies can also address if BAM15 can protect from deadly ischemic conditions that are longer in length or accompanied by cardiac complications to more closely mimic the conditions in which renal IRI occurs in a clinical setting.

The efficacy of BAM15 against renal IRI is highly significant. The highest dose of BAM15 (5 mg/kg) demonstrated plasma creatinine concentrations, immune cell infiltration, and ATN that were indistinguishable from animals that underwent a sham procedure. From these data it can be concluded that BAM15 confers complete protection from renal IRI, and may represent a medical advance that can prevent the effects of this deadly disease. Specific patients are at high risk for renal IRI, which makes uncoupling an attractive therapeutic target because it can be used prophylactically in the event of acute renal failure.

CONCLUDING REMARKS AND FUTURE DIRECTIONS

Synthetic mitochondrial uncouplers are invaluable tools for the analysis of mitochondrial function and they represent possible therapeutics for diabetes, obesity, neurodegeneration, cancer, ischemia-reperfusion injury, and other disorders linked to mitochondrial dysfunction. However, a possible factor limiting the use of available protonophore uncouplers is their unwanted activity at other membranes such as the plasma membrane.

This study identified and validated BAM15 as a bona-fide mitochondrial uncoupler that does not affect plasma membrane conductance and has a broad effective range. BAM15 is a major advance in mitochondrial bioenergetics research, as the maximal rate of mitochondrial respiration can be more accurately assessed with BAM15 compared to FCCP. Because the maximal rate of uncoupler-induced respiration can change not only across cell types but across phenotypes, known characteristics of mitochondrial respiratory defects in whole cells may not be accurate in many cases. It is not clear how much of the literature regarding mitochondrial bioenergetics dysfunction in disease has been altered by the narrow dosing ranges of current uncouplers. Future studies utilizing BAM15 may include bioenergetics analysis in cases in which FCCP has a phenotype-specific dosing range, such as insulin resistance models³⁷⁹.

The mechanism by which BAM15 does not affect plasma membrane electrophysiology is not clear, but may be due to specificity of BAM15 for the mitochondrial inner membrane and the pKa of the ionizable proton at the interface of a phospholipid bilayer. Thus, BAM15 may demonstrate cyclical protonophore activity in the PM, and may simply diffuse in and out of the membrane. This could also occur if a

membrane potential is required for BAM15 to have uncoupling activity, as the membrane potential in the mitochondria is much greater than the plasma membrane. Future studies utilizing patch-clamp methods that measure BAM15 ion diffusion in membranes containing different lipid compositions and membrane potentials may answer these questions.

BAM15 will also allow for a greater understanding of the role of mitochondrial uncoupling in health and disease. Because known mitochondrial uncouplers have many off-target effects, gaining an accurate assessment of the role of proton leak is extremely difficult, as there is no clear way to assure that a small molecule is not affecting other parts of the cell. To address this, we designed an inactive control for BAM15 (**Figure 23**, SHC121013) which is similar to BAM15 but does not have protonophore activity. SHC121013 allows for both *in vivo* and cell culture-based experiments to be properly controlled such that experimental outcomes observed with BAM15 are likely due to mitochondrial proton leak. Because current uncouplers have known protein-binding targets, it is also not clear how many conclusions of the actions of mitochondrial proton leak have been falsely attributed to the off-target effects of small molecule uncouplers. Future experimentation with the proper inactive controls designed in this work may have to be performed to validate previous findings and conclusions of mitochondrial uncoupling.

Low concentrations of uncouplers are demonstrated to have beneficial effects in cell culture and animal models of insulin resistance and obesity^{379,380}, neurodegeneration and ischemic reperfusion injury^{286,383,384} and cardiovascular disease^{385,386}. Our data demonstrated that BAM15 treatment dose-dependently protected from renal ischemic-reperfusion injury. These data are promising; however, future studies will be required to

determine if BAM15 is suitable for long-term treatment of pathologies that require constant exposure such as progressive metabolic disorders.

Collectively, BAM15 represents a valuable new tool for the study of mitochondrial function and its low cytotoxicity and lack of off-target membrane depolarization provides renewed optimism that mitochondrial uncouplers may again be useful for medical intervention in the myriad disorders linked to mitochondrial dysfunction.

PUBLICATIONS RESULTING FROM THIS WORK

Kenwood BM, Calderone J, Hoehn KL and Santos WL. *Structure-activity relationships of the mitochondrial protonophore BAM15*. In preparation.

Kenwood BM, Weaver JL, Bajwa A, Poon IK, Byrne FL, Murrow BA, Calderone JA, Huang L, Divakaruni AS, Tomsig JL, Okabe K, Columbus L, Lynch KR, Ravichandran KS, Yan Z, Uchiyama S, Santos WL, Rogers GW, Okusa MD, Bayliss DA, and Hoehn KL. *Identification of a Novel Mitochondrial Uncoupler that Does Not Depolarize the Plasma Membrane. **Molecular Metabolism***. 3(2):114-123, 2013.

REFERENCES

1. Rousset, S. *et al.* The biology of mitochondrial uncoupling proteins. *Diabetes* **53 Suppl 1**, S130–5 (2004).
2. Mueckler, M. M. The molecular biology of mammalian glucose transporters. *Curr. Opin. Nephrol. Hypertens.* **1**, 12–20 (1992).
3. Randle, P. J. Regulatory interactions between lipids and carbohydrates: the glucose fatty acid cycle after 35 years. *Diabetes. Metab. Rev.* **14**, 263–83 (1998).
4. Halestrap, B. A. P. The Mitochondrial Pyruvate Carrier. *Biochem. J.* 85–96 (1975).
5. Tracy, B. Y., Flora, C. L. & Reed, L. J. REGULATION OF THE ACTIVITY OF THE PYRUVATE MITOCHONDRIA BY PHOSPHORYLATION AND DEPHOSPHORYLATION. *Proc. Natl. Acad. Sci.* **62**, 234–241 (1968).
6. Cooper, R., Randle, P. & Denton, R. Stimulation of phosphorylation and inactivation of pyruvate dehydrogenase by physiological inhibitors of the pyruvate dehydrogenase reaction. *Nature* 808–809 (1975). at <http://www.nature.com/nature/journal/v257/n5529/abs/257808a0.html>
7. Lenz, H. *et al.* Stereochemistry of si-citrate synthase and ATP-citrate-lyase reactions. *Eur. J. Biochem.* **24**, 207–15 (1971).
8. Rose, I. A., Connell, E. L. O. & Connell, L. O. Mechanisms of Aconitase Action: I. THE HYDROGEN TRANSFER REACTION. *J. Biol. Chem.* 1870–1879 (1967).
9. Kornberg, A. & Pricer, W. Di- and triphosphopyridine nucleotide isocitric dehydrogenases in yeast. *J. Biol. Chem.* 123–136 (1951). at <http://www.jbc.org/content/189/1/123.short>
10. Massey, V. The composition of the ketoglutarate dehydrogenase complex. *Biochim. Biophys. Acta* **38**, 447–460 (1960).
11. Palmer, J. M. & Wedding, R. T. Purification and properties of succinyl-CoA synthetase from Jerusalem artichoke mitochondria. *Biochim. Biophys. Acta - Enzymol. Biol. Oxid.* **113**, 167–174 (1966).
12. Dervartanian, D. & Veeger, C. Studies on succinate dehydrogenase. I. Spectral properties of the purified enzyme and formation of enzyme-competitive inhibitor complexes. ... *Biophys. Acta (BBA)-Specialized Sect.* ... **92**, 233–247 (1964).

13. Walker, W. & Singer, T. Identification of the Covalently Bound Flavin of Succinate Dehydrogenase as 8 α -(Histidyl) Flavin Adenine Dinucleotide. *J. Biol. Chem.* **245**, 4224–4225 (1970).
14. Quastel, J. H. & Dampier Whetham, M. The Equilibria existing between Succinic, Fumaric, and Malic Acids in the presence of Resting Bacteria. *Biochem. J.* **18**, 519–534 (1924).
15. Mann, P. J. G. & Woolf, B. The action of salts on fumerase. *Biochem. J.* **24**, 427–434 (1930).
16. Wolfe, R. & Neilands, J. Some molecular and kinetic properties of heart malic dehydrogenase. *J. Biol. Chem.* **221**, 61–70 (1956).
17. Webb, L., Hill, E. & Banaszak, L. Conformation of nicotinamide adenine dinucleotide bound to cytoplasmic malate dehydrogenase. *Biochemistry* **12**, 1–9 (1973).
18. Liu, Y., Fiskum, G. & Schubert, D. Generation of reactive oxygen species by the mitochondrial electron transport chain. *J. Neurochem.* **80**, 780–787 (2002).
19. Galante, Y. M. & Hatefi, Y. Purification and molecular and enzymic properties of mitochondrial NADH dehydrogenase. *Arch. Biochem. Biophys.* **192**, 559–568 (1979).
20. Friedrich, T. The NADH:ubiquinone oxidoreductase (complex I) from *Escherichia coli*. *Biochim. Biophys. Acta* **1364**, 134–146 (1998).
21. Leif, H., Sled, V. D., Ohnishi, T., Weiss, H. & Friedrich, T. Isolation and characterization of the proton-translocating NADH: ubiquinone oxidoreductase from *Escherichia coli*. *Eur. J. Biochem.* **230**, 538–48 (1995).
22. Yu, C. & Yu, L. Preparations and properties of high purity succinate dehydrogenase and ubiquinol-cytochrome c reductase. *Biochim. Biophys. Acta* **591**, 409–420 (1980).
23. Starkov, a a & Fiskum, G. Myxothiazol induces H₂O₂ production from mitochondrial respiratory chain. *Biochem. Biophys. Res. Commun.* **281**, 645–50 (2001).
24. Li, Y., Park, J.-S., Deng, J.-H. & Bai, Y. Cytochrome c oxidase subunit IV is essential for assembly and respiratory function of the enzyme complex. *J. Bioenerg. Biomembr.* **38**, 283–91 (2006).
25. Mitchell, P. Coupling of phosphorylation to electron and hydrogen transfer by a chemi-osmotic type of mechanism. *Nature* **191**, 144–148 (1961).

26. Brand, M. D. & Nicholls, D. G. Assessing mitochondrial dysfunction in cells. *Biochem. J.* **435**, 297–312 (2011).
27. Korshunov, S. S., Skulachev, V. P. & Starkov, A. a. High protonic potential actuates a mechanism of production of reactive oxygen species in mitochondria. *FEBS Lett.* **416**, 15–18 (1997).
28. Hafner, R. P., Brown, G. C. & Brand, M. D. Analysis of the control of respiration rate, phosphorylation rate, proton leak rate and protonmotive force in isolated mitochondria using the “top-down” approach of metabolic control theory. *Eur. J. Biochem.* **188**, 313–9 (1990).
29. Symersky, J., Osowski, D., Walters, D. E. & Mueller, D. M. Oligomycin frames a common drug-binding site in the ATP synthase. *Proc. Natl. Acad. Sci. U. S. A.* **109**, 13961–5 (2012).
30. Pogoryelov, D. *et al.* Microscopic rotary mechanism of ion translocation in the F(o) complex of ATP synthases. *Nat. Chem. Biol.* **6**, 891–9 (2010).
31. Rouslin, W. Protonic Inhibition of the Mitochondrial Oligomycin-sensitive Adenosine 5' -Triphosphatase in Ischemic and Autolyzing Cardiac Muscle. *J. Biol. Chem.* **256**, 9657–9661 (1983).
32. Penefsky, H. S. Mechanism of inhibition of mitochondrial adenosine triphosphatase by dicyclohexylcarbodiimide and oligomycin: relationship to ATP synthesis. *Proc. Natl. Acad. Sci. U. S. A.* **82**, 1589–93 (1985).
33. Teruyo, A., Matsui, H., Wakizaka, A. & Homareda, H. Mechanism responsible for oligomycin-induced occlusion of Na⁺ within Na/K-ATPase. *J. Biol. ...* **271**, 25604–25610 (1996).
34. Brand, M. D. *et al.* The basal proton conductance of mitochondria depends on adenine nucleotide translocase content. *Biochem. J.* **392**, 353–62 (2005).
35. Nicholls, D. G. The Influence of Respiration and ATP Hydrolysis on the Proton-Electrochemical Gradient across the Inner Membrane of Rat-Liver Mitochondria as Determined by Ion Distribution. *Eur. J. Biochem.* **50**, 305–315 (1974).
36. Pietrobon, D., Azzone, G. F. & Walz, D. Effect of funiculosin and antimycin A on the redox-driven H⁺-pumps in mitochondria: on the nature of "leaks". *Eur. J. Biochem.* **117**, 389–94 (1981).
37. Pietrobon, D., Zoratti, M. & Azzone, G. F. Molecular Slipping in Redox and ATPase H⁺ Pumps. *Biochim. Biophys. Acta* **723**, 317–321 (1983).

38. Pietrobon, D., Zoratti, M., Azzone, G. F. & Caplan, S. R. Intrinsic Uncoupling of Mitochondrial Proton Pumps. *Biochemistry* **25**, 767–75 (1986).
39. Porter, R. K. & Brand, M. D. Mitochondrial proton conductance and H⁺/O ratio are independent of electron transport rate in isolated hepatocytes. *Biochem. J.* **310** (Pt 2, 379–82 (1995).
40. Brown, G. C. The relative proton stoichiometries of the mitochondrial proton pumps are independent of the proton motive force. *J. Biol. Chem.* **264**, 14704–9 (1989).
41. Brown, G. & Brand, M. On the Nature of Mitochondrial Proton Leak. *Biochim. Biophys. Acta (BBA)-Bioenergetics* **1059**, 55–62 (1991).
42. Brand, M. D. The proton leak across the mitochondrial inner membrane. *Biochim. Biophys. Acta* **1018**, 128–33 (1990).
43. Nobe, D., Brown, C., Olive, N. & Brand, D. Non-ohmic Proton Conductance of the Mitochondrial Inner Membrane in Hepatocytes. *J. Biol. Chem.* **265**, 12903–12909 (1990).
44. Mitchell, P. The protonmotive Q cycle: A general formulation. *FEBS Lett.* **59**, 137–139 (1975).
45. Rolfe, D. F. & Brand, M. D. Contribution of mitochondrial proton leak to skeletal muscle respiration and to standard metabolic rate. *Am. J. Physiol.* **271**, C1380–9 (1996).
46. Klingenberg, M. & Appel, M. The uncoupling protein dimer can form a disulfide cross-link between the mobile C-terminal SH groups. *Eur. J. Biochem.* **180**, 123–31 (1989).
47. Nonogaki, K. New insights into sympathetic regulation of glucose and fat metabolism. *Diabetologia* **43**, 533–49 (2000).
48. Golozoubova, V. *et al.* Only UCP1 can mediate adaptive nonshivering thermogenesis in the cold. *FASEB J.* **15**, 2048–2050 (2001).
49. Ukropec, J., Anunciado, R. P., Ravussin, Y., Hulver, M. W. & Kozak, L. P. UCP1-independent thermogenesis in white adipose tissue of cold-acclimated Ucp1^{-/-} mice. *J. Biol. Chem.* **281**, 31894–908 (2006).
50. Talbot, D. a *et al.* Uncoupling protein and ATP/ADP carrier increase mitochondrial proton conductance after cold adaptation of king penguins. *J. Physiol.* **558**, 123–35 (2004).

51. Gimeno, R. E. *et al.* Cloning and characterization of an uncoupling protein homolog: a potential molecular mediator of human thermogenesis. *Diabetes* **46**, 900–6 (1997).
52. Vidal-Puig, a, Solanes, G., Grujic, D., Flier, J. S. & Lowell, B. B. UCP3: an uncoupling protein homologue expressed preferentially and abundantly in skeletal muscle and brown adipose tissue. *Biochem. Biophys. Res. Commun.* **235**, 79–82 (1997).
53. Boss, O., Samec, S., Dulloo, A., Seydoux, J. & Giacobino, J.-P. Tissue-dependent upregulation of rat uncoupling protein-2 expression in response to fasting or cold. *FEBS Lett.* **412**, 111–114 (1997).
54. Liu, D. *et al.* Mitochondrial UCP4 Mediates an Adaptive Shift in Energy Metabolism and Increases the Resistance of Neurons to Metabolic and Oxidative Stress. *Neuromolecular Med.* **8**, 389–413 (2006).
55. Gao, C.-L. *et al.* UCP4 overexpression improves fatty acid oxidation and insulin sensitivity in L6 myocytes. *J. Bioenerg. Biomembr.* **43**, 109–18 (2011).
56. Locke, R. M., Rial, E., Scott, I. D. & Nicholls, D. G. Fatty acids as acute regulators of the proton conductance of hamster brown-fat mitochondria. *Eur. J. Biochem.* **129**, 373–80 (1982).
57. Eduardo Rial, Alison Poustie, D. G. N. Brown adipose-tissue mitochondria: the regulation of the 32 000-Mr uncoupling protein by fatty acids and purine nucleotides. *Eur. J. ...* **203**, 197–203 (1983).
58. Winkler, Edith, M. K. An improved procedure for reconstitution of the uncoupling protein and in-depth analysis of H⁺/OH⁻ transport. *Eur. J. Biochem.* **207**, 135–145 (1992).
59. Klingenberg, M. & Huang, S. G. Structure and function of the uncoupling protein from brown adipose tissue. *Biochim. Biophys. Acta* **1415**, 271–96 (1999).
60. Jabůrek, M., Varecha, M., Jezek, P. & Garlid, K. D. Alkylsulfonates as probes of uncoupling protein transport mechanism. Ion pair transport demonstrates that direct H(+) translocation by UCP1 is not necessary for uncoupling. *J. Biol. Chem.* **276**, 31897–905 (2001).
61. Garlid, K. D., Orosz, D. E., Modrianský, M., Vassanelli, S. & Jezek, P. On the mechanism of fatty acid-induced proton transport by mitochondrial uncoupling protein. *J. Biol. Chem.* **271**, 2615–20 (1996).

62. Hanus, J. Photoactivated Azido Fatty Acid Irreversibly Inhibits Anion and Proton Transport through the Mitochondrial Uncoupling Protein. *J. Biol. Chem.* **271**, 6199–6205 (1996).
63. Skulachev, V. P. Fatty acid circuit as a physiological mechanism of uncoupling of oxidative phosphorylation. *Fed. Eur. Biochem. Soc.* **294**, 158–162 (1991).
64. Gong, D.-W., He, Y., Karas, M. & Reitman, M. Uncoupling Protein-3 Is a Mediator of Thermogenesis Regulated by Thyroid Hormone, β -Adrenergic Agonists, and Leptin. *J. Biol. Chem.* **272**, 24129–24132 (1997).
65. Jaburek, M., Miyamoto, S., Di Mascio, P., Garlid, K. D. & Jezek, P. Hydroperoxy fatty acid cycling mediated by mitochondrial uncoupling protein UCP2. *J. Biol. Chem.* **279**, 53097–102 (2004).
66. Bezaire, V. *et al.* Constitutive UCP3 overexpression at physiological levels increases mouse skeletal muscle capacity for fatty acid transport and oxidation. *FASEB J.* **19**, 977–9 (2005).
67. Schrauwen, P., Saris, W. H. & Hesselink, M. K. An alternative function for human uncoupling protein 3: protection of mitochondria against accumulation of nonesterified fatty acids inside the mitochondrial matrix. *FASEB J.* **15**, 2497–502 (2001).
68. Schrauwen, P. *et al.* Etomoxir-induced increase in UCP3 supports a role of uncoupling protein 3 as a mitochondrial fatty acid anion exporter. *FASEB J.* **16**, 1688–1690 (2002).
69. Jaburek, M. *et al.* Transport Function and Regulation of Mitochondrial Uncoupling Proteins 2 and 3. *J. Biol. Chem.* **274**, 26003–26007 (1999).
70. Andreyev AY *et al.* The ATP/ADP-antiporter is involved in the uncoupling effect of fatty acids on mitochondria. *Eur. J. Biochem.* **182**, 585–92 (1989).
71. Cannon, B., Shabalina, I. G., Kramarova, T. V., Petrovic, N. & Nedergaard, J. Uncoupling proteins: a role in protection against reactive oxygen species--or not? *Biochim. Biophys. Acta* **1757**, 449–58 (2006).
72. Chance, B. & Williams, G. RESPIRATORY ENZYMES IN OXIDATIVE PHOSPHORYLATION: I. KINETICS OF OXYGEN UTILIZATION. *J. Biol. Chem.* **217**, 383–394 (1955).
73. Sansbury, B. E., Jones, S. P., Riggs, D. W., Darley-Usmar, V. M. & Hill, B. G. Bioenergetic function in cardiovascular cells: the importance of the reserve capacity and its biological regulation. *Chem. Biol. Interact.* **191**, 288–95 (2011).

74. Gong, G. *et al.* Oxidative capacity in failing hearts. *Am. J. Physiol. Heart Circ. Physiol.* **285**, H541–8 (2003).
75. Hill, B. G., Dranka, B. P., Zou, L., Chatham, J. C. & Darley-USmar, V. M. Importance of the bioenergetic reserve capacity in response to cardiomyocyte stress induced by 4-hydroxynonenal. *Biochem. J.* **424**, 99–107 (2009).
76. Yadava, N. & Nicholls, D. G. Spare respiratory capacity rather than oxidative stress regulates glutamate excitotoxicity after partial respiratory inhibition of mitochondrial complex I with rotenone. *J. Neurosci.* **27**, 7310–7 (2007).
77. Cairns, R. a, Harris, I. S. & Mak, T. W. Regulation of cancer cell metabolism. *Nat. Rev. Cancer* **11**, 85–95 (2011).
78. Wiley, C. & Beeson, C. Continuous Measurement of Glucose Utilization of Heart Myoblasts. *Anal. Biochem.* **304**, 139–146 (2002).
79. Owicki, J. & Parce, J. W. Biosensors based on the energy metabolism of living cells: the physical chemistry and cell biology of extracellular acidification. *Biosens. Bioelectron.* **7**, 255–272 (1992).
80. Ferrick, D. a, Neilson, A. & Beeson, C. Advances in measuring cellular bioenergetics using extracellular flux. *Drug Discov. Today* **13**, 268–274 (2008).
81. Treberg, J. R., Quinlan, C. L. & Brand, M. D. Evidence for two sites of superoxide production by mitochondrial NADH-ubiquinone oxidoreductase (complex I). *J. Biol. Chem.* **286**, 27103–10 (2011).
82. Murphy, M. P. How mitochondria produce reactive oxygen species. *Biochem. J.* **417**, 1–13 (2009).
83. Raha, S. & Robinson, B. H. Mitochondria, oxygen free radicals, disease and ageing. *Trends Biochem. Sci.* **25**, 502–8 (2000).
84. Quinlan, C. L. *et al.* Mitochondrial complex II can generate reactive oxygen species at high rates in both the forward and reverse reactions. *J. Biol. Chem.* **287**, 27255–64 (2012).
85. St-Pierre, J., Buckingham, J. a, Roebuck, S. J. & Brand, M. D. Topology of superoxide production from different sites in the mitochondrial electron transport chain. *J. Biol. Chem.* **277**, 44784–90 (2002).
86. Turrens, J. F. & Boveris, a. Generation of superoxide anion by the NADH dehydrogenase of bovine heart mitochondria. *Biochem. J.* **191**, 421–7 (1980).

87. Turrens, J. F., Freeman, B. A., Levitt, J. G. & Crapo, J. D. The effect of hyperoxia on superoxide production by lung submitochondrial particles. *Arch. Biochem. Biophys.* **217**, 401–410 (1982).
88. Genova, M. L. *et al.* The site of production of superoxide radical in mitochondrial Complex I is not a bound ubisemiquinone but presumably iron-sulfur cluster N2. *FEBS Lett.* **505**, 364–8 (2001).
89. Zhang, L. Generation of Superoxide Anion by Succinate-Cytochrome c Reductase from Bovine Heart Mitochondria. *J. Biol. Chem.* **273**, 33972–33976 (1998).
90. Brunelle, J. K. *et al.* Oxygen sensing requires mitochondrial ROS but not oxidative phosphorylation. *Cell Metab.* **1**, 409–14 (2005).
91. Guzy, R. D. *et al.* Mitochondrial complex III is required for hypoxia-induced ROS production and cellular oxygen sensing. *Cell Metab.* **1**, 401–8 (2005).
92. Chin, D.-H., Chiericato, G., Nanni, E. J. J. & Sawyer, D. T. Proton-induced disproportionation of superoxide ion in aprotic media. *J. Am. Chem. Soc.* **104**, 1296–1299 (1982).
93. Bielski, B. H. & Allen, A. O. Mechanism of the Disproportionation of Superoxide Radicals. *J. Phys. Chem.* **81**, 1048–1050 (1977).
94. Liochev, S. & Fridovich, I. Modulation of the Fumarases of *Escherichia coli* in Response to Oxidative Stress. *Arch. Biochem. Biophys.* **301**, 379–384 (1993).
95. Flint, D. H., Tuminello, J. F. & Emptage, M. H. The inactivation of Fe-S cluster containing hydro-lyases by superoxide. *J. Biol. Chem.* **268**, 22369–76 (1993).
96. Gardner, P. R. & Fridovich, I. Superoxide sensitivity of the *Escherichia coli* aconitase. *J. Biol. Chem.* **266**, 19328–33 (1991).
97. Turrens, J. F. Mitochondrial formation of reactive oxygen species. *J. Physiol.* **552**, 335–44 (2003).
98. Greenwald, R. A. SUPEROXIDE DISMUTASE AND CATALASE AS THERAPEUTIC AGENTS FOR HUMAN DISEASES. *Free Radic. Biol. Med.* **8**, 201–209 (1990).
99. Wei, L. & Dirksen, R. T. Mitochondrial superoxide flashes: From discovery to new controversies. *J. Gen. Physiol.* **139**, 425–34 (2012).
100. Da Silva Dantas, A. *et al.* Thioredoxin regulates multiple hydrogen peroxide-induced signaling pathways in *Candida albicans*. *Mol. Cell. Biol.* **30**, 4550–63 (2010).

101. Halliwell, B. Free Radicals and Other Reactive Species in Disease. *eLS* 1–7 (2005). doi:10.1038/npg.els.0003913
102. Powell, C. S. & Jackson, R. M. Mitochondrial complex I, aconitase, and succinate dehydrogenase during hypoxia-reoxygenation: modulation of enzyme activities by MnSOD. *Am. J. Physiol. Lung Cell. Mol. Physiol.* **285**, L189–98 (2003).
103. Cecarini, V. *et al.* Protein oxidation and cellular homeostasis: Emphasis on metabolism. *Biochim. Biophys. Acta* **1773**, 93–104 (2007).
104. Sohal, R. Role of oxidative stress and protein oxidation in the aging process 1, 2. *Free Radic. Biol. Med.* **33**, 37–44 (2002).
105. Smith, C. D. *et al.* Excess brain protein oxidation and enzyme dysfunction in normal aging and in Alzheimer disease. *Proc. Natl. Acad. Sci. U. S. A.* **88**, 10540–3 (1991).
106. Butterfield, D. & Lauderback, C. Lipid peroxidation and protein oxidation in Alzheimer's disease brain: potential causes and consequences involving amyloid β -peptide-associated free radical. *Free Radic. Biol. Med.* **32**, 1050–1060 (2002).
107. Kohr, M. J. *et al.* Simultaneous measurement of protein oxidation and S-nitrosylation during preconditioning and ischemia/reperfusion injury with resin-assisted capture. *Circ. Res.* **108**, 418–26 (2011).
108. Divald, A. *et al.* Myocardial ischemic preconditioning preserves postischemic function of the 26S proteasome through diminished oxidative damage to 19S regulatory particle subunits. *Circ. Res.* **106**, 1829–38 (2010).
109. Stadtman, E. R. & Levine, R. L. Protein oxidation. *Ann. N. Y. Acad. Sci.* **899**, 191–208 (2000).
110. Yin, H., Xu, L. & Porter, N. a. Free radical lipid peroxidation: mechanisms and analysis. *Chem. Rev.* **111**, 5944–72 (2011).
111. Yamamoto, Y. *et al.* Free radical chain oxidation and hemolysis of erythrocytes by molecular oxygen and their inhibition by vitamin E. *J. Nutr. ...* **32**, 475–479 (1986).
112. Niki, E. Lipid peroxidation: physiological levels and dual biological effects. *Free Radic. Biol. Med.* **47**, 469–84 (2009).
113. Chen, R., Yang, L. & McIntyre, T. M. Cytotoxic phospholipid oxidation products. Cell death from mitochondrial damage and the intrinsic caspase cascade. *J. Biol. Chem.* **282**, 24842–50 (2007).

114. Chen, R., Feldstein, A. E. & McIntyre, T. M. Suppression of mitochondrial function by oxidatively truncated phospholipids is reversible, aided by bid, and suppressed by Bcl-XL. *J. Biol. Chem.* **284**, 26297–308 (2009).
115. Avery, S. V. Molecular targets of oxidative stress. *Biochem. J.* **434**, 201–10 (2011).
116. Bo, H. *et al.* Regulation of mitochondrial uncoupling respiration during exercise in rat heart: role of reactive oxygen species (ROS) and uncoupling protein 2. *Free Radic. Biol. Med.* **44**, 1373–81 (2008).
117. Echtay, K. S. *et al.* Superoxide activates mitochondrial uncoupling proteins. *Nature* **415**, 96–9 (2002).
118. Echtay, K. S. *et al.* A signalling role for 4-hydroxy-2-nonenal in regulation of mitochondrial uncoupling. *EMBO J.* **22**, 4103–10 (2003).
119. Diano, S. & Horvath, T. L. Mitochondrial uncoupling protein 2 (UCP2) in glucose and lipid metabolism. *Trends Mol. Med.* **18**, 52–8 (2012).
120. Adjeitey, C. N.-K., Mailloux, R. J., Dekemp, R. a & Harper, M.-E. Mitochondrial uncoupling in skeletal muscle by UCP1 augments energy expenditure and glutathione content while mitigating ROS production. *Am. J. Physiol. Endocrinol. Metab.* **305**, E405–15 (2013).
121. Pi, J. & Collins, S. Reactive oxygen species and uncoupling protein 2 in pancreatic β -cell function. *Diabetes, Obes. Metab.* **12**, 141–148 (2010).
122. Andrews, Z. B. *et al.* UCP2 mediates ghrelin's action on NPY/AgRP neurons by lowering free radicals. *Nature* **454**, 846–51 (2008).
123. MacLellan, J., Gerrits, M. & Gowing, A. Physiological increases in uncoupling protein 3 augment fatty acid oxidation and decrease reactive oxygen species production without uncoupling respiration in. *Diabetes* **54**, 2343–2350 (2005).
124. Mailloux, R. J. *et al.* Hexokinase II acts through UCP3 to suppress mitochondrial reactive oxygen species production and maintain aerobic respiration. *Biochem. J.* **437**, 301–11 (2011).
125. Mailloux, R. J. *et al.* Glutathionylation acts as a control switch for uncoupling proteins UCP2 and UCP3. *J. Biol. Chem.* **286**, 21865–75 (2011).
126. Dłasková, A., Clarke, K. J. & Porter, R. K. The role of UCP 1 in production of reactive oxygen species by mitochondria isolated from brown adipose tissue. *Biochim. Biophys. Acta* **1797**, 1470–6 (2010).

127. Pi, J. *et al.* Persistent oxidative stress due to absence of uncoupling protein 2 associated with impaired pancreatic beta-cell function. *Endocrinology* **150**, 3040–8 (2009).
128. Senapedis, W. T., Kennedy, C. J., Boyle, P. M. & Silver, P. a. Whole genome siRNA cell-based screen links mitochondria to Akt signaling network through uncoupling of electron transport chain. *Mol. Biol. Cell* **22**, 1791–805 (2011).
129. Nakano, M. Determination of superoxide radical and singlet oxygen based on chemiluminescence of luciferin analogs. *Methods Enzym.* **186**, 585–591 (1990).
130. Kussmaul, L. & Hirst, J. The mechanism of superoxide production by NADH:ubiquinone oxidoreductase (complex I) from bovine heart mitochondria. *Proc. Natl. Acad. Sci. U. S. A.* **103**, 7607–12 (2006).
131. Klinman, J. P. How do enzymes activate oxygen without inactivating themselves? *Acc. Chem. Res.* **40**, 325–33 (2007).
132. Wikström, M. Two protons are pumped from the mitochondrial matrix per electron transferred between NADH and ubiquinone. *FEBS Lett.* **169**, 300–4 (1984).
133. Okun, J., Lümmer, P. & Brandt, U. Three classes of inhibitors share a common binding domain in mitochondrial complex I (NADH: ubiquinone oxidoreductase). *J. Biol. Chem.* **274**, 2625–2630 (1999).
134. Baradaran, R., Berrisford, J. M., Minhas, G. S. & Sazanov, L. a. Crystal structure of the entire respiratory complex I. *Nature* **494**, 443–8 (2013).
135. Angerer, H. *et al.* A scaffold of accessory subunits links the peripheral arm and the distal proton-pumping module of mitochondrial complex I. *Biochem. J.* **437**, 279–88 (2011).
136. Carroll, J. *et al.* Bovine complex I is a complex of 45 different subunits. *J. Biol. Chem.* **281**, 32724–7 (2006).
137. Carroll, J., Fearnley, I. M., Shannon, R. J., Hirst, J. & Walker, J. E. Analysis of the subunit composition of complex I from bovine heart mitochondria. *Mol. Cell. Proteomics* **2**, 117–26 (2003).
138. Esposti, M. D. Inhibitors of NADH-ubiquinone reductase: an overview. *Biochim. Biophys. Acta* **1364**, 222–235 (1998).
139. Zickermann, V., Barquera, B., Wikström, M. & Finel, M. Analysis of the pathogenic human mitochondrial mutation ND1/3460, and mutations of strictly conserved residues in its vicinity, using the bacterium *Paracoccus denitrificans*. *Biochemistry* **37**, 11792–6 (1998).

140. Prieur, I., Lunardi, J. & Dupuis, A. Evidence for a quinone binding site close to the interface between NUOD and NUOB subunits of Complex I. *Biochim. Biophys. Acta (BBA)*- ... **1504**, 173–178 (2001).
141. Ueno, K., Miyoshi, H., Ebisui, K. & Iwamura, H. Comparison of the inhibitory action of natural rotenone and its stereoisomers with various NADH-ubiquinone reductases. *Eur. J. Biochem.* **225**, 411–417 (1994).
142. Votyakova, T. V & Reynolds, I. J. DeltaPsi(m)-Dependent and -independent production of reactive oxygen species by rat brain mitochondria. *J. Neurochem.* **79**, 266–77 (2001).
143. Turrens, J., Alexandre, A. & Lehninger, A. Ubisemiquinone is the electron donor for superoxide formation by complex III of heart mitochondria. *Arch. Biochem. Biophys.* **237**, 408–14 (1985).
144. Takeshige, K. & Minakami, S. NADH- and NADPH-dependent formation of superoxide anions by bovine heart submitochondrial particles and NADH-ubiquinone reductase preparation. *Biochem. J.* **180**, 129–35 (1979).
145. Chen, Q., Vazquez, E. J., Moghaddas, S., Hoppel, C. L. & Lesnefsky, E. J. Production of reactive oxygen species by mitochondria: central role of complex III. *J. Biol. Chem.* **278**, 36027–31 (2003).
146. Hirst, J., King, M. S. & Pryde, K. R. The production of reactive oxygen species by complex I. *Biochem. Soc. Trans.* **36**, 976–80 (2008).
147. Si, Y., Shi, H. & Lee, K. Metabolic flux analysis of mitochondrial uncoupling in 3T3-L1 adipocytes. *PLoS One* **4**, e7000 (2009).
148. Vinogradov, a D. Catalytic properties of the mitochondrial NADH-ubiquinone oxidoreductase (complex I) and the pseudo-reversible active/inactive enzyme transition. *Biochim. Biophys. Acta* **1364**, 169–85 (1998).
149. Lambert, A. J. & Brand, M. D. Superoxide production by NADH:ubiquinone oxidoreductase (complex I) depends on the pH gradient across the mitochondrial inner membrane. *Biochem. J.* **382**, 511–7 (2004).
150. Anderson, R. F. *et al.* Electron-transfer pathways in the heme and quinone-binding domain of complex II (succinate dehydrogenase). *Biochemistry* **53**, 1637–46 (2014).
151. Sun, F. *et al.* Crystal structure of mitochondrial respiratory membrane protein complex II. *Cell* **121**, 1043–57 (2005).

152. Mitchell, P. PROTONMOTIVE REDOX MECHANISM OF THE CYTOCHROME b-c1 COMPLEX IN THE RESPIRATORY CHAIN: PROTONMOTIVE UBIQUINONE CYCLE. *FEBS Lett.* **56**, 1–6 (1975).
153. Bleier, L. & Dröse, S. Superoxide generation by complex III: from mechanistic rationales to functional consequences. *Biochim. Biophys. Acta* **1827**, 1320–31 (2013).
154. Orii, Y. & Miki, T. Oxidation Process of Bovine Heart Ubiquinol-Cytochrome c Reductase as Studied by Stopped-flow Rapid-scan Spectrophotometry and Simulations Based on the Mechanistic Q Cycle Model. *J. Biol. Chem.* **272**, 17594–17604 (1997).
155. Ohnishi, T. & Trumpower, B. L. Differential effects of antimycin on ubisemiquinone bound in different environments in isolated succinate . cytochrome c reductase complex. *J. Biol. Chem.* **255**, 3278–84 (1980).
156. Muller, F., Crofts, A. R. & Kramer, D. M. Multiple Q-Cycle Bypass Reactions at the Qo Site of the Cytochrome bc1 Complex. *Biochemistry* **41**, 7866–7874 (2002).
157. Potter, V. & Reif, A. Inhibition of an electron transport component by antimycin A. *J. Biol. Chem.* **194**, 287–297 (1952).
158. Ahmad, K., Schneider, H. & Strong, F. Studies on the biological action of Antimycin A. *Arch. Biochem. Biophys.* **28**, 281–294 (1950).
159. Slater, E. THE MECHANISM OF ACTION OF THE RESPIRATORY INHIBITOR, ANTIMYCIN. *Biochim. Biophys. Acta* **301**, 129–154 (1973).
160. Huang, L.-S., Cobessi, D., Tung, E. Y. & Berry, E. a. Binding of the respiratory chain inhibitor antimycin to the mitochondrial bc1 complex: a new crystal structure reveals an altered intramolecular hydrogen-bonding pattern. *J. Mol. Biol.* **351**, 573–97 (2005).
161. Quinlan, C. L., Gerencser, A. a, Treberg, J. R. & Brand, M. D. The mechanism of superoxide production by the antimycin-inhibited mitochondrial Q-cycle. *J. Biol. Chem.* **286**, 31361–72 (2011).
162. Sugioka, K. *et al.* Mechanism of O₂- generation in reduction and oxidation cycle of ubiquinones in a model of mitochondrial electron transport systems. *Biochim. Biophys. Acta* **936**, 377–85 (1988).
163. Boveris, A., Cadenas, E. & Stoppani, A. Role of ubiquinone in the mitochondrial generation of hydrogen peroxide. *Biochem. J.* **156**, 435–44 (1976).

164. Cadenas, E., Alberto, B., Ragan, C. & Stoppani, A. Production of superoxide radicals and hydrogen peroxide by NADH-ubiquinone reductase and ubiquinol-cytochrome c reductase from beef-heart mitochondria. *Arch. Biochem. Biophys.* **180**, 248–257 (1977).
165. Muller, F. L., Roberts, A. G., Bowman, M. K. & Kramer, D. M. Architecture of the Qo site of the cytochrome bc1 complex probed by superoxide production. *Biochemistry* **42**, 6493–9 (2003).
166. Dröse, S. & Brandt, U. The mechanism of mitochondrial superoxide production by the cytochrome bc1 complex. *J. Biol. Chem.* **283**, 21649–54 (2008).
167. Ksenzenko, M., Konstantinov, a a, Khomutov, G. B., Tikhonov, a N. & Ruuge, E. K. Effect of electron transfer inhibitors on superoxide generation in the cytochrome bc1 site of the mitochondrial respiratory chain. *FEBS Lett.* **155**, 19–24 (1983).
168. Cape, J. L., Bowman, M. K. & Kramer, D. M. A semiquinone intermediate generated at the Qo site of the cytochrome bc1 complex: importance for the Q-cycle and superoxide production. *Proc. Natl. Acad. Sci. U. S. A.* **104**, 7887–92 (2007).
169. Rottenberg, H., Covian, R. & Trumpower, B. L. Membrane potential greatly enhances superoxide generation by the cytochrome bc1 complex reconstituted into phospholipid vesicles. *J. Biol. Chem.* **284**, 19203–10 (2009).
170. Liangos, O. *et al.* Epidemiology and outcomes of acute renal failure in hospitalized patients: a national survey. *Clin. J. Am. Soc. Nephrol.* **1**, 43–51 (2006).
171. Aronson, S. & Blumenthal, R. Perioperative renal dysfunction and cardiovascular anesthesia: concerns and controversies. ... *Cardiothorac. Vasc. Anesth.* **5**, 567–586 (1998).
172. Chatterjee, P. K. Novel pharmacological approaches to the treatment of renal ischemia-reperfusion injury: a comprehensive review. *Naunyn. Schmiedeberg's Arch. Pharmacol.* **376**, 1–43 (2007).
173. Friedewald, J. J. & Rabb, H. Inflammatory cells in ischemic acute renal failure. *Kidney Int.* **66**, 486–91 (2004).
174. Huang, L. *et al.* Overexpression of stanniocalcin-1 inhibits reactive oxygen species and renal ischemia/reperfusion injury in mice. *Kidney Int.* **82**, 867–77 (2012).
175. Gueler, F., Gwinner, W., Schwarz, A. & Haller, H. Long-term effects of acute ischemia and reperfusion injury. *Kidney Int.* **66**, 523–7 (2004).

176. Halloran, P. F. *et al.* The “injury response”: a concept linking nonspecific injury, acute rejection, and long-term transplant outcomes. *Transplant. Proc.* **29**, 79–81 (1997).
177. Chertow, G. M., Levy, E. M., Hammermeister, K. E., Grover, F. & Daley, J. Independent association between acute renal failure and mortality following cardiac surgery. *Am. J. Med.* **104**, 343–8 (1998).
178. Bonegio, R. & Lieberthal, W. Role of apoptosis in the pathogenesis of acute renal failure. *Curr. Opin. Nephrol. Hypertens.* **11**, 301–8 (2002).
179. Savill, J. & Fadok, V. Corpse clearance defines the meaning of cell death. *Nature* **407**, 784–8 (2000).
180. Park, D. *et al.* Continued clearance of apoptotic cells critically depends on the phagocyte Ucp2 protein. *Nature* **477**, 220–4 (2011).
181. Hengartner, M. O. The biochemistry of apoptosis. *Nature* **407**, 770–6 (2000).
182. Elliott, M. R. *et al.* Nucleotides released by apoptotic cells act as a find-me signal to promote phagocytic clearance. *Nature* **461**, 282–6 (2009).
183. Burch, W., Paffe, S., Putz, B., Barthel, G. & Schulte-Hermann, R. Determination of the length of the histological stages of apoptosis in normal liver and in altered hepatic foci of rats. *Carcinogenesis* **5**, 847–53 (1990).
184. Nadasdy, T. *et al.* Human acute tubular necrosis: a lectin and immunohistochemical study. *Hum. Pathol.* **26**, 230–9 (1995).
185. Witzgall, R., Brown, D., Schwarz, C. & Bonventre, J. V. Localization of Proliferating Cell Nuclear Antigen, Vimentin, c-Fos, and Clusterin in the Postischemic Kidney. *J. Clin. Invest.* **93**, 2175–2188 (1994).
186. Serhan, C. N. & Savill, J. Resolution of inflammation: the beginning programs the end. *Nat. Immunol.* **6**, 1191–7 (2005).
187. Nath, K. & Norby, S. Reactive oxygen species and acute renal failure. *Am. J. Med.* **109**, 665–678 (2000).
188. Elliott, M. R. & Ravichandran, K. S. Clearance of apoptotic cells: implications in health and disease. *J. Cell Biol.* **189**, 1059–70 (2010).
189. Ravichandran, K. S. Find-me and eat-me signals in apoptotic cell clearance: progress and conundrums. *J. Exp. Med.* **207**, 1807–17 (2010).

190. Li, L. & Okusa, M. Macrophages, dendritic cells, and kidney ischemia-reperfusion injury. *Semin. Nephrol.* **30**, 268–277 (2010).
191. Francischetti, I., Moreno, J. B., Scholz, M. & Yoshida, W. B. Leukocytes and the inflammatory response in ischemia-reperfusion injury. *Rev. Bras. Cir. Cardiovasc.* **25**, 575–84 (2010).
192. Arslan, F. *et al.* Myocardial ischemia/reperfusion injury is mediated by leukocytic toll-like receptor-2 and reduced by systemic administration of a novel anti-toll-like receptor-2 antibody. *Circulation* **121**, 80–90 (2010).
193. Bonventre, J. V. Mechanisms of ischemic acute renal failure. *Kidney Int.* **43**, 1160–78 (1993).
194. Kobryn, C. E. & Mandel, L. J. Decreased protein phosphorylation induced by anoxia in proximal renal tubules. *Am. J. Physiol.* **267**, C1073–9 (1994).
195. Tsukamoto, T. & Nigam, S. Tight junction proteins form large complexes and associate with the cytoskeleton in an ATP depletion model for reversible junction assembly. *J. Biol. Chem.* **272**, 16133–16139 (1997).
196. Kinsey, G., Li, L. & Okusa, M. Inflammation in acute kidney injury. *Nephron Exp. Nephrol.* **109**, 1–7 (2008).
197. Jang, H. R. & Rabb, H. The innate immune response in ischemic acute kidney injury. *Clin. Immunol.* **130**, 41–50 (2009).
198. Weinberg, J. M. *et al.* Anaerobic and aerobic pathways for salvage of proximal tubules from hypoxia-induced mitochondrial injury. *Am. J. Physiol. Renal Physiol.* **279**, F927–43 (2000).
199. Epstein, F., Brezis, M. & Rosen, S. Hypoxia of the renal medulla—its implications for disease. *New Engl. J. ...* **332**, 647–655 (1995).
200. Lieberthal, W. & Nigam, S. Acute renal failure. II. Experimental models of acute renal failure: imperfect but indispensable. *Am. J. Physiol. Physiol.* **278**, F1–F12 (2000).
201. Bonventre, J. V. Recent Advances in the Pathophysiology of Ischemic Acute Renal Failure. *J. Am. Soc. Nephrol.* **14**, 2199–2210 (2003).
202. Bonventre, J. & Yang, L. Cellular pathophysiology of ischemic acute kidney injury. *J. Clin. Invest.* **121**, 4210–4221 (2011).
203. Beeuwkes, R. 3rd & Bonventre, J. Tubular organization and vascular-tubular relations in the dog kidney. *Am. J. Physiol.* **229**, 695–713 (1975).

204. Bagnasco, S., Good, D., Balaban, R. & Burg, M. Lactate production in isolated segments of the rat nephron. *Am J Physiol* **248**, F522–526 (1985).
205. Ravi Thadhani, Manuel Pascual, J. V. B. Acute renal failure. *N. Engl. J. Med.* **334**, 1448–1460 (1996).
206. Thakar, C. V *et al.* Identification of thrombospondin 1 (TSP-1) as a novel mediator of cell injury in kidney ischemia. *JCI* **115**, 3451–3459 (2005).
207. Flores, J., DiBona, D. R., Beck, C. H. & Leaf, a. The role of cell swelling in ischemic renal damage and the protective effect of hypertonic solute. *J. Clin. Invest.* **51**, 118–26 (1972).
208. Suwa, T., Hogg, J. C., Klut, M. E., Hards, J. & van Eeden, S. F. Interleukin-6 changes deformability of neutrophils and induces their sequestration in the lung. *Am. J. Respir. Crit. Care Med.* **163**, 970–6 (2001).
209. Li, L. *et al.* The chemokine receptors CCR2 and CX3CR1 mediate monocyte/macrophage trafficking in kidney ischemia-reperfusion injury. *Kidney Int.* **74**, 1526–37 (2008).
210. Awad, A. S. *et al.* Compartmentalization of neutrophils in the kidney and lung following acute ischemic kidney injury. *Kidney Int.* **75**, 689–98 (2009).
211. Kelly, K. *et al.* An oral platelet-activating factor antagonist, Ro-24-4736, protects the rat kidney from ischemic injury. *Am. J. ...* **271**, F1061–F1067 (1996).
212. Kelly, K. J. *et al.* Intercellular adhesion molecule-1-deficient mice are protected against ischemic renal injury. *J. Clin. Invest.* **97**, 1056–63 (1996).
213. Sugden, P. H. & Clerk, a. “Stress-Responsive” Mitogen-Activated Protein Kinases (c-Jun N-Terminal Kinases and p38 Mitogen-Activated Protein Kinases) in the Myocardium. *Circ. Res.* **83**, 345–352 (1998).
214. Nemoto, T. *et al.* Small molecule selectin ligand inhibition improves outcome in ischemic acute renal failure. *Kidney Int.* **60**, 2205–14 (2001).
215. Jo, S. K. *et al.* α -MSH decreases apoptosis in ischaemic acute renal failure in rats : possible mechanism of this beneficial effect. *Nephrol. Dial. Transplant.* **16**, 1583–1591 (2001).
216. Chiao, H. *et al.* Alpha-melanocyte-stimulating hormone inhibits renal injury in the absence of neutrophils. *Kidney Int.* **54**, 765–74 (1998).

217. Linas, S. L., Shanley, P. F., Whittenburg, D., Berger, E. & Repine, J. E. Neutrophils accentuate ischemia-reperfusion injury in isolated perfused rat kidneys. *Am. J. Physiol.* **255**, F728–35 (1988).
218. Klausner, J. M. *et al.* Postischemic renal injury is mediated by neutrophils and leukotrienes. *Am. J. Physiol.* **256**, F794–802 (1989).
219. Okusa, M. D., Linden, J., Macdonald, T., Huang, L. & Mark, D. Selective A_{2A} adenosine receptor activation reduces ischemia-reperfusion injury in rat kidney. Selective A_{2A} adenosine receptor activation reduces ischemia-reperfusion injury in rat kidney. (1999).
220. Rabb, H. *et al.* Pathophysiological role of T lymphocytes in renal ischemia-reperfusion injury in mice. *Am. J. Physiol. Renal Physiol.* **279**, F525–31 (2000).
221. Ishibashi, N., Weisbrot-Lefkowitz, M., Reuhl, K., Inouye, M. & Mirochnitchenko, O. Modulation of chemokine expression during ischemia/reperfusion in transgenic mice overproducing human glutathione peroxidases. *J. Immunol.* **163**, 5666–77 (1999).
222. Hellberg, P. O. & Källskog, T. O. Neutrophil-mediated post-ischemic tubular leakage in the rat kidney. *Kidney Int.* **36**, 555–61 (1989).
223. Riera, M. *et al.* Neutrophils accentuate renal cold ischemia-reperfusion injury. Dose-dependent protective effect of a platelet-activating factor receptor antagonist. *J. Pharmacol. Exp. Ther.* **280**, 786–94 (1997).
224. Day, Y., Huang, L., Ye, H., Linden, J. & Okusa, M. D. Renal ischemia-reperfusion injury and adenosine A_{2A} receptor-mediated tissue protection : role of macrophages. *Am. J. Physiol. Physiol.* **288**, F722–F731 (2005).
225. Jo, S.-K., Sung, S.-A., Cho, W.-Y., Go, K.-J. & Kim, H.-K. Macrophages contribute to the initiation of ischaemic acute renal failure in rats. *Nephrol. Dial. Transplant* **21**, 1231–9 (2006).
226. Holdsworth, S. R., Neale, T. J. & Wilson, C. B. Abrogation of Macrophage-dependent Injury in Experimental Glomerulonephritis in the Rabbit. *J. Clin. Invest.* **68**, 686–698 (1981).
227. Kaissling, B. & Le Hir, M. Characterization and distribution of interstitial cell types in the renal cortex of rats. *Kidney Int.* **45**, 709–720 (1994).
228. Shipley, J. Metalloelastase is required for macrophage-mediated proteolysis and matrix invasion in mice. *Proc. ...* **93**, 3942–3946 (1996).

229. Hoste, E. a J. *et al.* Assessment of renal function in recently admitted critically ill patients with normal serum creatinine. *Nephrol. Dial. Transplant* **20**, 747–53 (2005).
230. Verhave, J. C., Fesler, P., Ribstein, J., du Cailar, G. & Mimran, A. Estimation of renal function in subjects with normal serum creatinine levels: influence of age and body mass index. *Am. J. Kidney Dis.* **46**, 233–41 (2005).
231. Chertow, G. M., Burdick, E., Honour, M., Bonventre, J. V & Bates, D. W. Acute kidney injury, mortality, length of stay, and costs in hospitalized patients. *J. Am. Soc. Nephrol.* **16**, 3365–70 (2005).
232. Lassnigg, A. *et al.* Minimal Changes of Serum Creatinine Predict Prognosis in Patients after Cardiothoracic Surgery: A Prospective Cohort Study. *J. Am. Soc. Nephrol.* **15**, 1597–1605 (2004).
233. Loef, B. G. *et al.* Immediate postoperative renal function deterioration in cardiac surgical patients predicts in-hospital mortality and long-term survival. *J. Am. Soc. Nephrol.* **16**, 195–200 (2005).
234. Shemesh, O., Golbetz, H., Kriss, J. P. & Myers, B. D. Limitations of creatinine as a filtration marker in glomerulopathic patients. *Kidney Int.* **28**, 830–8 (1985).
235. Star, R. Treatment of acute renal failure. *Kidney Int.* **54**, 1817–1831 (1998).
236. Ying, W., Allen, C. E., Curtis, L. M., Aaron, K. J. & Sanders, P. W. Mechanism and prevention of acute kidney injury from cast nephropathy in a rodent model. *J. Clin. Invest.* **122**, 1777–1785 (2012).
237. Hoyer, J. R. & Seiler, M. W. Pathophysiology of Tamm-Horsfall protein. *Kidney Int.* **16**, 279–89 (1979).
238. Howie, A., Lote, C., Cunningham, A., Zaccone, G. & Fasulo, S. Distribution of immunoreactive Tamm-Horsefall protein in various species in the vertebrate classes. *Cell Tissue Res.* **274**, 15–19 (1993).
239. Sikri, K. L., Foster, C. L., MacHugh, N. & Marshall, R. D. Localization of Tamm-Horsfall glycoprotein in the human kidney using immuno-fluorescence and immuno-electron microscopical techniques. *J. Anat.* **132**, 597–605 (1981).
240. McKenzie, J. K. & McQueen, E. G. Immunofluorescent localization of Tamm-Horsfall mucoprotein in human kidney. *J. Clin. Pathol.* **22**, 334–9 (1969).
241. Tamm, I. & Horsfall, F. A mucoprotein derived from human urine which reacts with influenza, mumps, and Newcastle disease viruses. *J. Exp. Med.* **74**, 108–114 (1952).

242. Hunt, J. S., McGiven, a R., Groufsky, a, Lynn, K. L. & Taylor, M. C. Affinity-purified antibodies of defined specificity for use in a solid-phase microplate radioimmunoassay of human Tamm-Horsfall glycoprotein in urine. *Biochem. J.* **227**, 957–63 (1985).
243. Robinson, J. P. & Puett, D. Morphological and conformational studies of Tamm-Horsfall urinary glycoprotein. *Arch. Biochem. Biophys.* **159**, 615–621 (1973).
244. Wiggins, R. Uromucoid (Tamm-Horsfall glycoprotein) forms different polymeric arrangements on a filter surface under different physicochemical conditions. *Clin. Chim. acta* **162**, 329–340 (1987).
245. Toma, G., Bates, J. & Kumar, S. Uromodulin (Tamm-Horsfall Protein) Is a Leukocyte Adhesion Molecule. *Biochem. Biophys. Res. Commun.* **200**, 275–282 (1994).
246. Wangsiripaisan, A., Gengaro, P. E., Edelstein, C. L. & Schrier, R. W. Role of polymeric Tamm-Horsfall protein in cast formation: oligosaccharide and tubular fluid ions. *Kidney Int.* **59**, 932–40 (2001).
247. Bradley, J. R., Johnson, D. R. & Pober, J. S. Endothelial Activation by Hydrogen Peroxide. *Am. J. Pathol.* **142**, 1598–1609 (1993).
248. Engerson, T. D. *et al.* Conversion of xanthine dehydrogenase to oxidase in ischemic rat tissues. *J. Clin. Invest.* **79**, 1564–70 (1987).
249. Fernández, L. *et al.* Preconditioning protects liver and lung damage in rat liver transplantation: role of xanthine/xanthine oxidase. *Hepatology* **36**, 562–72 (2002).
250. Stripe, F. & Corte, E. Della. The regulation of rat liver xanthine oxidase. *J Biol Chem* **126**, 739–745 (1969).
251. Nordström G, Seeman T, H. P. Beneficial effect of allopurinol in liver ischemia. *Surgery* **97**, 679–684 (1985).
252. Lee, W.-Y. & Lee, S.-M. Synergistic protective effect of ischemic preconditioning and allopurinol on ischemia/reperfusion injury in rat liver. *Biochem. Biophys. Res. Commun.* **349**, 1087–93 (2006).
253. Manning, a. S., Coltart, D. J. & Hearse, D. J. Ischemia and reperfusion-induced arrhythmias in the rat. Effects of xanthine oxidase inhibition with allopurinol. *Circ. Res.* **55**, 545–548 (1984).
254. Stull, L. B., Leppo, M. K., Szweda, L., Gao, W. D. & Marbán, E. Chronic treatment with allopurinol boosts survival and cardiac contractility in murine postischemic cardiomyopathy. *Circ. Res.* **95**, 1005–11 (2004).

255. Landmesser, U. Vascular Oxidative Stress and Endothelial Dysfunction in Patients With Chronic Heart Failure: Role of Xanthine-Oxidase and Extracellular Superoxide Dismutase. *Circulation* **106**, 3073–3078 (2002).
256. Doehner, W. Effects of Xanthine Oxidase Inhibition With Allopurinol on Endothelial Function and Peripheral Blood Flow in Hyperuricemic Patients With Chronic Heart Failure: Results From 2 Placebo-Controlled Studies. *Circulation* **105**, 2619–2624 (2002).
257. Cappola, T. P. *et al.* Allopurinol Improves Myocardial Efficiency in Patients With Idiopathic Dilated Cardiomyopathy. *Circulation* **104**, 2407–2411 (2001).
258. Ekelund, U. E. G. *et al.* Intravenous Allopurinol Decreases Myocardial Oxygen Consumption and Increases Mechanical Efficiency in Dogs With Pacing-Induced Heart Failure. *Circ. Res.* **85**, 437–445 (1999).
259. Mellin, V. *et al.* Transient reduction in myocardial free oxygen radical levels is involved in the improved cardiac function and structure after long-term allopurinol treatment initiated in established chronic heart failure. *Eur. Heart J.* **26**, 1544–50 (2005).
260. Struthers, a D. *et al.* Effect of allopurinol on mortality and hospitalisations in chronic heart failure: a retrospective cohort study. *Heart* **87**, 229–34 (2002).
261. Hare, J. M. & Johnson, R. J. Uric acid predicts clinical outcomes in heart failure: insights regarding the role of xanthine oxidase and uric acid in disease pathophysiology. *Circulation* **107**, 1951–3 (2003).
262. Jaeschke, H. Glutathione disulfide formation and oxidant stress during acetaminophen-induced hepatotoxicity in mice in vivo: the protective effect of allopurinol. *J. Pharmacol. Exp. ...* **255**, 935–941 (1990).
263. Gonzalez-Flecha, B. & Boveris, A. Mitochondrial sites of hydrogen peroxide production in reperfused rat kidney cortex. *Biochim. Biophys. Acta* **3**, 361–366 (1995).
264. Zweier, J. L., Flaherty, J. T. & Weisfeldt, M. L. Direct measurement of free radical generation following reperfusion of ischemic myocardium. *Proc. Natl. Acad. Sci.* **84**, 1404–1407 (1987).
265. Zweier, J. L. *et al.* Measurement and characterization of postischemic free radical generation in the isolated perfused heart. *J. Biol. Chem.* **264**, 18890–5 (1989).
266. Walker, L. M. *et al.* Oxidative Stress and Reactive Nitrogen Species Generation during Renal Ischemia. *Toxicol. Sci.* **148**, 143–148 (2001).

267. Paller, M. S., Hoidal, J. R. & Ferris, T. F. Oxygen free radicals in ischemic acute renal failure in the rat. *J. Clin. Invest.* **74**, 1156–64 (1984).
268. Kulah, E. *et al.* Oxidized LDL accumulation in experimental renal ischemia reperfusion injury model. *Ren. Fail.* **29**, 409–15 (2007).
269. Kim, J., Jang, H. & Park, K. Reactive oxygen species generated by renal ischemia and reperfusion trigger protection against subsequent renal ischemia and reperfusion injury in mice. *Am. J. Physiol. Renal Physiol.* **298**, 158–166 (2010).
270. Kevin, L. G., Camara, A. K. S., Riess, M. L., Novalija, E. & Stowe, D. F. Ischemic preconditioning alters real-time measure of O₂ radicals in intact hearts with ischemia and reperfusion. *Am. J. Physiol. Heart Circ. Physiol.* **284**, H566–74 (2003).
271. Altug, S., Demiryürek, a T., Kane, K. a & Kanzik, I. Evidence for the involvement of peroxynitrite in ischaemic preconditioning in rat isolated hearts. *Br. J. Pharmacol.* **130**, 125–31 (2000).
272. Baines, C., Goto, M. & Downey, J. Oxygen radicals released during ischemic preconditioning contribute to cardioprotection in the rabbit myocardium. *J. Mol. Cell. ...* **216**, 207–216 (1997).
273. Chen, W., Gabel, S., Steenbergen, C. & Murphy, E. A Redox-Based Mechanism for Cardioprotection Induced by Ischemic Preconditioning in Perfused Rat Heart. *Circ. Res.* **77**, 424–429 (1995).
274. Das, D. K., Maulik, N., Sato, M. & Ray, P. S. Reactive oxygen species function as second messenger during ischemic preconditioning of heart. *Mol. Cell. Biochem.* **196**, 59–67 (1999).
275. Valen, G. *et al.* Preconditioning with hydrogen peroxide (H₂O₂) or ischemia in H₂O₂-induced cardiac dysfunction. *Free Radic. Res.* **29**, 235–245 (1998).
276. Zhou, X., Zhai, X. & Ashraf, M. Direct Evidence That Initial Oxidative Stress Triggered by Preconditioning Contributes to Second Window of Protection by Endogenous Antioxidant Enzyme in Myocytes. *Circulation* **93**, 1177–1184 (1996).
277. Patel, N. *et al.* TEMPONE reduces renal dysfunction and injury mediated by oxidative stress of the rat kidney. *Free Radic. Biol. ...* **33**, 1575–1589 (2002).
278. Chatterjee, P. K. *et al.* Tempol, a membrane-permeable radical scavenger, reduces oxidant stress-mediated renal dysfunction and injury in the rat. *Kidney Int.* **58**, 658–73 (2000).

279. Baker, G. L., Corry, R. J. & Autor, P. Oxygen free radical induced damage in kidneys subjected to warm ischemia and reperfusion. Protective effect of superoxide dismutase. *Ann. Surg.* **202**, 628–41 (1985).
280. Omar, B. & McCord, J. The cardioprotective effect of Mn-superoxide dismutase is lost at high doses in the postischemic isolated rabbit heart. *Free Radic. Biol. Med.* **9**, 473–478 (1990).
281. Elroy-Stein, O., Bernstein, Y. & Groner, Y. Overproduction of human Cu/Zn-superoxide dismutase in transfected cells: extenuation of paraquat-mediated cytotoxicity and enhancement of lipid peroxidation. *EMBO J.* **5**, 615–622 (1986).
282. Omar, B. *et al.* Cardioprotection by Cu,Zn-superoxide dismutase is lost at high doses in the reoxygenated heart. *Free Radic. Biol. ...* **9**, 465–471 (1990).
283. Nelson, S., Bose, S. & McCord, J. The toxicity of high-dose superoxide dismutase suggests that superoxide can both initiate and terminate lipid peroxidation in the reperfused heart. *Free Radic. Biol. Med.* **16**, 195–200 (1994).
284. Minners, J. *et al.* Dinitrophenol, cyclosporin A, and trimetazidine modulate preconditioning in the isolated rat heart: support for a mitochondrial role in cardioprotection. *Cardiovasc. Res.* **47**, 68–73 (2000).
285. Rodrigo, G. C., Lawrence, C. L. & Standen, N. B. Dinitrophenol pretreatment of rat ventricular myocytes protects against damage by metabolic inhibition and reperfusion. *J. Mol. Cell. Cardiol.* **34**, 555–69 (2002).
286. Korde, A. S., Pettigrew, L. C., Craddock, S. D. & Maragos, W. F. The mitochondrial uncoupler 2,4-dinitrophenol attenuates tissue damage and improves mitochondrial homeostasis following transient focal cerebral ischemia. *J. Neurochem.* **94**, 1676–84 (2005).
287. Minners, J. *et al.* Ischemic and Pharmacological Preconditioning in Girardi Cells and C2C12 Myotubes Induce Mitochondrial Uncoupling. *Circ. Res.* **89**, 787–792 (2001).
288. Nadtochiy, S. M., Tompkins, A. J. & Brookes, P. S. Different mechanisms of mitochondrial proton leak in ischaemia/reperfusion injury and preconditioning: implications for pathology and cardioprotection. *Biochem. J.* **395**, 611–8 (2006).
289. McLeod, C. J., Aziz, A., Hoyt, R. F., McCoy, J. P. & Sack, M. N. Uncoupling proteins 2 and 3 function in concert to augment tolerance to cardiac ischemia. *J. Biol. Chem.* **280**, 33470–6 (2005).
290. Mattiasson, G. *et al.* Uncoupling protein-2 prevents neuronal death and diminishes brain dysfunction after stroke and brain trauma. *Nat. Med.* **9**, 1062–8 (2003).

291. Sheikh-Hamad, D. Mammalian stanniocalcin-1 activates mitochondrial antioxidant pathways: new paradigms for regulation of macrophages and endothelium. *Am. J. Physiol.* ... **298**, 248–254 (2010).
292. Wang, Y. *et al.* Stanniocalcin-1 suppresses superoxide generation in macrophages through induction of mitochondrial UCP2. *J. Leukoc. Biol.* **86**, 981–8 (2009).
293. Pinchot, G. The mechanism of uncoupling of oxidative phosphorylation by 2, 4-dinitrophenol. *J. Biol. Chem.* **242**, 4577–83 (1967).
294. Perkins, R. G. Association of Schools of Public Health A Study of the Munitions Intoxications in France. **34**, 2335–2374 (2014).
295. Colman, E. Dinitrophenol and obesity: an early twentieth-century regulatory dilemma. *Regul. Toxicol. Pharmacol.* **48**, 115–7 (2007).
296. Barkan, I. D. Industry Invites Regulation: The Passage of the Pure Food and Drug Act of 1906. *Am. J. Public Health* **75**, 18–26 (1985).
297. Anderson, O. E. Pioneer Statute: The Pure Food and Drugs Act of 1906. *J. Public Law* **13**, 189–196 (1964).
298. Regier, C. The Struggle for Federal Food and Drugs Legislation. *Law Contemp. Probl.* **1**, 3–15 (1933).
299. Johnson, D. R. The history of the 1906 pure food and drugs act and the meat inspection act. *Food. Drug. Cosmet. Law J.* **37**, 5–9 (1982).
300. Swann, J. P. Drug abuse control under FDA, 1938-1968. *Public Health Rep.* **112**, 83–86 (1977).
301. Law, M. T. How do Regulators Regulate? Enforcement of the Pure Food and Drugs Act, 1907-38. *J. Law, Econ. Organ.* **22**, 459–489 (2005).
302. Cutting, W. C. & Tainter, M. L. Actions of Dinitrophenol. *Exp. Biol. Med.* **29**, 1268–1269 (1932).
303. Cutting, W., HG, M. & Tainter, M. Actions and uses of Dinitrophenol: Promising metabolic applications. *JAMA* **101**, 193–195 (1933).
304. ML, T., AB, S. & WC, C. Use of Dinitrophenol in obesity and related conditions: A progress report. *JAMA* **101**, 1472–1475 (1933).
305. Simkins, S. Dinitrophenol and desiccated thyroid in the treatment of obesity: A comprehensive clinical and laboratory study. *JAMA* **108**, 2110–2117 (1937).

306. JA, H., K, D. & MD, B. Mitochondrial uncoupling as a target for drug development for the treatment of obesity. *Obesity* **2**, 255–265 (2001).
307. Tainter, M., Cutting, W. & Hines, E. Effects of moderate doses of dinitrophenol on the energy exchange and nitrogen metabolism of patients under conditions of restricted dietary. *J. Pharmacol. ...* **55**, 326–353 (1935).
308. Tainter, M., Cutting, W. & Stockton, A. Use of Dinitrophenol in Nutritional Disorders: A Critical Survey of Clinical Results. *Am. J. Public Health* **24**, 1045–1053 (1934).
309. Masserman, J. H. & Goldsmith, H. Dinitrophenol: Its therapeutic and toxic actions in certain types of psychobiologic underactivity. *JAMA* **102**, 523–525 (1934).
310. Koch, R., Lee, R. & Tainter, M. Dinitrophenol on liver function. *West. J. Med.* **43**, 337–339 (1935).
311. Dunlop, D. The use of 2:4-Dinitrophenol as a metabolic stimulant. *BMJ* **1**, 524–527 (1934).
312. MacBryde, C. M. & Taussig, B. L. Functional changes in liver, heart and muscle, and loss of dextrose tolerance resulting from Dinitrophenol. *JAMA* **105**, (1935).
313. Rodin, F. H. Cataracts following the use of Dinitrophenol: A summary of thirty-two cases. *West. J. Med.* **44**, 276–279 (1936).
314. Horner, W. D. Cataract following Di-nitrophenol treatment for obesity. *Arch. Ophthalmol.* **16**, 447–461 (1936).
315. Grundlingh, J., Dargan, P. I., El-Zanfaly, M. & Wood, D. M. 2,4-dinitrophenol (DNP): a weight loss agent with significant acute toxicity and risk of death. *J. Med. Toxicol.* **7**, 205–12 (2011).
316. Wax, P. M. Elixirs, diluents, and the passage of the 1938 Federal Food, Drug and Cosmetic Act. *Ann. Intern. Med.* **122**, 456–61 (1995).
317. DNP (2,4-Dinitrophenol) 100mg Biomax. *Anab. 24* at <<http://anabolics24.com/buy-DNP-2-4-Dinitrophenol-100mg-Biomax.html>>
318. Lou, P.-H. *et al.* Mitochondrial uncouplers with an extraordinary dynamic range. *Biochem. J.* **407**, 129–40 (2007).
319. Liberman, E., Topaly, V., Tsofina, L., Jasaitis, A. & Skulachev, V. Mechanism of Coupling of Oxidative Phosphorylation and the Membrane Potential of Mitochondria. *Nature* **222**, 1076–1078 (1969).

320. Chevrollier, A., Loiseau, D., Reynier, P. & Stepien, G. Adenine nucleotide translocase 2 is a key mitochondrial protein in cancer metabolism. *Biochim. Biophys. Acta* **1807**, 562–7 (2011).
321. Miyoshi H, Tsujishita H, Tokutake N, F. T. Quantitative analysis of uncoupling activity of substituted phenols with a physicochemical substituent and molecular parameters. *Biochim. Biophys. Acta* **1**, 99–106 (1990).
322. Bakker, E. P., Arents, J. O. S. C., Hoebe, J. A. N. P. M. & Terada, H. Surface Potential and the Interaction of Weakly Acidic Uncouplers of Oxidative Phosphorylation with Liposomes and Mitochondria. *Biochim. Biophys. Acta* **387**, 491–506 (1975).
323. John Kasianowicz, Roland Benz, S. M. The kinetic mechanism by which CCCP (carbonyl cyanidem-Chlorophenylhydrazone) transports protons across membranes. *J. Membr. Biol.* **82**, 179–190 (1984).
324. Cohen, F., Eisenberg, M. & McLaughlin, S. The kinetic mechanism of action of an uncoupler of oxidative phosphorylation. *J. Membr. Biol.* **37**, 361–396 (1977).
325. Spycher, S., Smejtek, P., Netzeva, T. I. & Escher, B. I. Toward a class-independent quantitative structure-activity relationship model for uncouplers of oxidative phosphorylation. *Chem. Res. Toxicol.* **21**, 911–27 (2008).
326. Benz, R. & McLaughlin, S. The molecular mechanism of action of the proton ionophore FCCP (carbonylcyanide p-trifluoromethoxyphenylhydrazone). *Biophys. J.* **41**, 381–98 (1983).
327. McLaughlin, S. & Dilger, J. Transport of Protons Across Membranes by Weak Acids. *Physiol. Rev* **60**, 825–863 (1980).
328. Naven, R. T., Swiss, R., Klug-McLeod, J., Will, Y. & Greene, N. The development of structure-activity relationships for mitochondrial dysfunction: uncoupling of oxidative phosphorylation. *Toxicol. Sci.* **131**, 271–8 (2013).
329. Hopfer, U., Lehninger, A. & Thompson, T. PROTONIC CONDUCTANCE ACROSS PHOSPHOLIPID BILAYER MEMBRANES INDUCED BY UNCOUPLING AGENTS FOR OXIDATIVE PHOSPHORYLATION. *Proc. ...* **59**, 484–490 (1968).
330. McLaughlin, S. The Mechanism of Action of DNP on Phospholipid Bilayer Membranes. *J. Membr. Biol.* 361–372 (1972).
331. Finkelstein, A. WEAK-ACID UNCOUPLERS OF OXIDATIVE PHOSPHORYLATION. MECHANISM OF ACTION ON THIN LIPID MEMBRANES. *Biochim. Biophys. Acta (BBA)-Bioenergetics* **205**, 1–6 (1970).

332. Poonia, N. S. COMPLEXATION OF SODIUM AND POTASSIUM WITH MACROCYCLIC POLYETHERS; ACTIVATION OF THE COUNTER ANIONS. *J. Inorg. Nucl. Chem.* **37**, 1855–1858 (1975).
333. Parsegian, A. Energy of an Ion crossing a Low Dielectric Membrane: Solutions to Four Relevant Electrostatic Problems. *Nature* **221**, 844–846 (1969).
334. Escher, B. I., Hunziker, R., Schwarzenbach, R. P. & Westall, J. C. Kinetic Model To Describe the Intrinsic Uncoupling Activity of Substituted Phenols in Energy Transducing Membranes. *Environ. Sci. Technol.* **33**, 560–570 (1999).
335. Bakker, E., Bühlmann, P. & Pretsch, E. The phase-boundary potential model. *Talanta* **63**, 3–20 (2004).
336. Kürschner, M. *et al.* Effect of Fluorine Substitution on the Interaction of Lipophilic Ions with the Plasma Membrane of Mammalian Cells. *Biophys. J.* **79**, 1490–1497 (2000).
337. Reuss, O. R. *et al.* Interaction of fluorinated lipophilic ions with the plasma membrane of mammalian cells studied by electroration and dielectrophoresis. *J. Electrostat.* **56**, 419–434 (2002).
338. Krafft, M. & Riess, J. Highly fluorinated amphiphiles and colloidal systems, and their applications in the biomedical field. *Biochimie* **80**, 489–514 (1998).
339. Benz, R. Structural requirement for the rapid movement of charged molecules across membranes. Experiments with tetraphenylborate analogues. *Biophys. J.* **54**, 25–33 (1988).
340. Jackson, P. Differences between Effects of Undissociated and Anionic 2,4-Dinitrophenol on Permeability of Barley Roots. *Plant Physiol.* **70**, 1373–1379 (1982).
341. Barker, J. & Levitan, H. Phenols: effects on membrane permeability of molluscan neurons. *Brain Res.* **67**, 555–561 (1974).
342. Alekseev, A., Gomez, L., Aleksandrova, L., Brady, P. & Terzic, A. Opening of cardiac sarcolemmal KATP channels by dinitrophenol separate from metabolic inhibition. *J. Membr. Biol.* **214**, 203–214 (1997).
343. Bowei, W., Toshiaki, S., Kiyosue, T. & Arita, M. Blockade of 2,4-dinitrophenol induced ATP sensitive potassium current in guinea pig ventricular myocytes by class I antiarrhythmic drugs. *Cardiovasc. Res.* **26**, 1095–1101 (1992).
344. Yamada, M. Mitochondrial ATP-sensitive K⁺ channels, protectors of the heart. *J. Physiol.* **588**, 283–6 (2010).

345. Hanstein, W. & Hatefi, Y. Characterization and Localization of Mitochondrial Uncoupler Binding Sites with an Uncoupler Capable of Photoaffinity Labeling. *J. Biol. Chem.* **249**, 1356–1362 (1974).
346. Hatefi, Y. Discovery and Photoaffinity Labeling of the Mitochondrial Uncoupler Binding Site. *Ann. N. Y. Acad. Sci.* **346**, 434–443 (1980).
347. Katre, N. & Wilson, D. A specific uncoupler-binding protein in *Tetrahymena pyriformis* and *Paracoccus denitrificans*. *Biochim. Biophys. Acta* **593**, 224–229 (1980).
348. Kurup, C. & Sanadi, D. Photoaffinity labeling of uncoupler binding sites on mitochondrial membrane. *J Bioenerg Biomembr.* **9**, 1–15 (1977).
349. Wang, G., Richardson, S. & Thayer, S. Intracellular acidification is not a prerequisite for glutamate-triggered death of cultured hippocampal neurons. *Neurosci. Lett.* **186**, 139–144 (1995).
350. Serrano, O. K., Jovanovic, a & Terzic, a. Inhibition of both Na/H and bicarbonate-dependent exchange is required to prevent recovery of intracellular pH in single cardiomyocytes exposed to metabolic stress. *Biosci. Rep.* **19**, 99–107 (1999).
351. Brismar, T. & Collins, V. Effect of external cation concentration and metabolic inhibitors on membrane potential of human glial cells. *J. Physiol.* **460**, 365–383 (1993).
352. Park, K.-S. *et al.* FCCP depolarizes plasma membrane potential by activating proton and Na⁺ currents in bovine aortic endothelial cells. *Pflugers Arch.* **443**, 344–52 (2002).
353. To, M.-S. *et al.* Mitochondrial uncoupler FCCP activates proton conductance but does not block store-operated Ca(2⁺) current in liver cells. *Arch. Biochem. Biophys.* **495**, 152–8 (2010).
354. Buckler, K. J. & Vaughan-Jones, R. D. Effects of mitochondrial uncouplers on intracellular calcium, pH and membrane potential in rat carotid body type I cells. *J. Physiol.* **513** (Pt 3, 819–33 (1998).
355. Juthberg, S. K. & Brismar, T. Effect of metabolic inhibitors on membrane potential and ion conductance of rat astrocytes. *Cell. Mol. Neurobiol.* **17**, 367–77 (1997).
356. Kuruvilla, S. *et al.* Effects of minimally toxic levels of carbonyl cyanide P-(trifluoromethoxy) phenylhydrazone (FCCP), elucidated through differential gene expression with biochemical and morphological correlations. *Toxicol. Sci.* **73**, 348–61 (2003).

357. Tsiper, M. V *et al.* Differential mitochondrial toxicity screening and multi-parametric data analysis. *PLoS One* **7**, e45226 (2012).
358. Guarino, R. D. *et al.* Method for determining oxygen consumption rates of static cultures from microplate measurements of pericellular dissolved oxygen concentration. *Biotechnol. Bioeng.* **86**, 775–87 (2004).
359. Rogers, G. W. *et al.* High throughput microplate respiratory measurements using minimal quantities of isolated mitochondria. *PLoS One* **6**, e21746 (2011).
360. Johnson-Cadwell, L. I., Jekabsons, M. B., Wang, a, Polster, B. M. & Nicholls, D. G. “Mild Uncoupling” does not decrease mitochondrial superoxide levels in cultured cerebellar granule neurons but decreases spare respiratory capacity and increases toxicity to glutamate and oxidative stress. *J. Neurochem.* **101**, 1619–31 (2007).
361. Zielonka, J. & Kalyanaraman, B. Hydroethidine- and MitoSOX-derived red fluorescence is not a reliable indicator of intracellular superoxide formation: another inconvenient truth. *Free Radic. Biol. Med.* **48**, 983–1001 (2010).
362. Al Mehdi, A., Shuman, H. & Fisher, A. B. Intracellular generation of reactive during nonhypoxic lung ischemia oxygen species. *Am. J. Physiol.* **272**, L294–300 (1997).
363. Boveris, A. & Cadenas, E. Mitochondrial Production of Hydrogen Peroxide Regulation by Nitric Oxide and the Role of Ubisemiquinone. *IUBMB Life* **50**, 245–250 (2000).
364. O’Malley, Y. Q., Reszka, K. J. & Britigan, B. E. Direct oxidation of 2',7'-dichlorodihydrofluorescein by pyocyanin and other redox-active compounds independent of reactive oxygen species production. *Free Radic. Biol. Med.* **36**, 90–100 (2004).
365. Glebska, J. & Koppenol, W. H. Peroxynitrite-Mediated Oxidation of Dichlorodihydrofluorescein and Dihydrorhodamine. *Free Radic. Biol. Med.* **35**, 676–682 (2003).
366. Wrona, M., Patel, K. & Wardman, P. Reactivity of 2',7'-dichlorodihydrofluorescein and dihydrorhodamine 123 and their oxidized forms toward carbonate, nitrogen dioxide, and hydroxyl radicals. *Free Radic. Biol. Med.* **38**, 262–70 (2005).
367. Shchepinova, M. M. *et al.* Dodecyl and octyl esters of fluorescein as protonophores and uncouplers of oxidative phosphorylation in mitochondria at submicromolar concentrations. *Biochim. Biophys. Acta* **1837**, 149–58 (2014).

368. Hulikova, A., Vaughan-Jones, R. D. & Swietach, P. Dual role of CO₂/HCO₃⁽⁻⁾ buffer in the regulation of intracellular pH of three-dimensional tumor growths. *J. Biol. Chem.* **286**, 13815–26 (2011).
369. Griffiths, E. J. Mitochondria--potential role in cell life and death. *Cardiovasc. Res.* **46**, 24–7 (2000).
370. Steinbach, J. Acetylcholine responses on clonal myogenic cells in vitro. *J. Physiol.* **247**, 393–405 (1975).
371. Li, L., Huang, L., Ye, H. & Song, S. Dendritic cells tolerized with adenosine A2AR agonist attenuate acute kidney injury. *J. Clin. ...* **122**, (2012).
372. Li, L. *et al.* NKT cell activation mediates neutrophil IFN-gamma production and renal ischemia-reperfusion injury. *J. Immunol.* **178**, 5899–911 (2007).
373. Harris, J. M. & Chess, R. B. Effect of pegylation on pharmaceuticals. *Nat. Rev. Drug Discov.* **2**, 214–21 (2003).
374. Veronese, F. & Pasut, G. PEGylation, successful approach to drug delivery. *Drug Discov. Today* **10**, 1451–1458 (2005).
375. Ueda, Y. *et al.* Gastric mucosal changes induced by polyethylene glycol 400 administered by gavage in rats. *J. Toxicol. Sci.* **36**, 811–5 (2011).
376. Basit, a W. *et al.* The effect of polyethylene glycol 400 on gastrointestinal transit: implications for the formulation of poorly-water soluble drugs. *Pharm. Res.* **18**, 1146–50 (2001).
377. Sack, M. N. Mitochondrial depolarization and the role of uncoupling proteins in ischemia tolerance. *Cardiovasc. Res.* **72**, 210–9 (2006).
378. Modrianský, M. & Gabrielová, E. Uncouple my heart: the benefits of inefficiency. *J. Bioenerg. Biomembr.* **41**, 133–6 (2009).
379. Hoehn, K. L. *et al.* Insulin resistance is a cellular antioxidant defense mechanism. *Proc. Natl. Acad. Sci. U. S. A.* **106**, 17787–92 (2009).
380. Caldeira da Silva, C. C., Cerqueira, F. M., Barbosa, L. F., Medeiros, M. H. G. & Kowaltowski, A. J. Mild mitochondrial uncoupling in mice affects energy metabolism, redox balance and longevity. *Aging Cell* **7**, 552–60 (2008).
381. Wu, Y.-N., Munhall, A. C. & Johnson, S. W. Mitochondrial uncoupling agents antagonize rotenone actions in rat substantia nigra dopamine neurons. *Brain Res.* **1395**, 86–93 (2011).

382. Stout, A. K., Raphael, H. M., Kanterewicz, B. I., Klann, E. & Reynolds, I. J. Glutamate-induced neuron death requires mitochondrial calcium uptake. *Nat. Neurosci.* **1**, 366–73 (1998).
383. Maragos, W., Rockich, K., Dean, J. & Young, K. Pre-or post-treatment with the mitochondrial uncoupler 2, 4-dinitrophenol attenuates striatal quinolinate lesions. *Brain Res.* **966**, 312–316 (2003).
384. Pandya, J. D., Pauly, J. R. & Sullivan, P. G. The optimal dosage and window of opportunity to maintain mitochondrial homeostasis following traumatic brain injury using the uncoupler FCCP. *Exp. Neurol.* **218**, 381–9 (2009).
385. Brennan, J. P. *et al.* Mitochondrial uncoupling, with low concentration FCCP, induces ROS-dependent cardioprotection independent of KATP channel activation. *Cardiovasc. Res.* **72**, 313–21 (2006).
386. Brennan, J. P., Berry, R. G., Baghai, M., Duchen, M. R. & Shattock, M. J. FCCP is cardioprotective at concentrations that cause mitochondrial oxidation without detectable depolarisation. *Cardiovasc. Res.* **72**, 322–30 (2006).